DEVELOPMENT OF WOOD CELLULOSE-BASED FILMS FROM AQUEOUS SOLVENTS FOR SUSTAINABLE FOOD PACKAGING

Kehao Huang

The Department of Food Science and Agricultural Chemistry

McGill University, Montreal

June 2024

A thesis submitted to McGill University in partial fulfillment of the requirements of the degree of Doctor of Philosophy

Table of Contents

Abstract

Increasing concerns about non-degradable plastic packaging have prompted the development of sustainable alternatives. Cellulose-based materials, provide a viable solution due to their renewable nature and lower environmental impact. The development of effective cellulose solvents has facilitated the fabrication of regenerated cellulose (RC) films, enabling the production of environmentally friendly packaging materials. This thesis aimed to explore the development, properties, and applications of RC films as a biodegradable food packaging material, with wood pulps serving as a rich source of cellulose that can be industrially available. The objective of Chapter 3 was to investigate the effects of different aqueous solvents on the structure and properties of RC films derived from wood cellulose. Cellulose was dissolved in either 64 wt.% H_2SO_4 solution (RC-H4) or NaOH/urea aqueous solution (RC-N4). RC-H4 films had higher tensile strength (109.78 ± 2.14 MPa) and better folding endurance (20-28 times) compared to RC-N4 films (62.90 ± 2.27 MPa and un-foldable). Increasing cellulose contents in concentrated H_2SO_4 solution from 3 to 5 wt.% led to improved tensile strength (102.61 ± 1.99 to 132.93 ± 5.64 MPa) and unchanged foldability. Additionally, RC-H4 films exhibited better water vapor barrier property, transparency, and but lower thermal stability. These results facilitated the production of high-performance RC films obtained from two aqueous solvents. Chapter 4 examined the influence of wood origin and drying methods on the mechanical properties and water vapor barrier performance of RC films. Five different wood pulps were dissolved in NaOH/urea solution, and films were dried either at ambient conditions or by hot pressing. Results indicated that wood origin had minimal impact on RC film structure. However, hot pressing significantly enhanced tensile strength and water vapor barrier property of RC films. The hot-pressed RC film made from pine demonstrated comparable performance to commercial plastic wrap in preserving cherry tomatoes. The next step was to address the

hygroscopic nature of cellulose films, which can diminish their mechanical properties under humid conditions. Chapter 5 focused on enhancing the water resistance of cellulose films through dual modifications of chemical vapor deposition of organosilanes and the incorporation of cellulose nanocrystals (CNC). The modified films had unchanged tensile strength (~57 MPa) at RH 60% and reduced water vapor permeability. Besides, these films showed effective performance in cookie preservation tests, comparable to commercial plastic wrap, while maintaining disintegration rate. Chapter 6 explored the development of antimicrobial surfaces inspired by nanostructures found in nature to functionalize RC films. This chapter aimed to investigate the effect of surface charge on the antimicrobial properties of RC films with chevaux-de-frise-like nanostructures by coating RC films with differently charged CNC. Positively charged CNC showed the highest antibacterial activity, effectively reducing *E. coli* and *S. aureus* populations upon contact. All CNC-coated films demonstrated improved mechanical strength and water vapor barrier property. This chapter highlighted the potential of using CNC coatings to develop active packaging materials to prevent bacterial growth and enhance food safety. Overall, this thesis demonstrates that RC films, derived from abundant wood cellulose and processed using various aqueous solvents and modification strategies, offer promising alternatives to non-degradable plastic packaging.

Résumé

Les préoccupations croissantes concernant les emballages plastiques non dégradables ont conduit au développement d'alternatives durables. Les matériaux à base de cellulose offrent une solution viable en raison de leur nature renouvelable et de leur impact environnemental réduit. Le développement de solvants efficaces pour la cellulose a facilité la fabrication de films de cellulose régénérée (RC), permettant la production de matériaux d'emballage respectueux de l'environnement. Cette thèse visait à explorer le développement, les propriétés et les applications des films RC comme matériau d'emballage alimentaire biodégradable, avec les pâtes de bois servant de source riche en cellulose, disponible industriellement. L'objectif du Chapitre 3 était d'étudier les effets de différents solvants aqueux sur la structure et les propriétés des films RC dérivés de la cellulose de bois. La cellulose a été dissoute dans une solution de H2SO4 à 64 % en poids (RC-H4) ou dans une solution aqueuse de NaOH/urée (RC-N4). Les films RC-H4 avaient une résistance à la traction plus élevée (109,78 ± 2,14 MPa) et une meilleure endurance au pliage (20-28 fois) par rapport aux films RC-N4 (62,90 ± 2,27 MPa et non pliable). L'augmentation du contenu en cellulose dans la solution concentrée de H2SO4 de 3 à 5 % en poids a conduit à une amélioration de la résistance à la traction (102,61 ± 1,99 à 132,93 ± 5,64 MPa) sans modification de la pliabilité. De plus, les films RC-H4 ont montré une meilleure propriété de barrière à la vapeur d'eau, une transparence accrue, mais une stabilité thermique plus faible. Ces résultats ont facilité la production de films RC performants obtenus à partir de deux solvants aqueux. Le Chapitre 4 a examiné l'influence de l'origine du bois et des méthodes de séchage sur les propriétés mécaniques et la performance de la barrière à la vapeur d'eau des films RC. Cinq pâtes de bois différentes ont été dissoutes dans une solution de NaOH/urée, et les films ont été séchés soit à température ambiante, soit par pressage à chaud. Les résultats ont indiqué que l'origine du bois avait un impact minime sur la structure des films

RC. Cependant, le pressage à chaud a considérablement amélioré la résistance à la traction et la propriété de barrière à la vapeur d'eau des films RC. Le film RC pressé à chaud fabriqué à partir de pin a montré des performances comparables à celles du film plastique commercial pour la conservation des tomates cerises. L'étape suivante a été de traiter la nature hygroscopique des films en cellulose, qui peut diminuer leurs propriétés mécaniques dans des conditions humides. Le Chapitre 5 a concentré sur l'amélioration de la résistance à l'eau des films en cellulose grâce à des modifications doubles par dépôt chimique de vapeur d'organosilanes et incorporation de nanocristaux de cellulose (CNC). Les films modifiés avaient une résistance à la traction inchangée (~57 MPa) à RH 60 % et une perméabilité à la vapeur d'eau réduite. De plus, ces films ont montré une performance efficace dans les tests de conservation des cookies, comparable au film plastique commercial, tout en maintenant un taux de désintégration. Le Chapitre 6 a exploré le développement de surfaces antimicrobiennes inspirées des nanostructures trouvées dans la nature pour fonctionnaliser les films RC. Ce chapitre visait à étudier l'effet de la charge de surface sur les propriétés antimicrobiennes des films RC avec des nanostructures de type chevaux-de-frise en les recouvrant de CNC chargés différemment. Les CNC chargés positivement ont montré la plus grande activité antibactérienne, réduisant efficacement les populations d'E. coli et de S. aureus au contact. Tous les films recouverts de CNC ont démontré une résistance mécanique améliorée et une propriété de barrière à la vapeur d'eau accrue. Ce chapitre a souligné le potentiel de l'utilisation des revêtements CNC pour développer des matériaux d'emballage actifs afin de prévenir la croissance bactérienne et d'améliorer la sécurité alimentaire. Dans l'ensemble, cette thèse démontre que les films RC, dérivés de la cellulose de bois abondante et traités par divers solvants aqueux et stratégies de modification, offrent des alternatives prometteuses aux emballages plastiques non dégradables.

Acknowledgements

The four-year journey of my PhD has been incredible, and I am deeply grateful to the many people who have provided support, guidance, and encouragement throughout this process.

First and foremost, I would like to express my profound gratitude to my supervisor, Dr. Yixiang Wang. His unwavering support and insightful feedback have been fundamental to the completion of my doctoral thesis. Dr. Wang's optimistic and open-minded attitude towards life, coupled with his constructive suggestions for addressing experimental challenges, have significantly influenced my approach to both work and life. His broad knowledge across interdisciplinary fields and sharp insight have consistently guided me in refining my research into a well-crafted work. I am immensely grateful for his mentorship, not only in navigating complex experiments but also in providing valuable advice for my future career and personal development.

I would like to express my sincere gratitude to my committee members, Dr. Saji George and Dr. Xiaonan Lu, for their constructive criticism, thoughtful suggestions, and time invested. Their different perspectives and provision of experimental equipment have greatly enriched my work and helped me accomplish challenging tasks. Special thanks to Dr. Benjamin K. Simpson for his invaluable assistance and friendship throughout this process. I am also grateful to my colleagues at the Wang Lab. The collaborative environment and intellectual discussions we engaged in have been both inspiring and stimulating. Besides, I extend my heartfelt acknowledgment to all the participants and collaborators who contributed to this research. Your involvement and insights have been invaluable to the success of this project.

To my family and friends, your unwavering belief in me and continuous encouragement have been a constant source of motivation. My deepest gratitude to my parents for their boundless

love and support. Thank you for nurturing my dreams; your endless care and patient communication have consistently kept me positive and diligent. I also want to express my appreciation to my basketball and fitness friends; I treasure our friendship dearly, and you have brought joy and vitality to my research life. To my girlfriend, Ziyun Xu, your patience, understanding, and unwavering support have been my rock throughout this journey. Embracing the challenges and joys of life and enjoying the time we spent together is truly the greatest reward of all.

Thank you all for being a part of this incredible journey.

Contribution of Authors

The following authors contributed to the publication of work undertaken as part of this thesis: Kehao Huang[a], Yixiang Wang[a], Ossyane Chateaugiron[a,b], Louis Mairot[a,c], Anne Maltais[d], Jinxia Liu[e]

Authors affiliation

[a] Department of Food Science and Agricultural Chemistry, McGill University, Ste Anne de Bellevue, Quebec, H9X 3V9, Canada

[b] Chimie ParisTech, Université Paris Sciences et Lettres, Paris, Île-de-France, 75005, France

[c] Agri-food and bioprocessing college, UniLaSalle, Beauvais, Hauts-de-France, 60000, France

[d] Institut de Technologie des Emballages et du Génie Alimentaire (ITEGA), Montréal, Québec, H1N 1C1, Canada

[e] Department of Civil Engineering, McGill University, Montreal, Quebec, H3A 0C3, Canada

Contribution of work by co-authors for each paper:

PAPER 1: Huang, K., & Wang, Y. (2022). Recent applications of regenerated cellulose films and hydrogels in food packaging. *Current Opinion in Food Science*, *43*, 7-17. (Chapter 2)

Author contributions: Kehao Huang: conceptualization, visualization, and writing-original draft; Yixiang Wang: writing-reviewing & editing, and supervision.

PAPER 2: Huang, K., Chateaugiron, O., Mairot, L., & Wang, Y. (2024). Wood cellulose films with different foldabilities triggered by dissolution and regeneration from concentrated H_2SO_4 and NaOH/urea aqueous solutions. *International Journal of Biological Macromolecules*, *273*, 133141. (Chapter 3)

Author contributions: Kehao Huang: methodology, investigation, writing - original draft; Ossyane Chateaugiron: writing- reviewing and editing; Louis Mairot: writing- reviewing and editing; Yixiang Wang: conceptualization, supervision, writing- reviewing and editing, funding acquisition.

PAPER 3: Huang, K., Maltais, A., Liu, J., & Wang, Y. (2022). Wood cellulose films regenerated from NaOH/urea aqueous solution and treated by hot pressing for food packaging application. *Food Bioscience*, 50, 102177. (Chapter 4)

Author contributions: Kehao Huang: investigation, writing-original draft; Anne Maltais: writing-review & editing; Jinxia Liu: writing-review & editing; Yixiang Wang: conceptualization, supervision, funding acquisition, writing-review & editing.

PAPER 4: Huang, K., Maltais, A., & Wang, Y. (2023). Enhancing water resistance of regenerated cellulose films with organosilanes and cellulose nanocrystals for food packaging. *Carbohydrate Polymer Technologies and Applications*, *6*, 100391. (Chapter 5)

Author contributions: Kehao Huang: investigation, writing-original draft; Anne Maltais: writing-review & editing; Yixiang Wang: conceptualization, supervision, funding acquisition, writing-review & editing.

PAPER 5: Huang, K., & Wang, Y. (2022). Effect of surface charge on mechano-bactericidal activity of cellulose nanocrystals constructed chevaux-de-frise and meat preservation. *Food Packaging and Shelf Life*. Submitted. (Chapter 6)

Author contributions: Kehao Huang: investigation, writing-original draft; Yixiang Wang: conceptualization, supervision, funding acquisition, writing-review & editing.

PAPER 6: Huang, K., & Wang, Y. (2023). Recent advances in self-healing materials for food packaging. *Packaging Technology and Science*, *36*(3), 157-169.

Author contributions: Kehao Huang: conceptualization, visualization, writing-original draft; Yixiang Wang: writing-reviewing & editing, and supervision.

List of Figures

List of Tables

List of Abbreviations

[η]	Intrinsic viscosity
AFM	Atomic force microscopy
ANOVA	Analysis of variance
ARC	Acidochromic cotton cellulose
BC	Bacterial cellulose
C. albicans	*Candida albicans*
CFU	Colony formation unit
CI	Crystallinity index
CMC	Carboxymethyl cellulose
CNC	Cellulose nanocrystals
CNF	Cellulose nanofibrils
CVD	Chemical vapor deposition
DP	Degree of polymerization
DS	Degree of substitution
E. coli	*Escherichia coli*
ECH	Epichlorohydrin
FE-ESEM	Field emission environmental scanning electron microscope
FT-IR	Fourier transform infrared spectroscopy
GO	Graphene oxide

ILs	Ionic liquids
LBA	Luria-Bertani agar
MBA	Methylenebis acrylamide
MTMS	Methyltrimethoxysilane
M_v	Viscosity-Average molecular weight
NMMO	*N*-methylmorpholine-*N*-oxide
NPs	Nanoparticles
OP	Oxygen permeability
OTR	Oxygen transmission rate
P. aeruginosa	*Pseudomonas aeruginosa*
PBS	Phosphate-buffered saline
PEI	Polyethyleneimine
PFTS	1H,1H,2H,2H-perfluorooctyltriethoxysilane
PV	Peroxide value
PVA	Polyvinyl alcohol
PVP	Polyvinyl pyrrolidone
RC	Regenerated cellulose
RH	Relative humidity
S. aureus	*Staphylococcus aureus*
SEM	Surface electron microscope

TEM	Transmission electron microscopy
TEMPO	(2,2,6,6-tetramethylpiperidine-1-yl)oxyl
T_{max}	Maximum decomposition temperature
TSA	Tryptic soy agar
TVC	Total viable count
WCA	Water contact angle
WVP	Water vapor permeability
WVTR	Water vapor transmission rate
XRD	X-ray diffractometry

Chapter 1. General Introduction

1.1. Introduction

The widespread use of petroleum-based, non-degradable plastics has led to significant environmental challenges. In Canada, about 4 million tons of plastics are produced annually, with food packaging materials accounting for one-third of Canadian household waste. However, only 20% of plastics are recovered for reuse and recycling, resulting in persistent pollution, landfill overflow, and marine litter (Roy, Mohanty, & Misra, 2022). Additionally, the production and disposal of plastic packaging contribute significantly to greenhouse gas emissions, exacerbating climate change. Consequently, developing biodegradable food packaging materials is crucial to mitigate adverse environmental impacts.

In response to the environmental issues posed by traditional plastics, cellulose emerges as a promising alternative. Cellulose is the most abundant natural polymer on Earth, primarily found in the cell walls of plants (Gardner & Blackwell, 1974). It is a linear polysaccharide consisting of D-glucose units linked by β-1,4-glycosidic bonds (Zhao et al., 2022). This unique structure imparts cellulose with remarkable mechanical strength, making it a fundamental component in numerous industrial applications. Given its biodegradability, renewability, and non-toxicity, cellulose is an attractive material for sustainable development (Shaghaleh, Xu, & Wang., 2018). One of the most exciting advancements in cellulose research is the development of cellulose nanocrystals (CNC). CNC is usually derived from natural cellulose fibers through processes such as acid hydrolysis, TEMPO oxidation, and enzymatic isolation (Pirich et al., 2020). These nanocrystals are highly crystalline, with dimensions typically ranging from a few nanometers in width to several hundred nanometers in length. CNC exhibits exceptional mechanical properties, high surface area, and the ability to form strong hydrogen bonds (Dhar et al., 2015). These characteristics make CNC a versatile nanomaterial with potential applications in reinforcing mechanical and barrier properties of composite materials.

Despite the numerous advantages of cellulose, its insolubility in water and most organic solvents poses a significant challenge for processing. To overcome this, various methods for cellulose dissolution have been developed, utilizing solvents such as ionic liquids, *N*-methylmorpholine-*N*-oxide, and alkaline solutions (El Seoud et al., 2019). Once dissolved, cellulose can be regenerated by precipitating it from the solution using anti-solvents like water or ethanol. This regeneration process restructures cellulose into different morphologies, such as fibers, films, or hydrogels, while maintaining its intrinsic properties (Tu et al., 2021).

Regenerated cellulose (RC) films, produced through the dissolution and regeneration process, are gaining attention for their application in sustainable packaging. These films exhibit excellent mechanical properties, transparency, and biodegradability (Li, Zhang, & Xu., 2012). The potential of RC films is particularly significant for food packaging, where maintaining product freshness and extending shelf life are critical. The inclusion of CNC into RC films improves the mechanical strength and barrier properties against gases and moisture, which are essential for effective food packaging. Additionally, CNC can be functionalized to impart antimicrobial properties to the films, further extending the shelf life of food products and ensuring safety (Li et al., 2019).

The food packaging industry has established specific performance metrics to ensure the effectiveness and safety of packaging materials. For instance, plastic food wraps are expected to have a tensile strength of at least 15 MPa to withstand mechanical stresses during handling and storage (Han, 2014). Barrier properties are also critical, packaging materials with oxygen transmission rates (OTR) below 50 mL/m²/day/atm at 23 °C and 75% relative humidity are enough to preserve meat under vacuum condition, while OTR of 0.5 mL/m²/day/atm is recommended to preserve meat such as cured ham at 5 °C. Besides, water vapor transmission rate (WVTR) of less than 5 g/m²/day is required for effective preservation of perishable foods

like meat (Véronique, 2008; Robertson, 2013). By incorporating cellulose nanocrystals (CNC) into regenerated cellulose films, this research aims to develop sustainable food packaging materials that meet these industry requirements while maintaining biodegradability.

1.2. Rationale and objectives of the proposed research

The hypotheses of this project are that (1) RC films obtained from different solvents would have different structures and properties; (2) NaOH/urea aqueous solution would be effective to prepare RC films from different wood pulps and drying conditions would affect the properties of RC films; (3) modification of CNC and organosilane would improve water resistance and tensile strength of RC films, achieving better food preservation while maintaining the biodegradability, and (4) different surface charges would affect the mechano-bactericidal effect of CNC. The overall objective of this study is to develop wood cellulose-based sustainable food packaging.

The specific objectives of this research are:

1. To compare the structures and properties of RC films obtained from concentrated H_2SO_4 and NaOH/urea aqueous solutions (Chapter 3).

2. To investigate the structure and properties of RC films regenerated from various wood pulps in NaOH/urea aqueous solvent with air drying and hot-pressing treatment (Chapter 4).

3. To determine the structure, properties, and compostability of RC films after the modification of CNC and organosilanes (Chapter 5).

4. To determine the influence of differently charged CNC on the properties and mechano-bactericidal activities of nanostructured RC films (Chapter 6).

1.3. Organization of the thesis

This dissertation comprises seven chapters: Chapter 1 serves as the general introduction, offering an overview of the research background, rationale, and objectives. Chapter 2 conducts a thorough literature review, encompassing the relevant subject matters involved in this research. Chapters 3-6 each present individual full manuscript, delineating the methodology and research findings comprehensively. The connecting texts between these manuscripts facilitate a seamless transition, demonstrating the logical progression from one chapter to the next. Chapter 7, the conclusion and summary, articulates the fulfilment of research objectives, discusses the implications of findings, and provides recommendations for future research.

Chapter 2. Recent Applications of Regenerated Cellulose Films and Hydrogels in Food Packaging

2.1. Abstract

Nowadays, non-degradable plastic packaging materials have created significant disposal and pollution issues threatening human health and development. The utilization of biodegradable packaging materials can help address the issue. Cellulose is abundant and renewable, and cellulose-based materials have been regarded as an alternative to petroleum-based plastic food packaging. With the development of cellulose solvents, various regenerated cellulose films and hydrogels have been fabricated for different applications. In this review, we summarize the recent progress in the preparation of regenerated cellulose films and hydrogels, and highlight their potential applications as biodegradable packaging, active packaging, and intelligent packaging. Finally, the biodegradability and safety of cellulose-based materials are stated, and future opportunities and challenges in this active research area are described.

2.2. Introduction

Food packaging waste comprises approximately one-third of all Canadian household waste, and only 20% is recovered for reuse and recycling. Among them, synthetic plastics suffer from poor biodegradability and limited ways to reuse and recycle, and thus cause serious environmental issues. Food packaging developed from natural polymers provides an alternative solution and has attracted more and more attention. Cellulose is the most abundant renewable and biodegradable polymer on earth, and has several advantages such as inexpensiveness, low density, non-toxicity, versatility, and superb mechanical properties [1]. Cellulose-based food-packaging materials, for example paper and cloth, have been widely utilized. However, with the requirements of improved protection of food products, the exploration of novel food packaging with multiple functional properties is urgent. The development of various cellulose solvents enabled the processing of cellulose into different

forms of materials. Especially, after dissolution, regenerated cellulose (RC) films and hydrogels can be fabricated by modulating physical and chemical interactions. They possess three-dimensional porous structures, which allow the incorporation of functional fillers and are thus applied as active or intelligent packaging materials [2,3,4,5,6•,7,8]. According to the Web of Science search result, 10,254 research papers on cellulose-based materials have been published in the last two years, and 404 (3.94%) of them are related to food packaging applications. The utilization of cellulose-based materials in food packaging is promising and still has a huge potential. Several reviews have summarized different forms of cellulose-based materials such as cellulose films [9], fibers [10], hydrogels [11•], microspheres [12], and composites [1], without the focus on food packaging purpose. Therefore, in this review, we have summarized recent strategies for fabricating RC-based films and hydrogels and their potential applications in food packaging. The considerations of biodegradability and toxicity are highlighted, and future opportunities, challenges, and research directions are described.

2.3. Recent studies on RC film and hydrogel production

Extensive studies have discussed various cellulose solvents including *N*-methylmorpholine-*N*-oxide (NMMO), LiCl/DMAc, ionic liquids (ILs), and alkali/urea solutions to develop a more efficient and environmentally friendly method for cellulose dissolution and regeneration. The NMMO process can be used to dissolve up to 35 wt% cellulose, but the resultant solution is unstable; LiCl/DMAc solvent allows the dissolution of cellulose at room temperature but requires an activation step as a pretreatment; ILs have good thermal stability but may have side reactions during dissolution; and the alkali/urea solvent is easy to prepare but cannot be applied to dissolve cellulose with high molecular weight [13•]. Therefore, the selection of cellulose solvent is mainly depended on the types of cellulose raw materials and additives, availability of facility, and cost. Figure 2.1 demonstrates the common steps in the preparation of RC films

and hydrogels, and Figures 2.2 (a)-(d) illustrate the appearance of RC films produced from different raw materials and solvents. Recent research mainly focused on optimizing dissolution conditions and strategies of non-solvent regeneration that influence morphological and mechanical properties of RC films [14]. For instance, cellulose source [15], wood type (hard or soft) [16], pulping process (acid sulfite or kraft sulfate) [16], and coagulants [17] used to regenerate cellulose were compared to investigate their effects on the morphology of cellulose films. Besides, O_2 plasma irradiation was proposed as a novel cellulose pretreatment method to activate cellulose chains and eliminate glycosidic bonds, improving the dissolution of cellulose and mechanical properties of RC films [18]. The effect of dissolution temperature was highlighted by Wei et al. that in the range of -2 to -12.5 °C, a decrease in temperature resulted in more cellulose dissolution in NaOH/urea solution [19]. The RC film prepared at -10 °C was optimal due to its best mechanical properties, transparency, and thermostability.

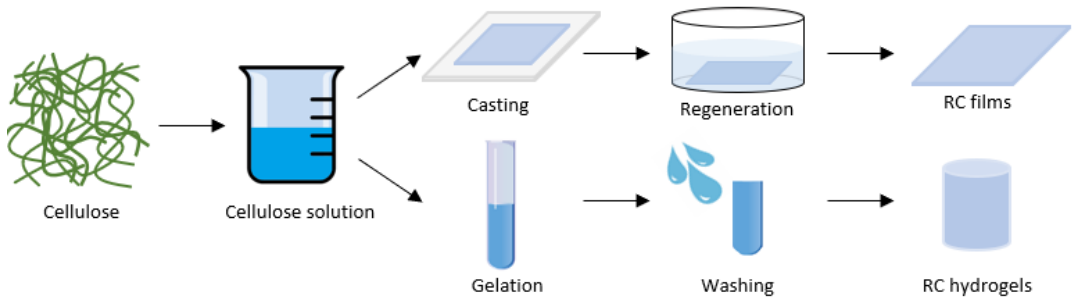

Figure 2.1. Preparation of RC films and hydrogels.

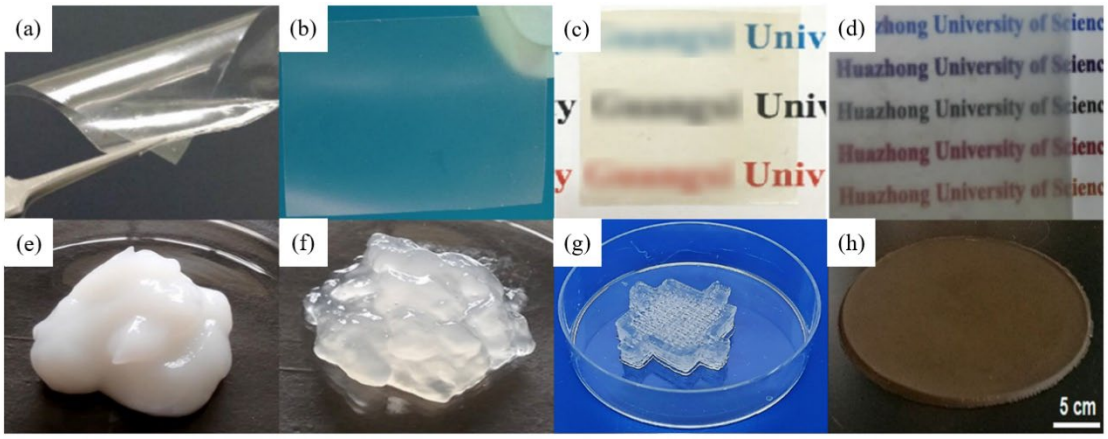

Figure 2.2. Photos of RC films (top) and hydrogels (bottom) prepared from (a) microcrystalline cellulose in LiCl/DMAc [26], (b) microcrystalline cellulose in NaOH/urea solution [27] Copyright 2020 Elsevier, (c) waste corrugated cardboard in AmimCl [28] Copyright 2020 American Chemical Society, (d) microcrystalline cellulose in BmimCl [29] Copyright 2020 Elsevier, (e) bagasse cellulose filaments (BCF) [6•] Copyright 2020 Elsevier, (f) oxidized BCF [6•] Copyright 2020 Elsevier, (g) oxidized birch fibers [30] Copyright 2021 Elsevier, and (h) cellulose from cotton fibers with amino-terminated hyperbranched polyamic anchored nanosilver [31] Copyright 2019 American Chemical Society.

The production of cellulose hydrogels is usually achieved by chemical or physical crosslinking [11•]. A new strategy namely double-crosslinking has been applied recently to obtain the hydrogels with dimensionally stable and recoverable double network structures [20,21]. For example, nanocellulose was crosslinked with epichlorohydrin (ECH) and metal salts ($FeCl_3$ or $CaCl_2$) to produce double-crosslinked hydrogels [22]. A three-dimensional network was formed due to the interconnected nanofibrils with no aggregation in crosslinked domains. A deformable cellulose hydrogel (126% of tensile strain) was formed via free radical polymerization of synthesized allyl cellulose with transparency of 89% at 550 nm and ionic

conductivity of 0.16 mS/cm [23]. This hydrogel was further immersed in saturated NaCl solution to initiate a double crosslinked network, which thus had an improved tensile strain (236%) and was still stretchable at -24 °C, due to the incorporation of physical crosslinking maintained the hydrogel integrity [24•]. A similar cellulose hydrogel with tensile strength of 3.1 MPa, transparency of 90% at 550 nm, and anti-freezing capacity was also reported, where ECH was used to crosslink cellulose dissolved in benzyltrimethyl ammonium hydroxide solution [25].

2.4. Potential applications of RC films in food packaging

Cellophane is the commercial transparent film regenerated from a viscose solution; however, carbon disulfide and other by-products of the viscose process cause serious environmental pollution [32]. Currently, RC films are prepared from eco-friendly solvent systems, and usually form composites with other polymers or additives to improve mechanical properties, optical properties, barrier properties, and thermostability. As shown in Figure 2.3, the applications of RC films in food packaging can be mainly classified into three aspects: biodegradable packaging, active packaging, and intelligent packaging. It was reported that commercial cellophane films have the tensile strength of about 18 MPa, initial degradation temperature of 150 °C, transparency of 91% at 800 nm, and incomplete degradation (94%) in the soil after 4 weeks [33•]. A pure cellulose film regenerated from durian rind waste was regarded as the alternative to cellophane [33•]. It had the smooth surface, transparency of 86%, tensile strength of 44 MPa, initial degradation temperature of 345 °C, and biodegradability (100% decomposed in 4 weeks). The cellulose film prepared from pulverized pineapple leaf fibers dissolved in IL showed comparable tensile strength and thermal stability, and the pineapple sample packaged by the RC film showed the decreased weight loss and well-maintained firmness and vitamin C content after 2 days [34•]. Another similar cellulose film regenerated from banana pseudo-stem

dissolved in IL also demonstrated the capacity to extend the storage life and commodity rate of mango to about 7 days [35]. The incorporation of nanoparticles (nanocellulose, metallic nanoparticles, etc.) and polymers (chitosan, xanthan gum, etc.) is the traditional way to reinforce the mechanical and barrier properties of RC films [36,37•,38]. A recent study recommended that the addition of Ca^{2+} in cellulose/ionic liquid solution promoted the interaction between cellulose chains and significantly improved the tensile strength (28.65 MPa to 85.86 MPa) and decomposition temperature (313 °C to 351 °C) of RC films; however, the transparency was reduced from ~64% to ~22% at 700 nm [28]. The modulation of polymer network structure is another way to enhance the performance. Ye et al. revealed that the well-ordered arrangement of polymers at nanoscale and macroscale enhanced the formation of highly anisotropic cellulose nanofibers, resulting in the improvement of mechanical and optical properties [39]. A double crosslinking method was used to control the aggregation of cellulose chains in cotton linter pulp (α-cellulose content >95%), yielding cellulose films with nanofibrous structures, tensile strength of 253.2 MPa), and transparency of 91% at 800 nm. Wang et al. dissolved the same feedstock in benzyltrimethyl ammonium hydroxide solvent followed by a simple water evaporation strategy to obtain RC films [40]. The fabricated film had a dense network, tensile strength of 158 MPa, light transmittance of 89.94% at 550 nm, and O_2 permeability of 1.37×10^{-17} cm^3 cm cm^{-2} s^{-1} Pa^{-1} in a 40% humidity environment [40]. At the same time, some research works focused on the improvement of low elasticity and high UV transparency of RC films [41], which may lead to ruptured packaging and deteriorated food. Bacterial cellulose (BC), which is free of lignin and hemicellulose, was used to fabricate RC films without any purification. The elongation, water vapor permeability, and visual appearance of BC films were improved by the addition of glycerol and polyvinyl alcohol (PVA), where glycerol showed a significant plasticizing effect and PVA filled the voids of films and

decreased porosity. Besides, the incorporation of 2 wt% of graphene oxide (GO) with abundant conjugated aromatic structures endowed cellulose films with reduced visible light transmittance (78%) and UVA (66.7%) and UVB (54.2%) shielding property [42]. The enhanced UV shielding capacity and hydrophobicity of cellulose films were also observed after the addition of CeO_2 [43]. Typical properties and potential applications of recently reported cellulose films are summarized in Table 2.1.

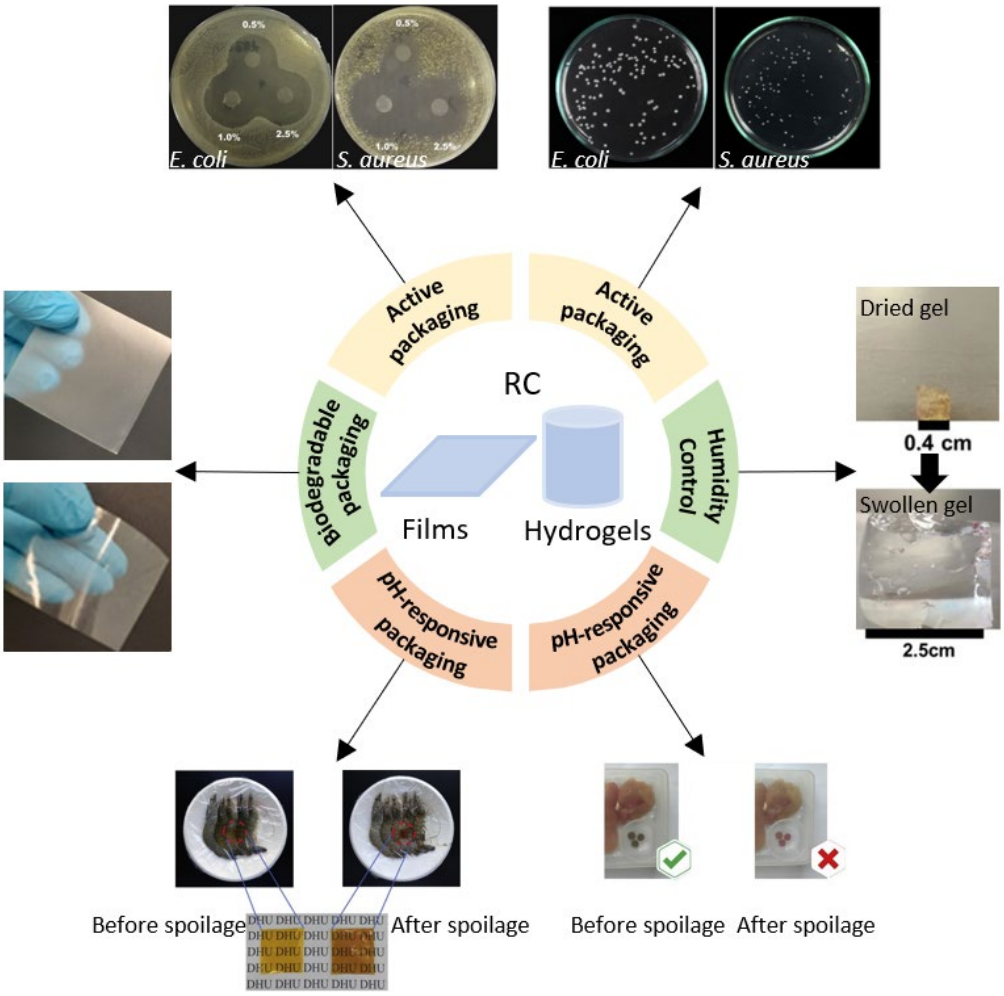

Figure 2.3. Potential applications of RC films and hydrogels in food packaging [6,38,44-47]. Copyright 2019 Elsevier; 2020 Elsevier; 2021 Elsevier; 2019 American Chemical Society; 2021 American Chemical Society.

Table 2.1. Typical properties and potential applications of recently reported RC films and hydrogels.

Types	Compositions	Tensile strength (MPa)	WVP (10^{-9} g/m·s·Pa)	Initial degradation temperature (°C)	Applications	References
Films	Durian rind C	44	/	270	"Green" and low-cost packaging	[33•]
	Pineapple leaf C	34	/	/	Pineapple packaging and preservation	[34•]
	Banana pseudo stem C	77	/	/	Mange packaging and preservation	[35]
	Waste cardboards C	85.86	/	/	Thermostable packaging	[28]
	Cotton linter pulps C	106	/	300	Super tough and clear packaging	[39]
	Cotton linter pulps C-Ag	158.2	/	290	Transparent packaging	[40]
	BC-Glycerol-PVA	13.78	0.20	/	Transparent packaging	[41]
	C-GO	78.5	/	/	UV shielding packaging	[42]
	Cotton linter pulps C-CeO_2	/	/	230	UV shielding packaging	[43]
	CMC-Cur-ZnO	41.8	1.67	210	Antioxidant and antimicrobial packaging	[2]
	BC-ZnO	92.4	/	337	Highly flexible packaging	[48]
	RC-ZnO	126.61	5.42	270	Antimicrobial packaging	[49]
	MCC-GSE	41.87	2.49	170.3	"Green" and low-cost packaging	[50]
	CNC-Gelatin	20	0.03	200	Biodegradable packaging	[51]
	BC-Gelatin-MgO	0.71	0.03	/	Egg packaging and preservation	[52]
	CNC-Gelatin-PVA	13.8	0.46	250	Biodegradable packaging	[53]
	Reactive CNF	47	3.40	260	Hydrophobic packaging	[54]
	CNF-ZnO-GSE	140	0.51	221	Antioxidant and antimicrobial packaging	[55]
	MC-CNF-SPA	46.6	0.02	230	Intelligent packaging	[56]
	FP-SCNF-FP	287	/	/	Low oxygen-permeable packaging	[57]
	OEO-Tween 80-CNF	24.63	/	/	Antimicrobial packaging	[58]
	OC-Nisin peptide	99.2	0.004	/	Antimicrobial packaging	[59]
	CMC-Starch	32.6	3.27	234	Transparent packaging	[60]
	Gellan gum-HEC-Lignin	39	2.18	148.2	Antioxidant packaging	[61]
	Cotton fabrics C-PVA-Dye	35	/	200	Intelligent packaging	[46•]
	C-Chitosan-Anthocyanins	/	/	/	Intelligent packaging	[62]
	C-Chitosan-Alizarin	/	/	/	Intelligent packaging	[63]
	Cotton fibers C-Ag	79	0.27	/	Active packaging	[31]
	CMC-Ag	58	4.78	/	Active packaging	[37•]
Hydrogels	CMC-ECH	/	/	/	Water absorbing packaging	[45]
	C-MBA	/	/	/	Water absorbing packaging	[64]
	BC-GG-PVP-CMC (film)	25.9	0.06	/	Blueberries packaging	[65]
	BC-PVP-CMC	/	/	/	Fruit packaging	[66]

Table 2.1. Continue.

Types	Compositions	Tensile strength (MPa)	WVP (10^{-9} g/m·s·Pa)	Initial degradation temperature (°C)	Applications	References
	C-Chitosan	/	/	/	Water absorbing packaging	[67]
	C-ECH	/	/	/	Good compressive packaging	[68]
	CMC-Fe^{3+}-PAAm	1.82	/	/	Highly stretchable packaging	[69]
	C-ECH-PEGDE	1.7	/	/	Highly stretchable packaging	[70]
	BC-Alginate-Cu ions	/	/	/	Active packaging	[71]
	BC-Cur-Cyclodextrins	/	/	220	Active packaging	[72]
	BC-Cur-Cyclodextrins-Ag	/	/	/	Active packaging	[73]
	NaCMC-HPMC-CA-GSE (film)	2.21	/	200	Active packaging	[74]
	CNC-Alginate-Ag	/	/	/	Active packaging	[75]
	BC-ECH-PEI	/	/	240	Active packaging	[76]
	DAC-QE-ZnO	/	/	/	Active packaging	[77•]
	C-ECH-ZnO	/	/	/	Active packaging	[78]
	ARC-PVA-Borax	0.04	/	250	Intelligent packaging	[79]
	TOBCF-Zn^{2+}	0.28	/	/	Intelligent packaging	[6•]
	CNC-Collagen	0.90	/	/	Biodegradable packaging	[80]
	C-PAAm	0.63	/	150	Highly flexible packaging	[81]
	CNF-$NaIO_4$-PVA	0.43	/	310.9	Thermostable packaging	[82]

Note: WVP, water vapor permeability; C, cellulose; BC, bacterial cellulose; PVA, polyvinyl alcohol; GO, graphene oxide; CMC, carboxymethyl cellulose; Cur, curcumin; RC, regenerated cellulose; GS, *Lemang* bamboo; MCC, microcrystalline cellulose; CNC, cellulose nanocrystals; CNF, cellulose nanofibrils; GSE, grape seed extracts; MC, methyl cellulose; SPA, saffron petal anthocyanin; FP, fluoropolymer; SCNF, succinylated cellulose nanofibers; OEO, oregano essential oil; OC, 2,3-dialdehyde cellulose; HEC, hydroxyethyl cellulose; ECH, epichlorohydrin; MBA, N,N'-methylene-bis-acrylamide; GG, guar gum; PVP, polyvinyl pyrrolidone; PAAm, polyacrylamide; PEGDE, poly(ethylene glycol) diglycidyl ether; NaCMC, sodium carboxymethylcellulose; HPMC, hydroxypropyl methylcellulose; CA, citric acid; PEI, polyethyleneimine; DAC, dialdehyde cellulose; QE, quercetin; ARC, acidochromic regenerated cellulose; TOBCF, TEMPO-oxidized bagasse cellulose filaments.

Active food packaging is one of many possible applications of RC films, in which antimicrobial agents could be incorporated to inhibit the growth of foodborne bacteria [37•,83,84,85]. A comparative study indicated that the CMC films incorporated with Ag, ZnO, and CuO nanoparticles (NPs) inhibited the growth of *E. coli* and *S. aureus* through the release of reactive oxygen species, where Ag NPs showed the best inhibition capacity [37•]. Gu et al. demonstrated that hyperbranched polyamide-amine could be used as a binder to ember Ag NPs and further control the release rate [31]. The films produced from cotton fibers exhibited a microbial inhibition capacity and maintained the freshness of cherry tomatoes for 9 days [31]. In recent years, an important trend in active packaging is the replacement of synthetic additives with natural antimicrobials such as essential oils and extracts [86]. For instance, poacic acid as a plant-based antimicrobial agent was added in cellulose film to suppress the growth of *S. aureus* [84], while oregano essential oil in the film showed an inhibition rate of 99.99% against *E. coli* and *L. monocytogenes* [58].

Intelligent cellulose-based films were also designed and employed to monitor the quality and condition of packaged food. Ding et al. [46•] used cotton fabrics to construct a pH-responsive RC film with PVA and acidochromic dye, which showed the pH-responsive color change within pH 7-12, tensile strength of 35 MPa, initial degradation temperature of about 150 °C, and leakage resistance in acidic and basic environments. The prepared intelligent film could be used to detect ammonia formation and indicate the freshness of shrimps [46•]. The methyl cellulose-based film loaded with saffron petal anthocyanin was reported with a wide pH-response range from 1 to 14, and successfully applied to indicate the freshness of lamb meat [56]. The anthocyanins-embedded cellulose/chitosan film had the pH response ranged from 2 to 12 and color stability for one month [62], while the similar cellulose/chitosan film embedded with alizarin was applied to monitor the spoilage of minced beef [63]. The pH value of minced

beef elevated from 6.2 to 6.76 after storage at 4 °C for 4 days, and the color of the film changed correspondingly from brown to purple, revealing the high microbial load (>7 log CFU/g) beyond the acceptable limit [63].

2.5. Potential applications of RC hydrogels in food packaging

Recent studies on RC hydrogels are summarized in Table 2.1. Compared to RC films, the applications of hydrogels in food packaging are relatively less. Cellulose hydrogels can be regarded as an attractive absorbent material with superhydrophilicity, good structural stability after water absorption, and negligible influence on the sensory attribute of food [45,87•], and be applied in food packaging to control the humidity and water activity of food. CMC, due to its good water holding capacity, was used to crosslink with ECH to form a superabsorbent cellulose hydrogel, which had the water retention capacity of 725 g water/g dry hydrogel [45]. Yang et al. provided a novel method to fabricate cellulose hydrogels by crosslinking with methylenebis acrylamide (MBA) in LiOH/urea solvents [64]. The interactions among water and ─OH and ─NH─ groups from polymer network endowed hydrogels with a water absorption capacity of 220 g water/g dry hydrogel. The composite hydrogel of CMC and PVP at a ratio of 1:1 could absorb 1134% water, and delayed the deterioration of blueberries for 15 days, while the addition of guar gum slightly decreased the water absorption capacity to 895% [65]. A similar CMC-PVP-BC-based hydrogel was applied to package table grapes, spinach, and tomatoes at room temperature for 30 days [66]. Alam and Cristopher noted that the water-absorption property of cellulose hydrogels was relevant to the concentration and chemical nature of polymers, and the optimal water absorption capacity (610 g water/g dry hydrogel) was found when cellulose hydrogels were crosslinked with 25% of chitosan [67]. However, one common limitation of hydrogel is inferior mechanical resistance, which can be improved by incorporating crosslinkers or forming composites. Huber et al. [68] increased the content of

undissolved micro-cellulose as a physical crosslinker (0-50 wt%) to improve the compressive strength of hydrogels from ~130 kPa to ~160 kPa, which reached to 300 kPa by further adding 10 wt% of ECH as a chemical crosslinker. The reinforcement of mechanical properties of CMC hydrogels via the incorporation of Fe^{3+} was also elucidated, and the increase of Fe^{3+} content at low iron ion concentration levels formed more tridentate coordinates with the carboxyl groups of CMC hydrogels [69]. However, the iron ions at high concentrations transformed tridentate into monodentate or bidentate, which deteriorated the toughness of hydrogels. Ye et al. constructed a double crosslinked cellulose hydrogel by using two cross-linking agents, ECH and polyethylene glycol diglycidyl ether, which exhibited the improved compressive strength (9.4 MPa) and tensile strength (1.7 MPa), and were 26.3 and 84 times higher than those of the single crosslinked hydrogel, respectively [70].

Like RC films, cellulose hydrogels were also employed as a three-dimensional matrix to fabricate antimicrobial or pH-responsive packaging by incorporating functional fillers. Compared to the dense structure of films, the porous network of cellulose hydrogels facilitates the transportation of bioactive compounds and enables quickly starting signaling pathways. The antimicrobial capacity was determined by the network density and concentration of active compounds [71]. Curcumin, a natural antioxidant and anti-inflammatory agent, was loaded in a BC hydrogel with a release rate of 76.99% in 6 h and significantly inhibited the growth of *S. aureus* [72]. The bactericidal effect was also found in the grapefruit seed extract-loaded cellulose hydrogel due to the existence of choline and ethanolamine [72]. Ag NPs were widely used to inhibit the growth of gram-negative bacteria (*P. aeruginosa*), gram-positive bacteria (*S. aureus*), and yeast (*C. albicans*) [73,75]. A novel strategy was proposed to produce hydrogels by using ECH to chemically crosslink BC and polyethyleneimine (PEI) in NaOH/urea solution [76]. The disruption of cell membranes by the polycationic nature of PEI caused a bactericidal

activity against *S. aureus* and *E. coli*. The synergistic effect of several antimicrobial compounds in cellulose hydrogels has also been studied. For example, chitosan was crosslinked with dialdehyde cellulose to form a hydrogel, which was embedded with ZnO NPs and two bioactive compounds (quercetin and onion peel drug) to inhibit the growth of *S. aureus* and *T. rubrum* [77•]. A similar effect was found in the RC hydrogel prepared from waste sugarcane bagasse with cellulose content of about 50% and filled with curcumin and ZnO NPs [78]. For the construction of intelligent packaging materials, two pH-responsive dyes (bromothymol blue and methyl red) were incorporated in a nanocellulose-based hydrogel as a food quality indicator to monitor the freshness of chicken breast [6•]. The hydrogels showed a noticeable color change from green to red after three days due to the emission of CO_2 from microbial growth, indicating the detected microbial loads exceeded the acceptable limit for consumption (>6 log CFU/g). A tough, self-healing, and pH-responsive hydrogel was produced from acidochromic cotton cellulose (ARC), PVA, and borax, which could recover to the original state within 15 s without any external force and display a color change from yellow to red and purple when pH value increased from 5 to 12 [79]. Besides, the addition of 0.6% ARC induced the entanglement of PVA and ARC, and thus increased the crosslink density of the hydrogel network, reinforcing the tensile strength from 5.2 kPa to 35.3 kPa [79]. However, it was noticed that the current applications of RC films and hydrogels as intelligent packaging mainly focused on pH-induced color change. More strategies could be considered when designing RC based intelligent materials for wider food-related applications.

2.6. Biodegradability and toxicity of cellulose-based materials

The biodegradability of cellulose may be affected by chemical modifications. Leppänen et al. reported that the biodegradation rate of RC depended on the degree of substitution (DS) [88]. RC from ionic liquid was completely degraded after 4 weeks in a natural composting

environment, while cellulose acetate with DS 2.5 prevented the attachment of enzymes and showed no biodegradability in enzymatic hydrolysis and natural composting environment [88]. However, cellulose acetate with DS lower than 1.8 can be degraded by esterase and enhanced by the synergistic effect of cellulase [89]. Cellulose nanocrystals are usually combined with RC to prepare all-cellulose materials; however, the incorporation of micro- and nanocellulose could hamper the water diffusion in the polymer matrix and affect the disintegration kinetics, leading to a decreased biodegradability [90-92]. Cui et al. demonstrated that okara cellulose hydrogels crosslinked by ECH could completely decompose in 28 days [93]. The presence of microorganisms in soil initiated the cleavage of crosslinkages and disrupted covalent bonds, resulting in the decomposed network structure of hydrogels [94]. Therefore, physical crosslinking and mild chemical modification of cellulose-based materials are preferred if the biodegradability/composability is a necessity. Regarding the safety and toxicity of cellulose-based materials, various forms of cellulose including raw cellulose and RC, as well as its derivatives such as CMC, cellulose acetate, ethyl cellulose, etc., have been regarded as safe food substances according to the U.S. Department of Agriculture and considered as the food additives by the FDA regulations. Nevertheless, the release and migration of functional additives from RC matrices should be carefully investigated. For instance, a shrimp lethal assay indicated that the minor amount of Ag NPs released from cellulose-based nanocomposite had no obvious toxicity to shrimp after an exposure of 24 h [95], but Ag NPs with high concentration (≥500 μg/mL) showed the significant cytotoxicity to Caco-2 and FHC human colon cells [96], and 100 ppm of Ag NPs remarkably decreased the vitality of hepatocellular carcinoma cells close to zero over 24 h [75]. It is generally considered that naturally available bioactive compounds are low-risk alternatives to metal particles in active packaging. However, it ignores the potential toxicity of bioactive compounds at high doses. For instance, β-

phellandrene (1425 and 2850 mg/kg) and 6-gingerol (20-80 μM) from ginger extract had genetic toxicity to human body [97], and hepatotoxicity effect was found with 140 mg - 1000 mg/day consumption of tea extract [98]. Therefore, the researchers should be cautious when designing functional packaging, no matter the additives are natural or manufactured. The dosage of bioactive additives released from packaging materials is one of the major factors to evaluate the safety issues.

2.7. Conclusions and outlook

Recent research focuses on optimizing dissolution conditions and developing new strategies to improve the properties of RC films and hydrogels, for example, the double-crosslinking method. Both cellulose films and hydrogels exhibit the potential to be applied in food packaging. Particularly, the RC films provide a solution for biodegradable wrapping materials, and the RC hydrogels can serve as a three-dimensional matrix for absorption and quick signal response. Various organic and inorganic fillers can be incorporated in RC films and hydrogels to enable special functionalities, such as antimicrobial property and pH-responsive color change. Generally speaking, RC materials are safe to be used for food packaging, but the release and migration of functional fillers should be evaluated. Future research in the following areas is required to promote their real applications:

1. The design of food packaging materials should be linked to a specific food product. Many research works generally focused on the improvement in mechanical and barrier properties of packaging materials, but did not mention the requirements for any food products. Therefore, for the development of novel packaging materials, various aspects such as initial status, storage condition, and quality change of food product should be understood in

advance, and the properties should be evaluated to see if they reach the targeted values rather than simply stating “good” or “improved”.

2. The feasibility of new packaging materials should be considered. Processes should be available for mass production, and all the modifications and additives should be economically practical. The selection of a cost-effective cellulose solvent system and the efficient recycling of solvent will help reduce the cost of RC materials.

3. The release and migration of functional fillers from RC packaging at different conditions (pH, temperature, solvent, food components, etc.) should be carefully studied. Suitable functional fillers and immobilization methods (e.g. stable during food processing and when contacting with food products) should be selected with the consideration of application of packaging materials. Generally speaking, chemically bonded active compounds are more stable compared to physically linked ones, but the fate of these chemicals in the environment after the materials are disposed and their effects on biodegradability should also be evaluated.

4. The utilization of artificial intelligence in the design of functional food packaging materials may be a future trend. Based on the structure of polymers and additives and preliminary experiment, the properties of targeted materials such as mechanical strength, flexibility, permeability, thermal stability, and biodegradability can be predicted, so as to facilitate the development of novel packaging materials and link them with specific food products.

2.8. References

Papers of particular interest, published within the period of review, have been highlighted as:

• of special interest

[1] Sharma A, Thakur M, Bhattacharya M, Mandal T, Goswami S: **Commercial application**

of cellulose nano-composites–A review. *Biotechnology Reports* 2019, **21**:e00316.

[2] Roy S, Rhim J-W: **Carboxymethyl cellulose-based antioxidant and antimicrobial active packaging film incorporated with curcumin and zinc oxide**. *International Journal of Biological Macromolecules* 2020, **148**:666-676.

[3] Xu Y, Liu X, Jiang Q, Yu D, Xu Y, Wang B, Xia W: **Development and properties of bacterial cellulose, curcumin, and chitosan composite biodegradable films for active packaging materials**. *Carbohydrate Polymers* 2021, **260**:117778.

[4] Salama HE, Aziz MSA: **Optimized carboxymethyl cellulose and guanidinylated chitosan enriched with titanium oxide nanoparticles of improved UV-barrier properties for the active packaging of green bell pepper**. *International Journal of Biological Macromolecules* 2020, **165**:1187-1197.

[5] Shaghaleh H, Hamoud YA, Xu X, Liu H, Wang S, Sheteiwy M, Dong F, Guo L, Qian Y, Li P: **Thermo-/pH-responsive preservative delivery based on TEMPO cellulose nanofiber/cationic copolymer hydrogel film in fruit packaging**. *International Journal of Biological Macromolecules* 2021, **183**:1911-1924.

[6] • Lu P, Yang Y, Liu R, Liu X, Ma J, Wu M, Wang S: **Preparation of sugarcane bagasse nanocellulose hydrogel as a colourimetric freshness indicator for intelligent food packaging**. *Carbohydrate Polymers* 2020, **249**:116831.

This cellulose hydrogel was produced from waste sugarcane bagasse and loaded with two natural dyes to indicate the quality of food, which had a wide pH response range. This low-cost and biodegradable hydrogel could be the future trend of food packaging materials.

[7] Sutthasupa S, Padungkit C, Suriyong S: **Colorimetric ammonia (NH_3) sensor based on an alginate-methylcellulose blend hydrogel and the potential opportunity for the**

development of a minced pork spoilage indicator. *Food Chemistry* 2021, **362**:130151.

[8] Ardila-Diaz LD, Oliveira TVd, Soares NdF: **Development and evaluation of the chromatic behavior of an intelligent packaging material based on cellulose acetate incorporated with polydiacetylene for an efficient packaging**. *Biosensors* 2020, **10**:59.

[9] Cazón P, Vázquez M: **Improving bacterial cellulose films by ex-situ and in-situ modifications: A review**. *Food Hydrocolloids* 2020:106514.

[10] Iglesias MC, Gomez-Maldonado D, Via BK, Jiang Z, Peresin MS: **Pulping processes and their effects on cellulose fibers and nanofibrillated cellulose properties: A review**. *Forest Products Journal* 2020, **70**:10-21.

[11] • Zainal SH, h Mohd NH, Suhaili N, Anuar FH, Lazim AM, Othaman R: **Preparation of cellulose-based hydrogel: A review**. *Journal of Materials Research and Technology* 2020.

This paper reviewed the recent advances in the preparation of cellulose-based hydrogels and discussed the relationship between the dissolution methods and properties of hydrogels. Besides, various crosslinkers for the formation of hydrogels were compared.

[12] Wei S, Ching YC, Chuah CH: **Preparation of aerogel beads and microspheres based on chitosan and cellulose for drug delivery: A review**. *International Journal of Biological Macromolecules* 2021.

[13] • Sayyed AJ, Deshmukh NA, Pinjari DV: **A critical review of manufacturing processes used in regenerated cellulosic fibres: Viscose, cellulose acetate, cuprammonium, LiCl/DMAc, ionic liquids, and NMMO based lyocell**. *Cellulose* 2019, **26**:2913-2940.

In this paper, a systematic review of six cellulose dissolution techniques and related

mechanisms and factors affecting the regeneration process was presented, which is beneficial for researchers to have a basic understanding of cellulose-based material preparation.

[14] Lindman B, Medronho B, Alves L, Costa C, Edlund H, Norgren M: **The relevance of structural features of cellulose and its interactions to dissolution, regeneration, gelation and plasticization phenomena**. *Physical Chemistry Chemical Physics* 2017, **19**:23704-23718.

[15] Ul-Islam M, Khan S, Ullah MW, Park JK: **Comparative study of plant and bacterial cellulose pellicles regenerated from dissolved states**. *International Journal of Biological Macromolecules* 2019, **137**:247-252.

[16] Sayyed AJ, Mohite LV, Deshmukh NA, Pinjari DV: **Structural characterization of cellulose pulp in aqueous NMMO solution under the process conditions of lyocell slurry**. *Carbohydrate Polymers* 2019, **206**:220-228.

[17] Ilyin SO, Makarova VV, Anokhina TS, Ignatenko VY, Brantseva TV, Volkov AV, Antonov SV: **Diffusion and phase separation at the morphology formation of cellulose membranes by regeneration from N-methylmorpholine N-oxide solutions**. *Cellulose* 2018, **25**:2515-2530.

[18] Lao TLB, Cordura SLA, Diaz LJL, Vasquez MR: **Influence of plasma treatment on the dissolution of cellulose in lithium chloride–dimethylacetamide**. *Cellulose* 2020, **27**:9801-9811.

[19] Wei Q-Y, Lin H, Yang B, Li L, Zhang L-Q, Huang H-D, Zhong G-J, Xu L, Li Z-M: **Structure and properties of all-cellulose composites prepared by controlling the dissolution temperature of a NaOH/urea solvent**. *Industrial & Engineering Chemistry Research* 2020, **59**:10428-10435.

[20] Li X, Wang H, Li D, Long S, Zhang G, Wu Z: **Dual ionically cross-linked double-network hydrogels with high strength, toughness, swelling resistance, and improved 3D printing Processability**. *ACS Applied Materials & Interfaces* 2018, **10**:31198-31207.

[21] Wu T, Yu S, Lin D, Wu Z, Xu J, Zhang J, Ding Z, Miao Y, Liu T, Chen T: **Preparation, characterization, and release behavior of doxorubicin hydrochloride from dual cross-linked chitosan/alginate hydrogel beads**. *ACS Applied Bio Materials* 2020, **3**:3057-3065.

[22] Xu H, Liu Y, Xie Y, Zhu E, Shi Z, Yang Q, Xiong C: **Doubly cross-linked nanocellulose hydrogels with excellent mechanical properties**. *Cellulose* 2019, **26**:8645-8654.

[23] Tong R, Chen G, Pan D, Qi H, Li Ra, Tian J, Lu F, He M: **Highly stretchable and compressible cellulose ionic hydrogels for flexible strain sensors**. *Biomacromolecules* 2019, **20**:2096-2104.

[24] • Tong R, Chen G, Pan D, Tian J, Qi H, Li Ra, Lu F, He M: **Ultrastretchable and antifreezing double-cross-linked cellulose ionic hydrogels with high strain sensitivity under a broad range of temperature**. *ACS Sustainable Chemistry & Engineering* 2019, **7**:14256-14265.

The authors introduced the enhanced structure and properties of cellulose hydrogels, which had good mechanical properties and were stretchable even in low-temperature environments.

[25] Wang Y, Zhang L, Lu A: **Transparent, antifreezing, ionic conductive cellulose hydrogel with stable sensitivity at subzero temperature**. *ACS Applied Materials & Interfaces* 2019, **11**:41710-41716.

[26] Sadeghifar H, Venditti RA, Pawlak JJ, Jur J: **Cellulose transparent and flexible films prepared from DMAc/LiCl solutions**. *BioResources* 2019, **14**:9021-9032.

[27] Cazón P, Vázquez M, Velázquez G: **Regenerated cellulose films with chitosan and polyvinyl alcohol: Effect of the moisture content on the barrier, mechanical and optical properties**. *Carbohydrate Polymers* 2020, **236**:116031.

[28] Xu H, Huang L, Xu M, Qi M, Yi T, Mo Q, Zhao H, Huang C, Wang S, Liu Y: **Preparation and properties of cellulose-based films regenerated from waste corrugated cardboards using [Amim] Cl/$CaCl_2$**. *ACS Omega* 2020, **5**:23743-23754.

[29] Qiao H, Li L, Wu J, Zhang Y, Liao Y, Zhou H, Li D: **High-strength cellulose films obtained by the combined action of shear force and surface selective dissolution**. *Carbohydrate Polymers* 2020, **233**:115883.

[30] Baniasadi H, Ajdary R, Trifol J, Rojas OJ, Seppälä J: **Direct ink writing of aloe vera/cellulose nanofibrils bio-hydrogels**. *Carbohydrate Polymers* 2021, **266**:118114.

[31] Gu R, Yun H, Chen L, Wang Q, Huang X: **Regenerated cellulose films with amino-terminated hyperbranched polyamic anchored nanosilver for active food packaging**. *ACS Applied Bio Materials* 2019, **3**:602-610.

[32] Fotie G, Limbo S, Piergiovanni L: **Manufacturing of food packaging based on nanocellulose: Current advances and challenges**. *Nanomaterials* 2020, **10**:1726.

[33] • Zhao G, Lyu X, Lee J, Cui X, Chen W-N: **Biodegradable and transparent cellulose film prepared eco-friendly from durian rind for packaging application**. *Food Packaging and Shelf Life* 2019, **21**:100345.

The authors provided an approach to fabricate cellulose films with good mechanical and optical properties from waste resources. The fast biodegradation process in the soil indicated its potential in biodegradable packaging.

[34] •Wei X, Zhang L, Wang J, Li J, Zhou W: **Preparation of cellulose film in ionic liquid**

by high shearing and application in pineapple preservation. *Materials Research Express* 2020, **7**:025313.

This is an interesting study that used pineapple leaves to extract cellulose, which was then used to preserve the fresh-cut pineapple. This research offered a promising process for producing, packaging, and marketing fruits with zero environmental pollution.

[35] Ai B, Zheng L, Li W, Zheng X, Yang Y, Xiao D, Shi J, Sheng Z: **Biodegradable cellulose film prepared from banana pseudo-stem using an ionic liquid for mango preservation**. *Frontiers in Plant Science* 2021, **12**:234.

[36] Shi J, Liu W, Jiang X, Liu W: **Preparation of cellulose nanocrystal from tobacco-stem and its application in ethyl cellulose film as a reinforcing agent**. *Cellulose* 2020, **27**:1393-1406.

[37] • Ebrahimi Y, Peighambardoust SJ, Peighambardoust SH, Karkaj SZ: **Development of antibacterial carboxymethyl cellulose-based nanobiocomposite films containing various metallic nanoparticles for food packaging applications**. *Journal of Food Science* 2019, **84**:2537-2548.

This paper focused on the antimicrobial properties of various commonly used metallic nanoparticles in cellulose-based hydrocolloids, which also included a comparison of the reinforcing effects in terms of mechanical properties, UV-barrier property, and water vapor permeability.

[38] Ju S, Zhang F, Duan J, Jiang J: **Characterization of bacterial cellulose composite films incorporated with bulk chitosan and chitosan nanoparticles: A comparative study**. *Carbohydrate Polymers* 2020, **237**:116167.

[39] Ye D, Lei X, Li T, Cheng Q, Chang C, Hu L, Zhang L: **Ultrahigh tough, super clear,**

and highly anisotropic nanofiber-structured regenerated cellulose films. *ACS Nano* 2019, **13**:4843-4853.

[40] Wang Y, Yuan L, Tian H, Zhang L, Lu A: **Strong, transparent cellulose film as gas barrier constructed via water evaporation induced dense packing**. *Journal of Membrane Science* 2019, **585**:99-108.

[41] Cazón P, Velazquez G, Vázquez M: **Characterization of mechanical and barrier properties of bacterial cellulose, glycerol and polyvinyl alcohol (PVOH) composite films with eco-friendly UV-protective properties**. *Food Hydrocolloids* 2020, **99**:105323.

[42] Zhang X-F, Song L, Wang Z, Wang Y, Wan L, Yao J: **Highly transparent graphene oxide/cellulose composite film bearing ultraviolet shielding property**. *International Journal of Biological Macromolecules* 2020, **145**:663-667.

[43] Wang W, Zhang B, Jiang S, Bai H, Zhang S: **Use of CeO_2 nanoparticles to enhance UV-shielding of transparent regenerated cellulose films**. *Polymers* 2019, **11**:458.

[44] Moradian M, Islam MS, van de Ven TG: **Insoluble regenerated cellulose films made from mildly carboxylated dissolving and kraft pulps**. *Industrial & Engineering Chemistry Research* 2021, **60**:5385-5393.

[45] Alam MN, Islam MS, Christopher LP: **Sustainable production of cellulose-based hydrogels with superb absorbing potential in physiological saline**. *ACS Omega* 2019, **4**:9419-9426.

[46] • Ding L, Li X, Hu L, Zhang Y, Jiang Y, Mao Z, Xu H, Wang B, Feng X, Sui X: **A naked-eye detection polyvinyl alcohol/cellulose-based pH sensor for intelligent packaging**. *Carbohydrate Polymers* 2020, **233**:115859.

In this paper, the acidochromic dye, 1-hydroxy-4-[4-(ethylsulfurate sulfonyl)-phenylazo]-

naphthalene, was incorporated to a cellulose-based film that had good mechanical properties, and was highly resistant to leaching under both acidic and alkaline conditions. This intelligent packaging material can indicate the freshness of shrimp for real-time monitoring.

[47] Song S, Liu Z, Abubaker MA, Ding L, Zhang J, Yang S, Fan Z: **Antibacterial polyvinyl alcohol/bacterial cellulose/nano-silver hydrogels that effectively promote wound healing**. *Materials Science and Engineering: C* 2021, **126**:112171.

[48] Abral H, Fajri N, Mahardika M, Handayani D, Sugiarti E, Kim H-J: **A simple strategy in enhancing moisture and thermal resistance and tensile properties of disintegrated bacterial cellulose nanopaper**. *Journal of Materials Research and Technology* 2020, **9**:8754-8765.

[49] Saedi S, Shokri M, Kim JT, Shin GH: **Semi-transparent regenerated cellulose/ZnONP nanocomposite film as a potential antimicrobial food packaging material**. *Journal of Food Engineering* 2021:110665.

[50] Hermawan D, Lai TK, Jafarzadeh S, Gopakumar DA, Hasan M, Owolabi FT, Aprilia NS, Rizal S, Khalil HA: **Development of seaweed-based bamboo microcrystalline cellulose films intended for sustainable food packaging applications**. *BioResources* 2019, **14**:3389-3410.

[51] Leite LS, Moreira FK, Mattoso LH, Bras J: **Electrostatic interactions regulate the physical properties of gelatin-cellulose nanocrystals nanocomposite films intended for biodegradable packaging**. *Food Hydrocolloids* 2021, **113**:106424.

[52] Wang Y, Luo W, Tu Y, Zhao Y: **Gelatin-based nanocomposite film with bacterial cellulose–MgO nanoparticles and its application in packaging of preserved eggs**. *Coatings* 2021, **11**:39.

[53] Oyeoka HC, Ewulonu CM, Nwuzor IC, Obele CM, Nwabanne JT: **Packaging and degradability properties of polyvinyl alcohol/gelatin nanocomposite films filled water hyacinth cellulose nanocrystals**. *Journal of Bioresources and Bioproducts* 2021.

[54] Li W, Wang S, Wang W, Qin C, Wu M: **Facile preparation of reactive hydrophobic cellulose nanofibril film for reducing water vapor permeability (WVP) in packaging applications**. *Cellulose* 2019, **26**:3271-3284.

[55] Roy S, Kim HC, Panicker PS, Rhim J-W, Kim J: **Cellulose nanofiber-based nanocomposite films reinforced with zinc oxide nanorods and grapefruit seed extract**. *Nanomaterials* 2021, **11**:877.

[56] Alizadeh-Sani M, Tavassoli M, McClements DJ, Hamishehkar H: **Multifunctional halochromic packaging materials: Saffron petal anthocyanin loaded-chitosan nanofiber/methyl cellulose matrices**. *Food Hydrocolloids* 2021, **111**:106237.

[57] Kim J-K, Choi B, Jin J: **Transparent, water-stable, cellulose nanofiber-based packaging film with a low oxygen permeability**. *Carbohydrate Polymers* 2020, **249**:116823.

[58] Chen S, Wu M, Lu P, Gao L, Yan S, Wang S: **Development of pH indicator and antimicrobial cellulose nanofibre packaging film based on purple sweet potato anthocyanin and oregano essential oil**. *International Journal of Biological Macromolecules* 2020, **149**:271-280.

[59] Wu Y, Li Q, Zhang X, Li Y, Li B, Liu S: **Cellulose-based peptidopolysaccharides as cationic antimicrobial package films**. *International Journal of Biological Macromolecules* 2019, **128**:673-680.

[60] Tavares KM, de Campos A, Luchesi BR, Resende AA, de Oliveira JE, Marconcini JM:

Effect of carboxymethyl cellulose concentration on mechanical and water vapor barrier properties of corn starch films. *Carbohydrate Polymers* 2020, **246**:116521.

[61] Rukmanikrishnan B, Ramalingam S, Rajasekharan SK, Lee J, Lee J: **Binary and ternary sustainable composites of gellan gum, hydroxyethyl cellulose and lignin for food packaging applications: Biocompatibility, antioxidant activity, UV and water barrier properties**. *International Journal of Biological Macromolecules* 2020, **153**:55-62.

[62] Tirtashi FE, Moradi M, Tajik H, Forough M, Ezati P, Kuswandi B: **Cellulose/chitosan pH-responsive indicator incorporated with carrot anthocyanins for intelligent food packaging**. *International Journal of Biological Macromolecules* 2019, **136**:920-926.

[63] Ezati P, Tajik H, Moradi M: **Fabrication and characterization of alizarin colorimetric indicator based on cellulose-chitosan to monitor the freshness of minced beef**. *Sensors and Actuators B: Chemical* 2019, **285**:519-528.

[64] Yang J, Medronho B, Lindman B, Norgren M: **Simple one pot preparation of chemical hydrogels from cellulose dissolved in cold LiOH/urea**. *Polymers* 2020, **12**:373.

[65] Bandyopadhyay S, Saha N, Brodnjak UV, Sáha P: **Bacterial cellulose and guar gum based modified PVP-CMC hydrogel films: Characterized for packaging fresh berries**. *Food Packaging and Shelf Life* 2019, **22**:100402.

[66] Saha N, Zaandra O, Bandyopadhyay S, Saha P: **Bacterial cellulose based hydrogel film for sustainable food packaging**. In *Advances in Sustainable Polymers*. Edited by: Springer; 2019:237-245.

[67] Alam MN, Christopher LP: **Natural cellulose-chitosan cross-linked superabsorbent hydrogels with superior swelling properties**. *ACS Sustainable Chemistry & Engineering* 2018, **6**:8736-8742.

[68] Huber T, Feast S, Dimartino S, Cen W, Fee C: **Analysis of the effect of processing conditions on physical properties of thermally set cellulose hydrogels**. *Materials* 2019, **12**:1066.

[69] Zhang H, Wu X, Qin Z, Sun X, Zhang H, Yu Q, Yao M, He S, Dong X, Yao F: **Dual physically cross-linked carboxymethyl cellulose-based hydrogel with high stretchability and toughness as sensitive strain sensors**. *Cellulose* 2020, **27**:9975-9989.

[70] Ye D, Chang C, Zhang L: **High-strength and tough cellulose hydrogels chemically dual cross-linked by using low-and high-molecular-weight cross-linkers**. *Biomacromolecules* 2019, **20**:1989-1995.

[71] Gutierrez E, Burdiles PA, Quero F, Palma P, Olate-Moya F, Palza H: **3D Printing of antimicrobial alginate/bacterial-cellulose composite hydrogels by incorporating copper nanostructures**. *ACS Biomaterials Science & Engineering* 2019, **5**:6290-6299.

[72] Gupta A, Keddie D, Kannappan V, Gibson H, Khalil I, Kowalczuk M, Martin C, Shuai X, Radecka I: **Production and characterisation of bacterial cellulose hydrogels loaded with curcumin encapsulated in cyclodextrins as wound dressings**. *European Polymer Journal* 2019, **118**:437-450.

[73] Gupta A, Briffa SM, Swingler S, Gibson H, Kannappan V, Adamus G, Kowalczuk M, Martin C, Radecka I: **Synthesis of silver nanoparticles using curcumin-cyclodextrins loaded into bacterial cellulose-based hydrogels for wound dressing applications**. *Biomacromolecules* 2020, **21**:1802-1811.

[74] Koneru A, Dharmalingam K, Anandalakshmi R: **Cellulose based nanocomposite hydrogel films consisting of sodium carboxymethylcellulose–grapefruit seed extract nanoparticles for potential wound healing applications**. *International Journal of*

Biological Macromolecules 2020, **148**:833-842.

[75] Bergonzi C, Remaggi G, Graiff C, Bergamonti L, Potenza M, Ossiprandi MC, Zanotti I, Bernini F, Bettini R, Elviri L: **Three-dimensional (3D) printed silver nanoparticles/alginate/nanocrystalline cellulose hydrogels: Study of the antimicrobial and cytotoxicity efficacy**. *Nanomaterials* 2020, **10**:844.

[76] Wahid F, Bai H, Wang F-P, Xie Y-Y, Zhang Y-W, Chu L-Q, Jia S-R, Zhong C: **Facile synthesis of bacterial cellulose and polyethyleneimine based hybrid hydrogels for antibacterial applications**. *Cellulose* 2020, **27**:369-383.

[77] • George D, Maheswari PU, Begum KMS: **Synergic formulation of onion peel quercetin loaded chitosan-cellulose hydrogel with green zinc oxide nanoparticles towards controlled release, biocompatibility, antimicrobial and anticancer activity**. *International Journal of Biological Macromolecules* 2019, **132**:784-794.

The synergistic effect of zinc oxide nanoparticles and bioactive compounds on the antimicrobial properties of cellulose hydrogel was revealed. The cell proliferation and anticancer effect of hydrogel indicated good biocompatibility and functionality.

[78] Anagha B, George D, Maheswari PU, Begum KMS: **Biomass derived antimicrobial hybrid cellulose hydrogel with green ZnO nanoparticles for curcumin delivery and its kinetic modelling**. *Journal of Polymers and the Environment* 2019, **27**:2054-2067.

[79] Ding L, Chen L, Hu L, Feng X, Mao Z, Xu H, Wang B, Sui X: **Self-healing and acidochromic polyvinyl alcohol hydrogel reinforced by regenerated cellulose**. *Carbohydrate Polymers* 2021, **255**:117331.

[80] Ghorbani M, Roshangar L: **Construction of collagen/nanocrystalline cellulose based-hydrogel scaffolds: synthesis, characterization, and mechanical properties**

evaluation. *International Journal of Polymeric Materials and Polymeric Biomaterials* 2021, **70**:142-148.

[81] Yang B, Hua WQ, Li L, Zhou ZH, Xu L, Bian FG, Ji X, Zhong GJ, Li ZM: **Robust hydrogel of regenerated cellulose by chemical crosslinking coupled with polyacrylamide network**. *Journal of Applied Polymer Science* 2019, **136**:47811.

[82] Zhu L, Liu Y, Jiang Z, Sakai E, Qiu J, Zhu P: **Highly temperature resistant cellulose nanofiber/polyvinyl alcohol hydrogel using aldehyde cellulose nanofiber as cross-linker**. *Cellulose* 2019, **26**:5291-5303.

[83] Gómez-García M, Sol C, de Nova PJ, Puyalto M, Mesas L, Puente H, Mencía-Ares Ó, Miranda R, Argüello H, Rubio P: **Antimicrobial activity of a selection of organic acids, their salts and essential oils against swine enteropathogenic bacteria**. *Porcine Health Management* 2019, **5**:1-8.

[84] Hu Y, Guo Q, Liu P, Zhu R, Lu F, Ramaswamy S, Wu Y, Xu F, Zhang X: **Fabrication of novel cellulose-based antibacterial film loaded with poacic acid against *Staphylococcus aureus***. *Journal of Polymers and the Environment* 2021, **29**:745-754.

[85] Oliva C, Huang W, El Badri S, Lee MAL, Ronholm J, Chen L, Wang Y: **Concentrated sulfuric acid aqueous solution enables rapid recycling of cellulose from waste paper into antimicrobial packaging**. *Carbohydrate Polymers* 2020, **241**:116256.

[86] Breijyeh Z, Jubeh B, Karaman R: **Resistance of Gram-negative bacteria to current antibacterial agents and approaches to resolve it**. *Molecules* 2020, **25**:1340.

[87] • Batista RA, Espitia PJP, Quintans JdSS, Freitas MM, Cerqueira MÂ, Teixeira JA, Cardoso JC: **Hydrogel as an alternative structure for food packaging systems**. *Carbohydrate Polymers* 2019, **205**:106-116.

This paper generally highlighted the factors involved in the development and performance evaluation of hydrogels and discussed the potential applications of hydrogels in food packaging.

[88] Leppänen I, Vikman M, Harlin A, Orelma H: **Enzymatic degradation and pilot-scale composting of cellulose-based films with different chemical structures**. *Journal of Polymers and the Environment* 2020, **28**:458-470.

[89] Haske-Cornelius O, Pellis A, Tegl G, Wurz S, Saake B, Ludwig R, Sebastian A, Nyanhongo GS, Guebitz GM: **Enzymatic systems for cellulose acetate degradation**. *Catalysts* 2017, **7**:287.

[90] Ong HL, Owi WT, Sam ST, Akil HM: **Revealing the water resistance, thermal and biodegradation properties of *Citrus aurantifolia* crosslinked tapioca starch/nanocellulose bionanocomposites**. *Journal of Polymers and the Environment* 2020, **28**:3256-3269.

[91] Trifol J, Plackett D, Szabo P, Daugaard AE, Giacinti Baschetti M: **Effect of crystallinity on water vapor sorption, diffusion, and permeation of pla-based nanocomposites**. *ACS Omega* 2020, **5**:15362-15369.

[92] Souza VGL, Fernando AL: **Nanoparticles in food packaging: Biodegradability and potential migration to food—A review**. *Food Packaging and Shelf Life* 2016, **8**:63-70.

[93] Cui X, Lee JJ, Chen WN: **Eco-friendly and biodegradable cellulose hydrogels produced from low cost okara: Towards non-toxic flexible electronics**. *Scientific Reports* 2019, **9**:1-9.

[94] Sethi S, Kaith BS, Kaur M, Sharma N, Khullar S: **A hydrogel based on dialdehyde carboxymethyl cellulose–gelatin and its utilization as a bio adsorbent**. *Journal of Chemical Sciences* 2020, **132**:1-16.

[95] Marrez DA, Abdelhamid AE, Darwesh OM: **Eco-friendly cellulose acetate green synthesized silver nano-composite as antibacterial packaging system for food safety**. *Food Packaging and Shelf Life* 2019, **20**:100302.

[96] Yu Z, Wang W, Dhital R, Kong F, Lin M, Mustapha A: **Antimicrobial effect and toxicity of cellulose nanofibril/silver nanoparticle nanocomposites prepared by an ultraviolet irradiation method**. *Colloids and Surfaces B: Biointerfaces* 2019, **180**:212-220.

[97] Oketch-Rabah HA, Roe AL, Rider CV, Bonkovsky HL, Giancaspro GI, Navarro V, Paine MF, Betz JM, Marles RJ, Casper S, et al.: **United States Pharmacopeia (USP) comprehensive review of the hepatotoxicity of green tea extracts**. *Toxicology Reports* 2020, **7**:386-402.

[98] Beristain-Bauza SDC, Hernández-Carranza P, Cid-Pérez TS, Ávila-Sosa R, Ruiz-López II, Ochoa-Velasco CE: **Antimicrobial activity of ginger (*Zingiber officinale*) and its application in food products**. *Food Reviews International* 2019, **35**:407-426.

Connecting Text

Chapter 2 summarized the recent studies on the production methods of RC films and hydrogels and their properties and functions as food packaging materials. RC films as a solution of biodegradable food packaging materials was pointed out. In chapter 3, the effects of two aqueous solvents on the structure and properties of wood cellulose films were explored. Firstly, RC films were produced by dissolving wood cellulose in either a concentrated H_2SO_4 solution or a NaOH/urea aqueous solution. Secondly, the mechanical properties and flexibility of RC films from different solutions were compared. Thirdly, the structure of RC films was studied by scanning electron microscopy, molecular weight test, Fourier-transform infrared spectroscopy, and X-ray diffraction. Finally, the effect of RC film structure on the moisture uptake, water vapor permeability, optical properties, and thermal stability was investigated.

Chapter 3. Wood Cellulose Films with Different Foldabilities Triggered by Dissolution and Regeneration from Concentrated H_2SO_4 and NaOH/Urea Aqueous Solutions

3.1. Abstract

Forests are a major source of wealth for Canadians, and cellulose makes up the "skeleton" of wood fibers. Concentrated H_2SO_4 and NaOH/urea aqueous solutions are two efficient solvents that can rapidly dissolve cellulose. Our preliminary experiment obtained regenerated wood cellulose films with different mechanical properties from these two solvents. Therefore, herein, we aim to investigate the effects of aqueous solvents on the structure and properties of wood cellulose films. Regenerated cellulose (RC) films were produced by dissolving wood cellulose in either 64 wt% H_2SO_4 solution (RC-H4) or NaOH/urea aqueous solution (RC-N4). RC-H4 showed the higher tensile strength (109.78 ± 2.14 MPa), better folding endurance (20-28 times), and higher torsion angle (42°) than RC-N4 (62.90 ± 2.27 MPa, un-foldable, and 12°). The increased cellulose contents in the H_2SO_4 solutions from 3 to 5 wt% resulted in an improved tensile strength from 102.61 ± 1.99 to 132.93 ± 5.64 MPa and did not affect the foldability. RC-H4 also exhibited better water vapor barrier property ($1.52 \pm 0.04 \times 10^{-7}$ g m^{-1} h^{-1} Pa^{-1}), superior transparency (~90% transmittance at 800 nm), but lower thermal stability compared to RC-N4. This work provides special insights into the regenerated wood cellulose from two aqueous solvents and is expected to facilitate the development of high-performance RC films from abundant forestry resources.

3.2. Introduction

The accumulation of non-degradable plastic waste poses an environmental menace, perpetuating pollution and causing harm to ecosystems. The development of renewable and biodegradable materials is imperative to reduce dependence on conventional petroleum-based plastics, alleviating environmental damage and promoting a sustainable future. Cellulose, the most abundant natural polymer on Earth, has emerged as a promising substitute for non-

renewable resources due to its significant industrial applications and unique properties like biocompatibility and biodegradability.

However, cellulose faces application limitations due to its intricate structure marked by extensive intra- and intermolecular hydrogen bonding. This structural stability renders cellulose insoluble in most common liquids, hindering its widespread utility. Solvents like *N*-methylmorpholine-*N*-oxide (NMMO), ionic liquids (ILs), and LiCl/DMAc have been developed for cellulose dissolution and regeneration [1]. Despite the partial success, the dissolution of cellulose by these solvents often accompanies undesirable properties. For instance, NMMO-solubilized cellulose solutions are thermally unstable; ILs are expensive and may lead to side reactions during dissolution; and LiCl/DMAc requires an activation process before dissolution. Besides, the recyclability and sustainability of these solvents remain some concerns [2]. Aqueous NaOH/urea solution is considered as an industrially feasible "green" solvent that can rapidly dissolve 4 wt% cellulose with a molecular weight of $<1.14 \times 10^5$ g/mol in 2 mins at −10 °C [3]. The dissolved cellulose can be shaped into desirable forms such as fibers [4,5], films [6], hydrogels [7,8], and composite materials [9,10] through the processes of spinning, casting, coating, etc. However, the NaOH/urea aqueous solution has the limitations in cellulose molecular weight and concentration [11], so an extra acid hydrolysis treatment is usually performed to decrease the molecular weights of the wood fibers before dissolution and the contents of cellulose are generally lower than 4 wt% [12,13].

The interaction between H_2SO_4 and cellulose has been studied for centuries. Numerous studies have demonstrated that concentrated solutions of H_2SO_4 (63-72 wt%) are capable of breaking hydrogen bonds and penetrating the crystalline and non-crystalline domains of cellulose, resulting in the lower molecular weight cellulose, nanocellulose, and even sugar [14,15,16]. Besides, earlier studies have shown that a gradual reduction in the temperature of concentrated

H_2SO_4 aqueous solutions from elevated temperatures to room or lower temperatures limited the hydrolysis of cellulose, leading to dissolution without significantly affecting the molecular weight of the cellulose. For instance, 1 g/mL of microcrystalline cellulose dissolved in 70 wt% H_2SO_4 at 5 °C had a yield of 72.7% after precipitation with water [17]. Huang et al. disclosed that 64 wt% H_2SO_4 aqueous solution was capable of dissolving 5 wt% cellulose at −20 °C within 2 min with a slight decrease of the molecular weight of cellulose from 4.10×10^5 g/mol to 3.34×10^5 g/mol [18]. Chen et al. designed a two-step concentrated H_2SO_4 dissolution system that was capable of dissolving 150 g/L of cellulose within 5 min at −10 °C [19]. The regenerated cellulose (RC) hydrogels had a yield of 97.1% and a polymerization degree of 71% of those of original cotton cellulose [19]. Besides, a few attempts have been made to dissolve the low contents of cellulose (2-3 wt%) in 64 wt% H_2SO_4 solution at low temperatures to produce RC films with tensile strengths of about 60-70 MPa [18,20,21].

To explore the potential applications of wood cellulose through dissolution and regeneration from aqueous solvents, our preliminary experiment showed significant differences in the mechanical properties and flexibility of wood cellulose films fabricated with concentrated H_2SO_4 and NaOH/urea aqueous solutions, which have never been reported. Therefore, this study aimed to explain the differences by comparing the structures and properties of RC films obtained from these two aqueous solutions. Their mechanical properties, flexibility, morphology, molecular weight, crystallinity, optical properties, and thermal stability were studied in detail, which sought to provide valuable insights into the sustainable processing of wood cellulose through aqueous solvents.

3.3. Materials and methods

3.3.1 Materials

The bleached spruce pulps were provided by FP Innovations (Pointe-Claire, QC, Canada). Sulfuric acid (95.0-98.0%) was purchased from Millipore-Sigma (Oakville, ON, Canada). Sodium hydroxide (>97.0%) and urea (>99.6%) were obtained from Fisher Scientific (Ottawa, ON, Canada).

3.3.2 Preparation of wood cellulose films

The pretreatments and dissolution of spruce pulps in NaOH/urea solution were based on our previous study with slight modifications [22]. The recovery rate of spruce pulps after acid hydrolysis was 91.58 ± 2.07%. Cellulose solution was casted with 1 mm thickness and coagulated in a 5 wt% H_2SO_4 aqueous bath at 25 °C for 7 min to produce RC films. The air-dried RC films obtained from NaOH/urea solution were labeled as RC-N4. The dissolution of spruce pulps in acid solvent began with the addition of 3, 4, and 5 wt% ground hydrolyzed spruce pulps into 64 wt% H_2SO_4 solutions at −20 °C, respectively. The solutions were stirred for 10 min at 1500 rpm under an ice bath, centrifuged at 120 *g* for 1 min to remove bubbles, and then casted with a thickness of 1 mm on a glass plate, followed by coagulation in 10 wt% NaOH at 25 °C for 7 min. The RC films obtained from the H_2SO_4 solutions were dried in air at room temperature and coded as RC-H, and RC-H3, RC-H4, and RC-H5 based on their cellulose contents.

3.3.3 Characterization of wood cellulose films

3.3.3.1 Mechanical properties and flexibility

RC films were conditioned (25 °C and 60% relative humidity) and tested for mechanical properties by using ADMET MTEST Quattro eXpert 7600 series (MA, USA) with a load cell of 250 lb. and a crosshead speed of 5 mm/min [22].

A torsion angle test was performed to determine the flexibility of RC films [23]. The conditioned RC films were cut into stripes with dimensions of 50 mm × 10 mm (length × width) and measured by the ADMET MTEST Quattro eXpert 9000 torsion testing system with a grip distance of 20 mm and a rotating speed of 3 deg./s until breakage.

The folding endurance of RC films was manually tested by iteratively folding RC film in a consistent position until it broke. The total count of folds required for RC films to develop cracks was designated as the folding value [24,25].

3.3.3.2 Morphological analysis

A Hitachi TM1000 SEM (Hitachi Co. Ltd., Tokyo, Japan) with an acceleration voltage of 4 kV was used to observe morphologies of RC films [21].

3.3.3.3 Molecular weight and yield rate

The determination of viscosity-average molecular weight (M_v) was conducted according to the TAPPI T230 standard test method [26]. The yield rate was calculated based on the ratio of the mass of air-dried RC films to the mass of hydrolyzed spruce pulps for dissolution.

3.3.3.4 Density and porosity

The density and apparent porosity of RC films were calculated based on previous study [27].

3.3.3.5 Fourier transform infrared spectroscopy (FT-IR)

The structure of RC films was determined by a Cary 630 Fourier-transform infrared spectroscope equipped with an ATR sampling module (FT-IR, Agilent Technologies, Santa Clara, CA, USA) [28].

3.3.3.6 X-ray diffractometry (XRD)

The crystalline profile of RC films was measured by a high-resolution X-ray diffractometer

(Empyrean, Malvern Panalytical Ltd, Malvern, UK) [29].

3.3.3.7 Moisture uptake

RC films were cut into squares (40 mm × 40 mm) and dried in an oven until a constant weight (m_i) was attained. The moisture absorption measurement was performed under 60% relative humidity at 25 °C for 4 days and the weight of films (m_d) was recorded. The moisture uptake percentage was calculated based on Eq. (1):

$$Moisture\ uptake\ (\%) = \frac{m_d - m_i}{m_i} \times 100\% \quad (1)$$

3.3.3.8 Water vapor permeability (WVP)

The water vapor permeability of RC films was determined by following ASTM E96-92 standard method [30].

3.3.3.9 Optical properties

RC films with similar thickness of about 12 ± 1 μm were fabricated to compare optical properties. The optical transmittance of RC films was measured by a DU 800 UV/vis spectrophotometer (Beckman Coulter, Brea, CA) in the range of 400-800 nm, using air as background.

3.3.3.10 Thermogravimetric analysis

TGA of RC films was performed using the thermogravimetric analyzer Discovery 5500 (TA Instruments Inc., New Castle, DE, USA). Thermograms of samples were collected from 30 to 600 °C with a heating rate of 10 °C/min in nitrogen (10 mL/min).

3.3.4 Statistical analysis

All tests were performed in triplicates, and the data were presented as the mean ± standard deviation. One-way analysis of variance (ANOVA) and Duncan's multiple-range test were employed for statistical analysis by SPSS statistical software (version 26, IBM SPSS Inc., New York, NY) with significant differences at $p < 0.05$.

3.4. Results and discussion

In our preliminary experiment, RC films obtained from concentrated H_2SO_4 solution had better flexibility. The mechanical properties of RC films are shown in Fig. 3.1A. RC-H4 exhibited a higher tensile strength of 109.78 ± 2.14 MPa compared to RC-N4 (62.90 ± 2.27 MPa). Notably, RC-H5 showed the highest tensile strength of 132.93 ± 5.64 MPa and elongation percentage of 3.91 ± 0.19%, indicative of increased cellulose chains available for extension and rearrangement. The tensile strength of RC-H5 was higher than RC films from corn stalk pulp fines in DMAc/LiCl solution (106.11 MPa) [31], wood pulp cellulose in ionic liquids (124.5 MPa) [32], cotton linter in NaOH/urea solution (108.1 MPa) [10], corncob in NMMO aqueous solution (73.1 MPa) [33], hardwood pulp cellulose in LiBr aqueous solution (67 MPa) [34], and wood pulp cellulose in CO_2/DBU/DMSO system (91 MPa) [35]. As shown in Fig. 3.1B-D, the flexibility of RC films was determined by rolling, bending, and folding. All four RC films were rollable and bendable. However, RC-N4 fractured at the first folding, while all RC-H films showed only slight cracks after 20-28 folding cycles. Besides, as shown in Table 3.1, RC-N4 exhibited a low torsion angle of 11.84 ± 2.02°. Three RC films obtained from H_2SO_4 solutions withstood a larger torsion angle of about 42°.

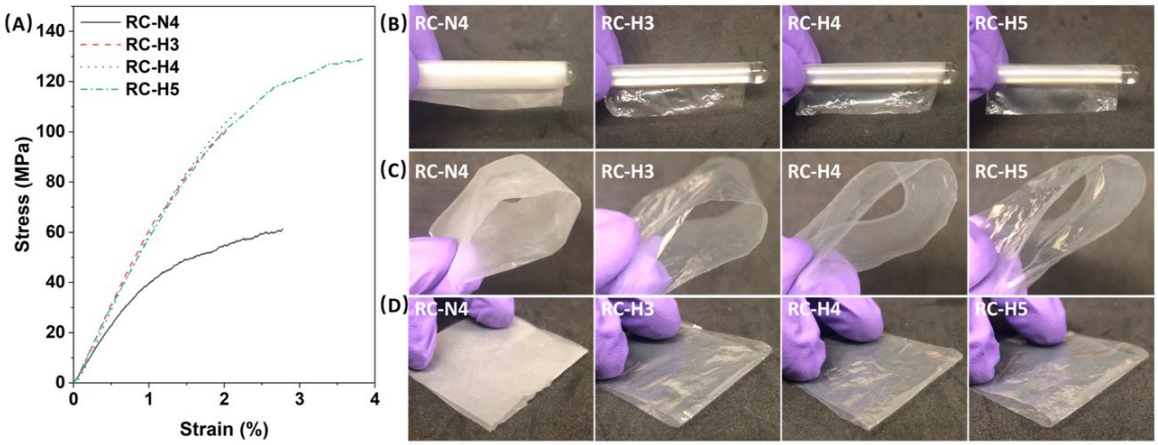

Fig. 3.1. (A) Stress-strain curves of RC films. Photos of RC films during (B) rolling, (C) bending, and (D) folding.

Table 3.1. Tensile strength, tensile strain, Young's modulus, and torsion angle of RC films.

Samples	Tensile strength (MPa)	Tensile strain (%)	Young's modulus (GPa)	Torsion angle (°)
RC-N4	62.90 ± 2.27^{d}	2.56 ± 0.30^{b}	4.50 ± 0.16^{b}	11.84 ± 2.02^{b}
RC-H3	102.61 ± 1.99^{c}	1.95 ± 0.10^{c}	5.95 ± 0.06^{a}	45.26 ± 3.96^{a}
RC-H4	109.78 ± 2.14^{b}	2.21 ± 0.07^{c}	6.00 ± 0.02^{a}	42.07 ± 6.67^{a}
RC-H5	132.93 ± 5.64^{a}	3.91 ± 0.19^{a}	6.04 ± 0.06^{a}	41.78 ± 1.60^{a}

The morphology of RC films was observed by SEM and is shown in Fig. 3.2A. No obvious undissolved fibers were found on the surface of RC films obtained from H_2SO_4 and NaOH/urea aqueous solutions. RC-N4 had an uneven and rough surface, which was attributed to the inevitable shrinkage of the film during the regeneration and drying process [36,37]. In contrast, RC-H3, RC-H4, and RC-H5 showed similar even and smooth surfaces. It was worth noting that, by applying similar amounts of cellulose solutions (about 1 mm thickness), the thickness of RC-N4 was the largest (29.28 ± 1.07 μm). RC-H3, RC-H4, and RC-H5 exhibited similar

layered structures with decreased thicknesses of 11.41 ± 0.24 μm, 13.09 ± 0.27 μm, and 13.47 ± 0.15 μm, respectively. The different thicknesses of RC-N4 and RC-H films could be linked to the different porosities caused by various coagulation rates. Li, Zhang, and Xu observed that raising the coagulation temperature from 25 °C to 45 °C augmented the diffusion speed of the coagulant [38]. This enhancement resulted in a notable increase in the average pore size on both the surface (from 342 nm to 809 nm) and the cross-section (from 140 nm to 343 nm), which facilitated the formation of a thicker film with larger pore sizes.

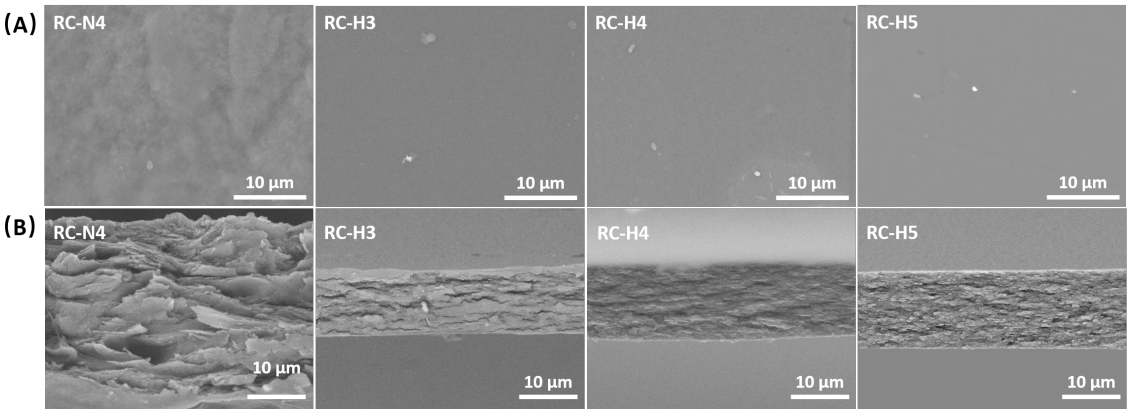

Fig. 3.2. SEM images of (A) surface and (B) cross-section of RC films.

The M_v value of the original spruce pulp was 3.46 × 10^5 g/mol, which was decreased to 1.91 × 10^5 g/mol after acid hydrolysis. RC-N4 showed a slightly decreased M_v value of 1.62 × 10^5 g/mol, while three RC films prepared from concentrated H_2SO_4 aqueous solution had the M_v values of about 5 × 10^4 g/mol. However, RC-H films had the higher yield rates in the range of 84.06% to 86.35% compared to 80.17 ± 2.87% of RC-N4 films. Since NaOH/urea aqueous solution is more efficient to dissolve cellulose with molecular weight <1.14 × 10^5 g/mol, the undissolved cellulose fibers with high molecular weight might be eliminated after centrifugation and led to the decreased yield rate of RC-N4 [3]. As shown in Fig. 3.3A, the density of RC-H4 (1.22 ± 0.02 g/cm^3) was obviously higher than that of RC-N4 (0.93 ± 0.01

g/cm^3). The increase of the cellulose contents from 3 wt% to 5 wt% resulted in the denser films with higher densities from 1.16 ± 0.04 g/cm^3 to 1.28 ± 0.03 g/cm^3 and reduced porosities from 28.67 ± 2.52% to 21.41 ± 1.99%. It was due to the increased cellulose chain entanglement at a higher cellulose concentration [18], leading to the significant improvement in tensile strength from 102.61 ± 1.99 to 132.93 ± 5.64 MPa. It was reported that the fast coagulation rate during the regeneration process would facilitate the lateral shrinkage of RC films [39,40], which might lead to a rougher film surface, lower film density, and larger film thickness of RC-N4 films [41]. At the same time, the decreased cavities and free space in RC-H films contributed to their higher tensile strength [42].

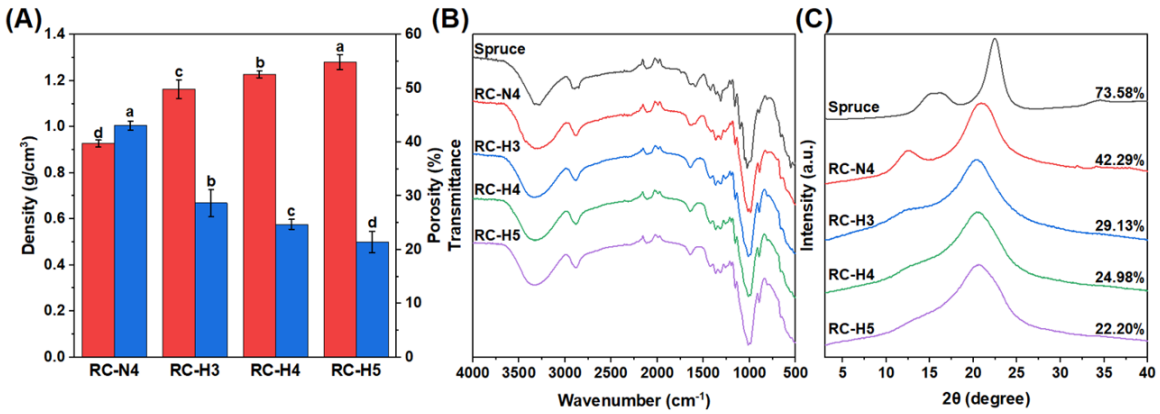

Fig. 3.3. (A) Density and porosity, (B) FT-IR spectra, and (C) XRD patterns and crystallinity index of RC films.

FT-IR spectra and XRD diffraction patterns were collected to investigate the effect of aqueous solutions on the structure of RC films. As shown in Fig. 3.3B, all RC films displayed similar FT-IR spectra to spruce pulps, indicating no chemical reactions during the dissolution and regeneration process. Characteristic absorption bands of spruce and RC films were observed at around 3600–3000, 2886, 1427, and 893 cm^{-1}, which were ascribed to O─H stretching vibration of hydroxyl groups, C─H stretching vibration, ─CH_2 symmetrical bending vibration

of cellulose I crystalline structure, and ─C─O─C─ bridge stretching of the amorphous region and cellulose II crystalline structure, respectively [43,44]. However, changes in the intensity of peaks were observed. For instance, two sharp peaks at 3340 and 3273 cm^{-1} were flattened and broadened after dissolution and regeneration, which were related to the intra- and intermolecular hydrogen bonds in cellulose, respectively [45]. The concentrated H_2SO_4 aqueous solution dissolved cellulose by breaking interchain hydrogen bonds in cellulose, and the rearrangement of cellulose happened during regeneration and drying [46]. The disturbed intermolecular interactions partially reformed during the rapid coagulation process, leading to decreased peak intensities. The asymmetric ─CH_2 bending vibration at 1427 cm^{-1} belonged to the cellulose I crystalline structure, while the ─C─O─C─ bridge stretching at 893 cm^{-1} represented the amorphous region and cellulose II crystalline structure [22]. The ratio of peaks at 1427 and 893 cm^{-1} was defined as the "crystallinity index" (CI), which decreased after dissolution and regeneration, indicating the reduced crystallinity and transition from cellulose I structure to cellulose II structure. Fig. 3.3C presents the change of cellulose polymorph. Spruce pulps showed diffraction peaks at 14.8° ($1\bar{1}0$), 16.3° (110), 22.5° (200), and 34.5° (004) with a CI value of about 73.6%, representing a typical cellulose I structure [21]. After dissolution and regeneration, RC-N4 showed a cellulose II structure with a broad diffraction peak at 21.0° and a small broad peak at 12.6° and a decreased CI value of about 42.3%, which was coordinated with FT-IR results [47]. However, the main peak of three RC-H films slightly shifted to a lower 2θ of 20.5°, and the intensity of diffraction peak at 12.6° reduced or even disappeared. These results suggested an expansion of the cellulose I lattice rather than a transformation to cellulose II, resulting in an amorphous RC film with lower CI values. It was because the hydrated sulfate ions disrupted the formation of hydrogen bonding network during regeneration, leading to an increase in disordered regions [48]. Similar amorphous structures

were observed in RC films prepared from microcrystalline cellulose [49] and eucalyptus [50] dissolved in ionic liquids and cotton cellulose powder [51] dissolved in LiCl/DMAc solution. Besides, the increased cellulose contents from 3 wt% to 5 wt% further decreased the CI values from 29.13% to 22.20%, which was ascribed to the increased chain entanglement and interruption of free chain mobility during coagulation [52]. However, this result diverged from previous studies, which have reported that cellulose with higher molecular weights and CI values led to higher tensile strength of RC films [53,54,55,56]. Therefore, in our opinion, the high mechanical strength and good foldability of RC-H films should be attributed to the high density and amorphous structure. Similar results were observed in cellulose nanofiber films, where the increased density from 0.8 to 1.0 g/cm^3 improved tensile strength from about 55 to 80 MPa [57]. Besides, amorphous cellulose has been reported to be more flexible and mobile due to its less ordered structure compared to crystalline cellulose [58]. The structural and foldability differences between RC-N4 and RC-H films are elucidated in Fig. 3.4. The disruption of interchain hydrogen bonds in cellulose occurred during dissolution, and the regeneration triggered different crystalline and entangled structures. RC-N4 films exhibited higher molecular weight, increased crystallinity, higher porosity, and brittleness. In contrast, RC-H films were characterized by lower molecular weight, more amorphous structure, higher density, and better foldability.

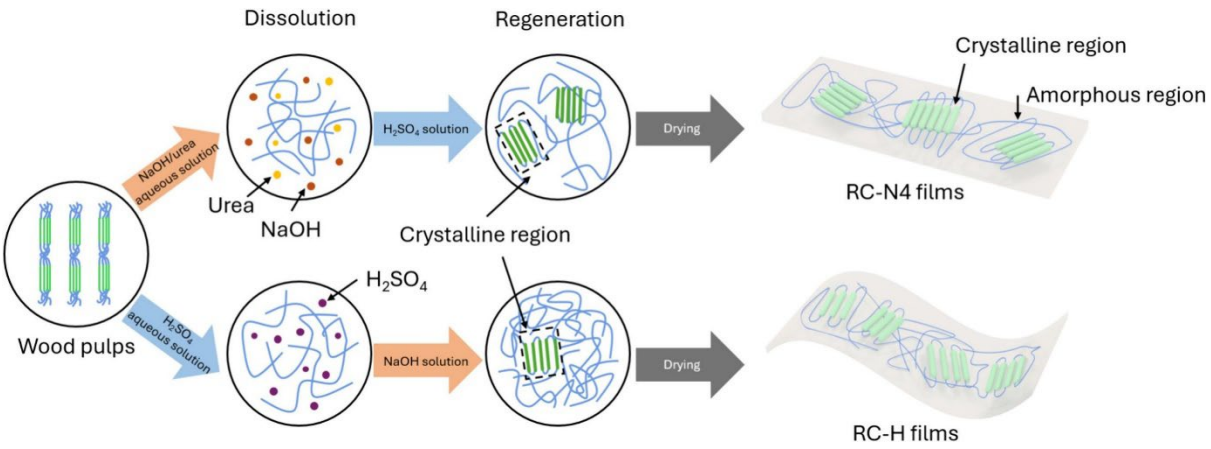

Fig. 3.4. Proposed mechanisms of wood cellulose dissolution and regeneration from NaOH/urea and concentrated H_2SO_4 aqueous solutions.

To evaluate the potential applications of wood cellulose films regenerated from two aqueous solutions, their other physical properties were studied and compared. In Fig. 3.5A, the moisture uptake percentage of different RC films was depicted. Previous studies have suggested that crystalline cellulose, characterized by a more ordered structure, tends to exhibit lower moisture sensitivity compared to amorphous cellulose, particularly at RH below 75% [59]. However, our findings deviated from this expectation, and all RC films demonstrated a similar moisture uptake of about 15 wt%. This discrepancy could be attributed to the interplay between moisture sorption and material porosity. Although RC-N4 exhibited a higher CI, its lower density and higher porosity facilitated moisture absorption within the films [60,61]. The comparison of WVP values of RC-N4 and RC-H films is illustrated in Fig. 3.5B. The RC-N4 showed a higher WVP value of $4.82 \pm 0.28 \times 10^{-7}$ g m^{-1} h^{-1} Pa^{-1}, whereas three RC-H films had significantly lower WVP values, ranging from 1.25 ± 0.02 to $1.52 \pm 0.04 \times 10^{-7}$ g m^{-1} h^{-1} Pa^{-1}. It was ascribed to the more convoluted path formed by higher film density. The increase in cellulose content from 3 to 5 wt% didn't show any significant effects on moisture uptake percentage and WVP of RC-H films. The slightly increased values of RC-H5 might be attributed to the enhanced

affinity of film to moisture and the intensified capillary force at a high cellulose content [62]. The WVP values of RC-H films were lower than the RC films fabricated from microcrystalline cellulose in 1-butyl-3-methylimidazolium chloride (4.68×10^{-7} g m^{-1} h^{-1} Pa^{-1}) [63], bamboo pulps in 1-ally-3-methylimidazolium chloride (2.51×10^{-7} g m^{-1} h^{-1} Pa^{-1}) [64], cotton linter in NaOH/urea aqueous solution (8.21×10^{-6} g m^{-1} h^{-1} Pa^{-1}) [65], microcrystalline cellulose in LiCl/DMAc (2.29×10^{-5} g m^{-1} h^{-1} Pa^{-1}) [66], and cellulose pulp in NMMO solvent (1.43×10^{-5} g m^{-1} h^{-1} Pa^{-1}) [67].

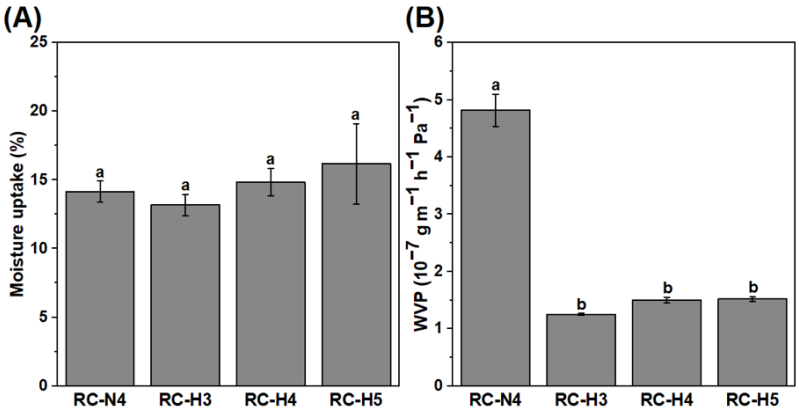

Fig. 3.5. (A) Moisture uptake and (B) WVP of RC films.

As shown in Fig. 3.6A, the transmittance of RC-N4 was lower than those of RC-H films. The RC-N4 film had the higher porosity, which refracted the incident light and resulted in less light being transmitted through the film. The increased cellulose contents led to a higher density of RC-H films, which prevented light scattering and decreased the opacity of films. This phenomenon could be explained by Snell's Law that photon scattering primarily occurs at interfaces with different refractive indexes, so the higher porosity resulted in more interfaces within the films and more scattered light [68,69]. The optical transparency of RC-H films at 800 nm was about 90%, which was comparable to those of RC films prepared from cotton linter in LiOH/urea solution (91.2%) [70], durian rind in LiCl/DMAc solution (86%) [71],

wood pulps in $ZnCl_2 \cdot 3H_2O$ solution (about 90%) [72], and higher than those of wood pulps in NaOH solution (about 75%) [73], bed sheet in H_2SO_4 solution (about 50%) [21], cotton linter in NaOH/urea solution (about 60%) [10], and wood pulps in DMSO (about 80%) [74].

The TGA and DTG curves of RC films were presented in Fig. 3.6B and C, respectively. All the films showed a slight weight loss of about 10% up to 250 ℃, corresponding to the dehydration of RC films. The main weight loss occurred in the range of 270-390 ℃, which was due to the decomposition and carbonization of cellulose [75]. The maximum decomposition temperature (T_{max}) of RC-N4 was about 348.38 ℃, which was higher than those of RC-H3 (343.02 ℃), RC-H4 (324.51 ℃), and RC-H5 (322.78 ℃). It could be explained by the different amounts of cellulose crystalline structures, where cellulose with a higher CI value had a higher decomposition temperature, and therefore better thermal stability [76].

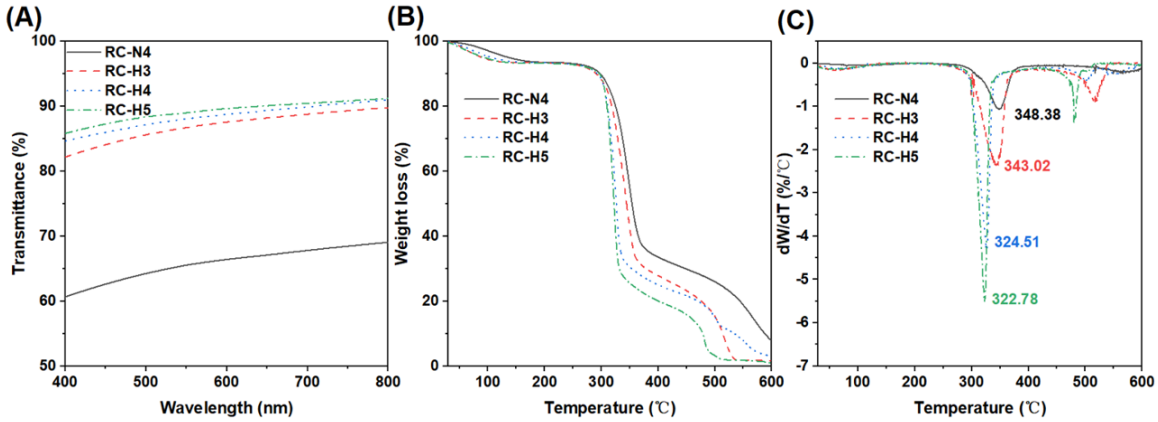

Fig. 3.6. (A) Optical property of RC films. (B) TGA and (C) DTG curves of RC films.

3.5. Conclusion

Both concentrated H_2SO_4 and NaOH/urea aqueous solutions are efficient to convert wood pulps into RC films. However, the structure and properties of RC films from different aqueous solutions varied. The RC films generated from NaOH/urea solution exhibited the loose layered structure with high CI value and the brittle feature, while the films obtained from H_2SO_4

solution showed the high density with more amorphous region and the good foldability. Especially, the RC-H5 films showed the highest tensile strength (132.93 ± 5.64 MPa) and tensile strain (3.91 ± 0.19%), and could be folded up to 28 times before breakage. The moisture uptake of RC films was determined by both the crystalline structure and porosity, but the water vapor barrier property was more affected by the density of RC films. The RC-N4 films had a high CI value, resulting in the lower light transmittance and better thermal stability. It is the first time to compare wood cellulose films regenerated from different aqueous solutions, and these findings will provide valuable insights into the construction of cellulose films as a sustainable alternative to nondegradable plastics.

3.6. References

[1] Sayyed, A. J., Deshmukh, N. A., & Pinjari, D. V. (2019). A critical review of manufacturing processes used in regenerated cellulosic fibres: viscose, cellulose acetate, cuprammonium, LiCl/DMAc, ionic liquids, and NMMO based lyocell. *Cellulose, 26*(5), 2913-2940.

[2] Wang, S., Lu, A., & Zhang, L. (2016). Recent advances in regenerated cellulose materials. *Progress in Polymer Science, 53*, 169-206.

[3] Cai, J., & Zhang, L. (2005). Rapid dissolution of cellulose in LiOH/urea and NaOH/urea aqueous solutions. *Macromolecular Bioscience, 5*(6), 539-548.

[4] Ke, G., Tan, S., Wang, Y., Chen, S., & Liu, K. (2023). Extraction and characterization of cellulosic fibers from cattail leaves by aqueous sodium hydroxide/urea. *Cellulose, 30*(11), 6799-6810.

[5] Xie, K., Tu, H., Dou, Z., Liu, D., Wu, K., Liu, Y., Chen, F., Zhang, L., & Fu, Q. (2021). The effect of cellulose molecular weight on internal structure and properties of regenerated

cellulose fibers as spun from the alkali/urea aqueous system. *Polymer, 215*, 123379.

[6] Zhu, Q., Wang, J., Sun, J., & Wang, Q. (2020). Preparation and characterization of regenerated cellulose biocomposite film filled with calcium carbonate by in situ precipitation. *BioResources, 15*(4), 7893.

[7] Niu, L., Zhang, D., Liu, Y., Zhou, X., Wang, J., Wang, C., & Chu, F. (2020). Combination of acid treatment and dual network fabrication to stretchable cellulose based hydrogels with tunable properties. *International Journal of Biological Macromolecules, 147*, 1-9.

[8] Wong, L. C., Poh, J. H., Tan, W. T., Khor, B.-K., Murugaiyah, V., Leh, C. P., & Goh, C. F. (2023). Cellulose hydrogel development from unbleached oil palm biomass pulps for dermal drug delivery. *International Journal of Biological Macromolecules, 224*, 483-495.

[9] Delgado, J. F., Salvay, A. G., Arroyo, S., Bernal, C. R., & Foresti, M. L. (2023). Effect of dissolution time on the development of all-cellulose composites using the NaOH/urea solvent system. *Polysaccharides, 4*(1), 65-77.

[10] Wei, Q.-Y., Lin, H., Yang, B., Li, L., Zhang, L.-Q., Huang, H.-D., Zhong, G.-J., Xu, L., & Li, Z.-M. (2020). Structure and properties of all-cellulose composites prepared by controlling the dissolution temperature of a NaOH/urea solvent. *Industrial & Engineering Chemistry Research, 59*(22), 10428-10435.

[11] Qi, H., Chang, C., & Zhang, L. (2008). Effects of temperature and molecular weight on dissolution of cellulose in NaOH/urea aqueous solution. *Cellulose, 15*, 779-787.

[12] Shi, Z., Yang, Q., Cai, J., Kuga, S., & Matsumoto, Y. (2014). Effects of lignin and hemicellulose contents on dissolution of wood pulp in aqueous NaOH/urea solution. *Cellulose, 21*, 1205-1215.

[13] Shi, Z., Yang, Q., Kuga, S., & Matsumoto, Y. (2015). Dissolution of wood pulp in aqueous NaOH/urea solution via dilute acid pretreatment. *Journal of Agricultural and Food Chemistry, 63*(27), 6113-6119.

[14] Roman, M., & Winter, W. T. (2004). Effect of sulfate groups from sulfuric acid hydrolysis on the thermal degradation behavior of bacterial cellulose. *Biomacromolecules, 5*(5), 1671-1677.

[15] Sherrard, E., & Blanco, G. (1923). Some of the products obtained in the hydrolysis of white spruce wood with dilute sulfuric acid under steam pressure. *Industrial & Engineering Chemistry, 15*(6), 611-616.

[16] Sun, B., Zhang, M., Hou, Q., Liu, R., Wu, T., & Si, C. (2016). Further characterization of cellulose nanocrystal (CNC) preparation from sulfuric acid hydrolysis of cotton fibers. *Cellulose, 23*, 439-450.

[17] Hashaikeh, R., & Abushammala, H. (2011). Acid mediated networked cellulose: preparation and characterization. *Carbohydrate Polymers, 83*(3), 1088-1094.

[18] Huang, W., Wang, Y., Zhang, L., & Chen, L. (2016). Rapid dissolution of spruce cellulose in H_2SO_4 aqueous solution at low temperature. *Cellulose, 23*, 3463-3473.

[19] Chen, G., Hong, F. F., Yuan, J., Li, L., Fang, M., Wei, W., Wang, X., & Wei, Y. (2022). Super solvent of cellulose with extra high solubility for tunable cellulose structure with versatile application. *Carbohydrate Polymers, 296*, 119917.

[20] Wang, L., Huang, S., & Wang, Y. (2022). Recycling of waste cotton textile containing elastane fibers through dissolution and regeneration. *Membranes, 12*(4), 355.

[21] Zhou, C., & Wang, Y. (2021). Recycling of waste cotton fabrics into regenerated cellulose films through three solvent systems: a comparison study. *Journal of Applied Polymer*

Science, 138(48), 51255.

[22] Huang, K., Maltais, A., Liu, J., & Wang, Y. (2022). Wood cellulose films regenerated from NaOH/urea aqueous solution and treated by hot pressing for food packaging application. *Food Bioscience, 50*, 102177.

[23] Erceg, T., Vukić, N., Šovljanski, O., Stupar, A., Šergelj, V., Aćimović, M., Baloš, S., Ugarković, J., Šuput, D., & Popović, S. (2022). Characterization of films based on cellulose acetate/poly (caprolactone diol) intended for active packaging prepared by green chemistry principles. *ACS Sustainable Chemistry & Engineering, 10*(28), 9141-9154.

[24] Mahesh, A., Shastri, N., & Sadanandam, M. (2010). Development of taste masked fast disintegrating films of levocetirizine dihydrochloride for oral use. *Current Drug Delivery, 7*(1), 21-27.

[25] Mandal, A., & Chakrabarty, D. (2019). Studies on mechanical, thermal, and barrier properties of carboxymethyl cellulose film highly filled with nanocellulose. *Journal of Thermoplastic Composite Materials, 32*(7), 995-1014.

[26] Loureiro, P. E., Cadete, S. M., Tokin, R., Evtuguin, D. V., Lund, H., & Johansen, K. S. (2021). Enzymatic fibre modification during production of dissolving wood pulp for regenerated cellulosic materials. *Frontiers in Plant Science, 12*, 717776.

[27] Aulin, C., Gällstedt, M., & Lindström, T. (2010). Oxygen and oil barrier properties of microfibrillated cellulose films and coatings. *Cellulose, 17*(3), 559-574.

[28] Hutton-Prager, B., Adenekan, K., Sypnewski, M., Smith, A., Meadows, M., & Calicdan, C. (2021). Hydrophobic development and mechanical properties of cellulose substrates supercritically impregnated with food-grade waxes. *Cellulose, 28*, 1633-1646.

[29] Sun, L., Han, J., Wu, J., Huang, W., Li, Y., Mao, Y., Wang, L., & Wang, Y. (2022). Cellulose pretreatment with inorganic salt hydrate: dissolution, regeneration, structure and morphology. *Industrial Crops and Products, 180*, 114722.

[30] de Souza Coelho, C. C., Silva, R. B. S., Carvalho, C. W. P., Rossi, A. L., Teixeira, J. A., Freitas-Silva, O., & Cabral, L. M. C. (2020). Cellulose nanocrystals from grape pomace and their use for the development of starch-based nanocomposite films. *International Journal of Biological Macromolecules, 159*, 1048-1061.

[31] Han, Q., Gao, X., Zhang, H., Chen, K., Peng, L., & Jia, Q. (2019). Preparation and comparative assessment of regenerated cellulose films from corn (Zea mays) stalk pulp fines in DMAc/LiCl solution. *Carbohydrate Polymers, 218*, 315-323.

[32] Xie, Y., Gao, H., Zhang, P., Qin, C., Nie, Y., & Liu, X. (2022). Preparation of degradable wood cellulose films using ionic liquids. *ACS Applied Polymer Materials*, *4*(5), 3598-3607.

[33] Li, D., Chen, Y., Xie, Y., & Feng, Q. (2023). Direct dissolution of unbleached pulp from corncob and wheat straw in N-methylmorpholine-N-oxide. *International Journal of Biological Macromolecules, 252*, 126485.

[34] Zhang, X., Xiao, N., Wang, H., Liu, C., & Pan, X. (2018). Preparation and characterization of regenerated cellulose film from a solution in lithium bromide molten salt hydrate. *Polymers, 10*(6), 614.

[35] Jin, L., Gan, J., Hu, G., Cai, L., Li, Z., Zhang, L., Zheng, Q., & Xie, H. (2019). Preparation of cellulose films from sustainable CO_2/DBU/DMSO system. *Polymers, 11*(6), 994.

[36] Ibrahim, N. A., Salleh, K. M., Fudholi, A., & Zakaria, S. (2022). Drying regimes on regenerated cellulose films characteristics and properties. *Membranes, 12*(5), 445.

[37] Zhang, Q., Wang, Z., Hao, S., & Huang, J. (2021). Preparation of all-cellulose composites based on controlled dissolution procedure. *Starch-Stärke, 73*(9-10), 2000280.

[38] Li, R., Zhang, L., & Xu, M. (2012). Novel regenerated cellulose films prepared by coagulating with water: structure and properties. *Carbohydrate Polymers*, *87*(1), 95-100.

[39] Geng, H., Yuan, Z., Fan, Q., Dai, X., Zhao, Y., Wang, Z., & Qin, M. (2014). Characterisation of cellulose films regenerated from acetone/water coagulants. *Carbohydrate Polymers, 102*, 438-444.

[40] Ruan, D., Zhang, L., Mao, Y., Zeng, M., & Li, X. (2004). Microporous membranes prepared from cellulose in NaOH/thiourea aqueous solution. *Journal of Membrane Science, 241*(2), 265-274.

[41] From, M., Larsson, P. T., Andreasson, B., Medronho, B., Svanedal, I., Edlund, H., & Norgren, M. (2020). Tuning the properties of regenerated cellulose: effects of polarity and water solubility of the coagulation medium. *Carbohydrate Polymers, 236*, 116068.

[42] Fan, J., Yang, B., Wang, Y., Gao, M., & Guan, R. (2022). Enhancing the tensile strength and heat resistance induced by high-density Ω phases in an Al–Cu–Mg–Ag alloy. *Journal of Materials Research and Technology, 18*, 3347-3357.

[43] Dam, S., Thakur, A., Das, D., Amarendra, G., & Hussain, S. (2018). Temperature dependent Raman studies of free standing thin films of cellulose. *Materials Research Express, 5*(12), 126401.

[44] El Oudiani, A., Msahli, S., & Sakli, F. (2017). In-depth study of agave fiber structure using Fourier transform infrared spectroscopy. *Carbohydrate Polymers, 164*, 242-248.

[45] Jiang, S., Liu, X., Wang, Z., Zhou, L., Meng, Z., Wang, X., Chen, G., Wang, S., & Jiang,

Y. (2023). In situ lignin modification enabling enhanced interfibrillar interactions in lignocellulosic nanomaterials toward structural applications. *ACS Sustainable Chemistry & Engineering*, *11*(20), 7705-7718.

[46] Lindman, B., Karlström, G., & Stigsson, L. (2010). On the mechanism of dissolution of cellulose. *Journal of Molecular Liquids, 156*(1), 76-81.

[47] French, A. D., & Santiago Cintrón, M. (2013). Cellulose polymorphy, crystallite size, and the Segal crystallinity index. *Cellulose, 20*, 583-588.

[48] Xing, L., Hu, C., Zhang, W., Guan, L., & Gu, J. (2020). Transition of cellulose supramolecular structure during concentrated acid treatment and its implication for cellulose nanocrystal yield. *Carbohydrate Polymers, 229*, 115539.

[49] Cheng, G., Varanasi, P., Li, C., Liu, H., Melnichenko, Y. B., Simmons, B. A., Kent, M. S., & Singh, S. (2011). Transition of cellulose crystalline structure and surface morphology of biomass as a function of ionic liquid pretreatment and its relation to enzymatic hydrolysis. *Biomacromolecules, 12*(4), 933-941.

[50] Sun, Y.-C., Xu, J.-K., Xu, F., & Sun, R.-C. (2013). Structural comparison and enhanced enzymatic hydrolysis of eucalyptus cellulose via pretreatment with different ionic liquids and catalysts. *Process Biochemistry, 48*(5-6), 844-852.

[51] Zhang, B.-x., Azuma, J.-i., & Uyama, H. (2015). Preparation and characterization of a transparent amorphous cellulose film. *RSC Advances, 5*(4), 2900-2907.

[52] Bang, Y. H., Lee, S., Park, J. B., & Cho, H. H. (1999). Effect of coagulation conditions on fine structure of regenerated cellulosic films made from cellulose/N-methylmorpholine-N-oxide/H_2O systems. *Journal of Applied Polymer Science, 73*(13), 2681-2690.

[53] Kumpikaitė, E., Varnaitė-Žuravliova, S., Tautkutė-Stankuvienė, I., & Laureckienė, G. (2021). Comparison of mechanical and end-use properties of grey and dyed cellulose and cellulose/protein woven fabrics. *Materials, 14*(11), 2860.

[54] Lettow, J. H., Yang, H., Nealey, P. F., & Rowan, S. J. (2021). Effect of graft molecular weight and density on the mechanical properties of polystyrene-grafted cellulose nanocrystal films. *Macromolecules, 54*(22), 10594-10604.

[55] Mazlan, N. S. N., Zakaria, S., Gan, S., Hua, C. C., & Baharin, K. W. (2019). Comparison of regenerated cellulose membrane coagulated in sulphate based coagulant. *Cerne, 25*, 18-24.

[56] Müller, C. M., Laurindo, J. B., & Yamashita, F. (2009). Effect of cellulose fibers on the crystallinity and mechanical properties of starch-based films at different relative humidity values. *Carbohydrate Polymers, 77*(2), 293-299.

[57] Amini, E., Hafez, I., Tajvidi, M., & Bousfield, D. W. (2020). Cellulose and lignocellulose nanofibril suspensions and films: A comparison. *Carbohydrate Polymers, 250*, 117011.

[58] Wan Ishak, W. H., Rosli, N. A., & Ahmad, I. (2020). Influence of amorphous cellulose on mechanical, thermal, and hydrolytic degradation of poly (lactic acid) biocomposites. *Scientific Reports, 10*(1), 11342.

[59] Sweygers, N., Depuydt, D. E., Eyley, S., Thielemans, W., Mosleh, Y., Ivens, J., Dewil, R., Appels, L., & Van Vuure, A. W. (2022). Prediction of the equilibrium moisture content based on the chemical composition and crystallinity of natural fibres. *Industrial Crops and Products, 186*, 115187.

[60] Garg, M., Apostolopoulou-Kalkavoura, V., Linares, M., Kaldéus, T., Malmström, E., Bergström, L., & Zozoulenko, I. (2021). Moisture uptake in nanocellulose: the effects

of relative humidity, temperature and degree of crystallinity. *Cellulose*, *28*, 9007-9021.

[61] Mihranyan, A., Llagostera, A. P., Karmhag, R., Strømme, M., & Ek, R. (2004). Moisture sorption by cellulose powders of varying crystallinity. *International Journal of Pharmaceutics, 269*(2), 433-442.

[62] Lundahl, M. J., Cunha, A. G., Rojo, E., Papageorgiou, A. C., Rautkari, L., Arboleda, J. C., & Rojas, O. J. (2016). Strength and water interactions of cellulose I filaments wet-spun from cellulose nanofibril hydrogels. *Scientific Reports*, *6*(1), 30695.

[63] Amalini, A. N., Haida, M. K. N., Imran, K., & Haafiz, M. K. M. (2019). Relationship between dissolution temperature and properties of oil palm biomass based-regenerated cellulose films prepared via ionic liquid. *Materials Chemistry and Physics, 221*, 382-389.

[64] Wu, R.-L., Wang, X.-L., Wang, Y.-Z., Bian, X.-C., & Li, F. (2009). Cellulose/soy protein isolate blend films prepared via room-temperature ionic liquid. *Industrial & Engineering Chemistry Research, 48*(15), 7132-7136.

[65] Reddy, J. P., Varada Rajulu, A., Rhim, J.-W., & Seo, J. (2018). Mechanical, thermal, and water vapor barrier properties of regenerated cellulose/nano-SiO_2 composite films. *Cellulose, 25*, 7153-7165.

[66] Saedi, S., Shokri, M., Kim, J. T., & Shin, G. H. (2021). Semi-transparent regenerated cellulose/ZnONP nanocomposite film as a potential antimicrobial food packaging material. *Journal of Food Engineering, 307*, 110665.

[67] Jo, C., Kim, S. S., Rukmanikrishnan, B., Ramalingam, S., DS, P., & Lee, J. (2022). Properties of cellulose pulp and polyurethane composite films fabricated with curcumin by using NMMO ionic liquid. *Gels, 8*(4), 248.

[68] Yang, H., Jacucci, G., Schertel, L., & Vignolini, S. (2022). Cellulose-based scattering enhancers for light management applications. *ACS Nano*, *16*(5), 7373-7379.

[69] Zhu, H., Parvinian, S., Preston, C., Vaaland, O., Ruan, Z., & Hu, L. (2013). Transparent nanopaper with tailored optical properties. *Nanoscale, 5*(9), 3787-3792.

[70] Ye, D., Lei, X., Li, T., Cheng, Q., Chang, C., Hu, L., & Zhang, L. (2019). Ultrahigh tough, super clear, and highly anisotropic nanofiber-structured regenerated cellulose films. *ACS Nano, 13*(4), 4843-4853.

[71] Zhao, G., Lyu, X., Lee, J., Cui, X., & Chen, W.-N. (2019). Biodegradable and transparent cellulose film prepared eco-friendly from durian rind for packaging application. *Food Packaging and Shelf Life, 21*, 100345.

[72] Gao, Y., Huang, C., Ge, D., Liao, Y., Chen, Y., Li, S., & Yu, H.-Y. (2024). Highly efficient dissolution and reinforcement mechanism of robust and transparent cellulose films for smart packaging. *International Journal of Biological Macromolecules, 254*, 128046.

[73] Tian, S., Jiang, J., Zhu, P., Yu, Z., Oguzlu, H., Balldelli, A., Wu, J., Zhu, J., Sun, X., & Saddler, J. (2022). Fabrication of a transparent and biodegradable cellulose film from Kraft pulp via cold alkaline swelling and mechanical blending. *ACS Sustainable Chemistry & Engineering, 10*(32), 10560-10569.

[74] Sirvio, J. A., & Lakovaara, M. (2021). A fast dissolution pretreatment to produce strong regenerated cellulose nanofibers via mechanical disintegration. *Biomacromolecules, 22*(8), 3366-3376.

[75] Bengtsson, A., Hecht, P., Sommertune, J., Ek, M., Sedin, M., & Sjöholm, E. (2020). Carbon fibers from lignin–cellulose precursors: Effect of carbonization conditions. *ACS Sustainable Chemistry & Engineering, 8*(17), 6826-6833.

[76] Beroual, M., Boumaza, L., Mehelli, O., Trache, D., Tarchoun, A. F., & Khimeche, K. (2021). Physicochemical properties and thermal stability of microcrystalline cellulose isolated from esparto grass using different delignification approaches. *Journal of Polymers and the Environment, 29*(1), 130-142.

Connecting Text

In Chapter 3, we investigated the effects of concentrated H_2SO_4 and NaOH/urea aqueous solutions on the structure and properties of RC films, highlighting differences in mechanical properties and foldability triggered by these two solutions. However, the use of concentrated H_2SO_4 in industrial applications poses significant challenges due to its high corrosion risk, safety concerns, and environmental implications. Besides, the higher porosity of RC films produced from NaOH/urea aqueous solution is beneficial for reagent accessibility and subsequent modifications. Therefore, we selected NaOH/urea aqueous solution for fabricating RC films in the following chapters. In Chapter 4, we produced RC films from different wood species and drying methods and compared their mechanical and water vapor barrier properties. Firstly, five types of wood pulps were pretreated and dissolved in NaOH/urea solution. Secondly, the resulting films were dried either under ambient conditions or by hot pressing. Thirdly, we compared the structure, mechanical, and barrier properties of the RC films. Finally, RC films with highest tensile strength and water vapor barrier property were selected to compare to plastic wrap for preserving cherry tomatoes.

Chapter 4. Wood Cellulose Films Regenerated from NaOH/Urea Aqueous Solution and Treated by Hot Pressing for Food Packaging Application

4.1. Abstract

Cellulose films made from 'green' solvent provide the possibility to mitigate environmental pollution caused by non-degradable plastic packaging. Herein, regenerated cellulose films were prepared from five wood pulps in NaOH/urea aqueous solution, dried either at ambient conditions or by hot pressing, and tested as biodegradable packaging materials. The results revealed that different wood origins did not cause much difference in the structure of cellulose films. However, hot-pressing could not only efficiently remove water from wet films, but also significantly improve the tensile strength and water vapor barrier property of regenerated films. The RC-P-HP film had the tensile strength of 85.00±3.26 MPa, Young's modulus of 6.45±0.36 GPa, and water vapor permeability of $3.59\pm0.14\times10^{-7}$ $gm^{-1}h^{-1}Pa^{-1}$, and exhibited the similar capacity as the commercial plastic wrap during the preservation of cherry tomatoes for up to 16 days. Therefore, this study demonstrates a feasible strategy to fabricate wood cellulose films for biodegradable food packaging.

4.2. Introduction

Food packaging waste accounts for approximately one-third of all household waste in Canada (Diggle & Walker, 2020). Among them, plastic waste has low secondary market value and high resistance to degradation and only 20% is collected for reuse and recycling (Diggle & Walker, 2020; Huang & Wang, 2022). The accumulation of this non-degradable waste has severe impacts on marine and terrestrial ecosystems, resulting in the urgent demand for eco-friendly food packaging materials. Cellulose is the most abundant biopolymer and has been explored as a potential alternative to petroleum-based plastics owing to its availability, renewability, and biodegradability (Shi, Wu, Luo, Yu, & Li, 2022). Wood is the most important source of cellulose, and the type of wood (e.g. hardwood and softwood) and processing conditions such

as pulping and bleaching can affect the structure of isolated cellulose (Tang et al., 2021). Wood cellulose has been studied for applications in papermaking, textiles, biomedical, and high-performance materials (Jia et al., 2018). Recently, the development of packaging materials from wood cellulose nanofibrils (CNF) has been reported. For example, Missio et al. (2020) fabricated an antioxidative film by combining CNF from *Acacia mearnsii* bark and tannins. Tayeb, Tajvidi, and Bousfield (2020) developed an oil barrier packaging material using CNF from a bleached softwood kraft pulp, and Muthoka, Panicker, Agumba, Pham, and Kim (2021) infiltrated CNF and chitosan into bleached fir veneer wood to form a transparent package.

Besides the utilization of CNF, natural cellulose fibers can also be easily converted into different materials through dissolution and regeneration (Huang, Wang, Zhang, & Chen, 2016). Traditional solvents for cellulose dissolution, such as *N*-methylmorpholine-*N*-oxide (NMMO), LiCl/DMAc, and ionic liquids (ILs), have significant disadvantages involving tedious handling processes, high energy consumption, and/or inefficient recyclability (Huang et al., 2016). The NaOH/urea aqueous system is a "green" solvent of cellulose that can disrupt the intra-/intermolecular hydrogen bonds of the supramolecular structure within cellulose (Cai & Zhang, 2005). It has been reported that the NaOH/urea system can be used to rapidly dissolve unbleached softwood kraft pulp and spruce pulp at low temperatures after a mechanical or chemical pretreatment (Shi et al., 2018; Gong, Wang, Tian, Zheng, & Chen, 2014). However, the structure and properties of regenerated cellulose (RC) films from various wood pulps have not yet been well studied. Moreover, drying methods of cellulose films, such as air drying, freeze-drying, oven drying, and hot pressing, can also affect the performance of the films. Among them, hot pressing is a convenient way to dry cellulose films in a short time using elevated temperatures and pressures (Rol, Billot, Bolloli, Beneventi, & Bras, 2020). Qing, Sabo, Wu, Zhu, and Cai (2015) found that the hot-pressed cellulose nanofibril (CNF) films showed

improved mechanical properties compared to the freeze-dried and air/oven-dried samples. Similar results were observed by Hasan, Wang, and Tajvidi (2021) that the CNF films treated by hot pressing exhibited decreased water vapor and oxygen permeability due to better consolidation of layers in the film structures.

Therefore, to develop wood cellulose films as biodegradable food packaging materials, in this work, various hardwood (aspen, eucalyptus, and maple) and softwood (pine and spruce) pulps were dissolved in NaOH/urea aqueous solution, and the corresponding RC films were dried either in the air at room temperature or by hot pressing. The structure and properties of RC films were characterized, and the RC film with the best mechanical and barrier properties was selected to preserve fresh cherry tomatoes.

4.3. Materials and methods

4.3.1 Materials

The bleached kraft pulps of aspen, eucalyptus, maple, pine, and spruce were kindly provided by FPInnovations (QC, Canada). Sulfuric acid (95.0-98.0%) was purchased from Sigma-Aldrich (Oakville, ON, Canada). Sodium hydroxide (>97.0%) and urea (>99.6%) were purchased from Fisher Scientific (Mississauga, ON, Canada). Distilled water was utilized throughout this study.

4.3.2 Preparation of wood cellulose films

The wood pulp (2g) was placed in 200mL of H_2SO_4 solution for 48h at 25°C with continuous stirring at 200rpm to reduce the molecular weight of cellulose via hydrolysis, where the concentrations of H_2SO_4 solutions were 30wt.% for aspen, pine and spruce pulps, and 25wt.% for eucalyptus and maple pulps. After acid hydrolysis, the samples were thoroughly washed with water, dried in an oven at 100°C for 16h, and dissolved (4wt.%) in the aqueous solution

containing NaOH/urea/H_2O in a 7:12:81 wt ratio. The solvent and wood pulps were pre-cooled to -20℃ and stirred at 2000rpm for 8min. The obtained solutions were centrifuged at 120×g for 5min at 25℃ to degas and precipitate the insoluble fractions, and then cast on the glass plate and coagulated in 5 wt.% H_2SO_4 aqueous bath at 25℃ for 5min to produce RC films. In one treatment, the wet RC films prepared from aspen, eucalyptus, maple, pine, and spruce were air dried at 25℃ and coded as RC-A-AD, RC-E-AD, RC-M-AD, RC-P-AD, RC-S-AD, respectively. In another aspect, the wet films were dried between two stainless steel plates of a hot press machine (3895, Carver Inc., USA) at 90℃ and 0.4MPa for 10min, followed by hot pressing at 120℃ and 18MPa for 10min. The hot-pressed RC films were labelled as RC-A-HP, RC-E-HP, RC-M-HP, RC-P-HP, RC-S-HP, respectively.

4.3.3 Characterization of wood cellulose films

The recovery rate of cellulose after acid hydrolysis was calculated using a gravimetric method by the Equation (1):

$$Recovery\ rate\ (\%) = \frac{W_2}{W_1} \times 100\% \tag{1}$$

Where W_1 is the dry weight of wood pulps before acid hydrolysis, and W_2 is the dry weight of wood pulps after acid hydrolysis.

Before viscosity-average molecular weight (M_v) measurement, original wood pulps, acid hydrolyzed wood pulps, and hot-pressed RC films were stored at 25℃ and 50% RH for 4 days to ensure same water content. The intrinsic viscosity [η] of each sample was conducted according to the TAPPI T230 standard test method. The degree of polymerization (DP) was determined by the Mark-Houwink-Sakurada equation, and the M_v values were calculated by multiplying DP by the molar mass of anhydrous glucose unit (162g/mol).

$$DP^{0.9} = 1.65[\eta] \quad (2)$$

Before density measurement, RC films (5 cm×5 cm) were conditioned at 25°C and 50% RH for 4 days. The thickness of the films was determined with a micrometer (resolution of 0.001 mm, Mitutoyo 547-400S, Japan) at 10 random points. The density was calculated by the ratio of weight and volume, and the apparent porosity was calculated based on the densities of RC films (ρ_f) and crystalline cellulose (ρ_c = 1.63g/cm^3) as shown in Equation (3) (Aulin, Gällstedt, & Lindström, 2010):

$$Porosity\ (\%) = \frac{\rho_c - \rho_f}{\rho_c} \times 100\% \quad (3)$$

The FT-IR spectra of RC films were recorded on an Agilent Technologies Cary 630 FT-IR spectrometer (Agilent Technologies Inc., CA, USA) as the average of 64 scans with a resolution of 2 cm^{-1}. The crystalline profile of wood pulps and RC films was measured using a high-resolution X-ray diffractometer (Empyrean, Malvern Panalytical Ltd, Malvern, UK) with copper Kα radiation (1.54178 Å) in 2θ ranging from 4° to 40°. The surface morphology of RC films was observed by a Hitachi TM1000 SEM (Hitachi Co. Ltd., Tokyo, Japan) with an acceleration voltage of 4kV. The samples were sputter-coated with a 4nm layer of gold-palladium using a Leica EM ACE200 coater (ON, Canada) prior to observation.

The tensile strength, elongation at break, and Young's modulus of RC films were tested at 25°C and 50% RH by using an ADMET MTEST Quattro eXpert 7600 single-column testing system (MA, USA) with a load cell of 250 lb. and a crosshead speed of 5 mm/min. The water vapor permeability (WVP) of RC films was determined based on the ASTM E96-92 standard (ASTM, 1995). A dried film was taped on the top of a glass flask containing 3g of anhydrous calcium chloride. The sealed glass flask was then located in a desiccator with water to reach a relative humidity of 100%. The weight change of the flask was recorded periodically at 25°C. The WVP

($g\ m^{-1}\ h^{-1}\ Pa^{-1}$) of films was calculated by the Equation (4):

$$WVP = \frac{\Delta m \times k}{A \times \Delta T \times \Delta P} \tag{4}$$

Where Δm is the weight change of the flask (g) during time ΔT (h), k is the thickness of each RC film (m), A is the exposed area of the film ($7.85 \times 10^{-5} m^2$), and ΔP is the partial water vapor pressure difference between two sides of the film (Pa). The oxygen transmission rate (OTR) of RC films was determined at 23°C and 0% RH using the Mocon Ox-Tran Model 2/22 (Mocon, Minneapolis, USA). The oxygen permeability (OP) was calculated by the Equation (5):

$$OP = \frac{OTR \times \ell}{\Delta P'} \tag{5}$$

where OTR is oxygen transmission rate, ℓ is the film thickness, and $\Delta P'$ is the partial pressure of oxygen (kPa).

4.3.4 Study of shelf life

The evaluation of the preservation effect of cellulose films on fruits was based on the methods of Guo, Chen, Wu, Li, and Sun (2020) with slight modifications. Fresh cherry tomatoes washed with deionized water were placed in glass jars and covered with polyvinyl chloride plastic wrap (Kirkland Signature Stretch-Tite Plastic Wrap - 11 7/8×750 Feet) and RC-P-HP. The tomatoes without any package were set as the control. All samples were stored at 25°C and 50% RH for a maximum of 3 weeks to monitor the appearance and weight loss.

4.3.5 Statistical analysis

Each measurement was performed in triplicate, and the experimental data were presented as the mean ± standard deviation. Analysis of variance (ANOVA) was applied for the statistical analysis, followed by multiple comparison tests via Duncan's multiple-range test. All the analyses were carried out through SPSS statistical software (version 26, IBM SPSS Inc., New

York, NY) with significant differences within samples at $p < 0.05$.

4.4. Results and discussion

As listed in Table 4.1, all the samples had a high recovery rate (~90%) after acid hydrolysis. The M_v values of original wood pulps ranged from 2.87×10^5 to 6.28×10^5g/mol, which decreased to the range of 1.53×10^5 to 2.33×10^5g/mol after acid hydrolysis. The molecular weight of hot-pressed RC films was relatively lower because a few insoluble fractions (~0.3%) were removed by centrifugation and the slight degradation happened during dissolution and regeneration process (Wang, Zhao & Deng, 2008).

Table 4.1. Recovery rate and molecular weight (M_v) of wood pulps and hot-pressed films.

Wood pulps	Recovery rates (%)	M_v (g/mol)		
		Original wood pulps	After acid hydrolysis	Hot-pressed films
Aspen	89.53±0.35	6.28×10^5	2.33×10^5	1.70×10^5
Eucalyptus	92.25±1.11	4.41×10^5	1.53×10^5	1.15×10^5
Maple	90.01±1.73	2.87×10^5	1.70×10^5	9.23×10^4
Pine	91.85±2.01	5.26×10^5	1.90×10^5	1.46×10^5
Spruce	92.42±1.86	4.54×10^5	1.85×10^5	7.51×10^4

The average thickness of RC films produced by air-drying was 33±3μm, while the hot-pressed RC films were significantly thinner (27±1μm). As shown in Fig. 4.1, different sources of wood pulps did not affect the density and porosity of RC films, but the hot pressing treatment remarkably increased the density from approximately 0.95g/cm^3 to 1.15g/cm^3 and reduced the porosity from about 35% to 22.5%. Similar results have been reported that RC films dried with applied pressure could form dense structures (Shahi, Min, Sapkota, & Rangari, 2020). The

decreased free space and cavities in RC films could contribute to the improvement in mechanical strength and gas barrier properties (Aulin et al., 2010; Wakabayashi, Fujisawa, Saito, & Isogai, 2020).

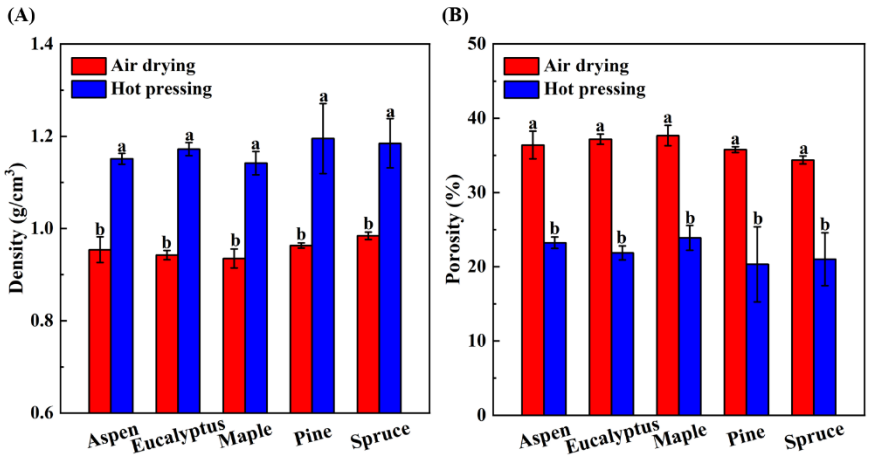

Fig. 4.1. Density (A) and porosity (B) of RC films. Different letters on the tops of columns represented the significant difference (p<0.05).

FT-IR spectra and XRD diffraction patterns of various wood pulps and RC films were collected to investigate the effects of cellulose dissolution and regeneration in NaOH/urea aqueous solution and different drying methods on cellulose structure. As shown in Fig. 4.2 A-C, all samples displayed similar FT-IR spectra with no new peaks after dissolution, regeneration and drying, which demonstrated no chemical modifications happened during film production. However, changes in the intensity of the peaks were observed. For instance, the intensities of absorption peaks at around 3360 and 3269cm^{-1} decreased after dissolution and regeneration, while the hot-pressed films presented even lower intensities than the air-dried films. These two peaks were attributed to the O─H stretching vibration of the hydroxyl groups, which indicated the intra- and intermolecular hydrogen bonds in cellulose, respectively (Zhou & Wang, 2021). The hydrogen bonds were broken during the dissolution, and the rearrangement happened during the regeneration and drying process. The rapid coagulation and drying process of RC

films led to the disturbed intermolecular interaction and decreased intensities at 3330 and 3269cm^{-1} (Lindman, Medronho, Alves, Costa, Edlund, & Norgren, 2017). Besides, the peak at 1427cm^{-1} was the absorption band of the crystalline cellulose due to asymmetric ─CH_2 bending vibration, while the peak at 898 cm^{-1} was the ─C─O─C─ bridge stretching, representing the amorphous region and cellulose II crystalline structure (Md Salim, Asik, & Sarjadi, 2021) The ratio of peak intensities at 1427 and 898cm^{-1} was defined as "crystallinity index", which was decreased after dissolution and regeneration, indicating the decrease in crystallinity and the transition from cellulose I to cellulose II structure (Md Salim et al., 2021; Zhou et al., 2021). As shown in Fig. 4.2 D-E, the wood pulps displayed similar diffraction peaks at about 14.8° ($1\bar{1}0$), 16.3° (110), 22.5° (200), and 34° (040), which were typical cellulose I structure (Zhou et al., 2021). After the dissolution and regeneration process, the RC films showed cellulose II structure with broad diffraction peaks at 20.2° and 22.6°, corresponding to (110) and (020) crystallographic planes, respectively (Razali et al., 2022). The crystallinity indices (CI) of RC films were significantly lower than those of the wood pulps. It indicated a crystal transformation of cellulose I to cellulose II during dissolution and regeneration, which was in accordance with the FT-IR results. The sources of wood pulps did not affect the diffraction patterns of RC films.

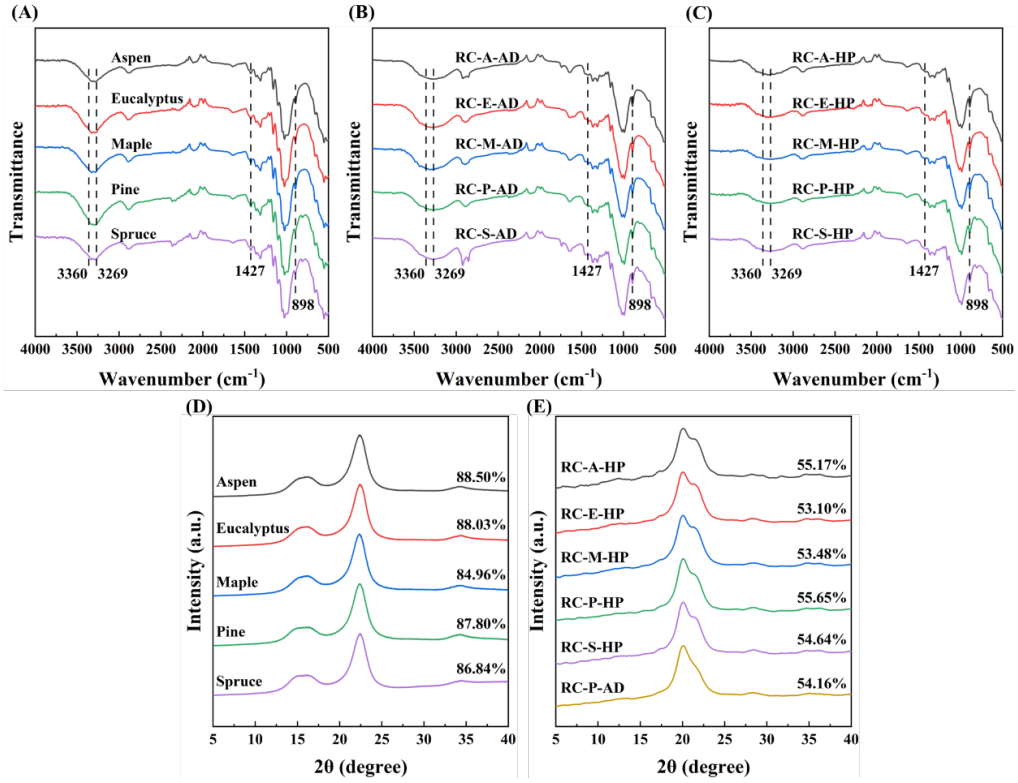

Fig. 4.2. Fourier transform infrared spectroscopy spectra of wood pulp cellulose (A), air-dried RC films (B), and hot-pressed RC films (C). X-ray diffraction patterns and crystallinity index of wood cellulose pulps (D) and RC films (E).

The morphology of RC films dried by different methods was observed by SEM. As shown in Fig. 4.3 A, no obvious undissolved fibers were observed on the surface of RC films, indicating a good solubility of hydrolyzed wood pulp cellulose in NaOH/urea aqueous solution. However, the air-dried RC films showed uneven and rough surfaces and layered cross-sections (Fig. 4.3 B), which might be due to the inevitable non-uniform shrinkage during the air-drying process (Ketola et al., 2018). In contrast, the hot-pressed RC films possessed smooth and uniform surfaces and dense internal structures. It was because the hot pressing treatment could facilitate the stretch and rearrangement of cellulose chains and effectively reduce the free space and cavities in the RC films (Wang et al., 2013). Moreover, the air-dried RC films were not as

transparent as the hot-pressed ones (Fig. 4.3 C). It was due to the uneven structure and larger thickness of air-dried RC films. The high transparency of RC films is beneficial for displaying the food products in packaging.

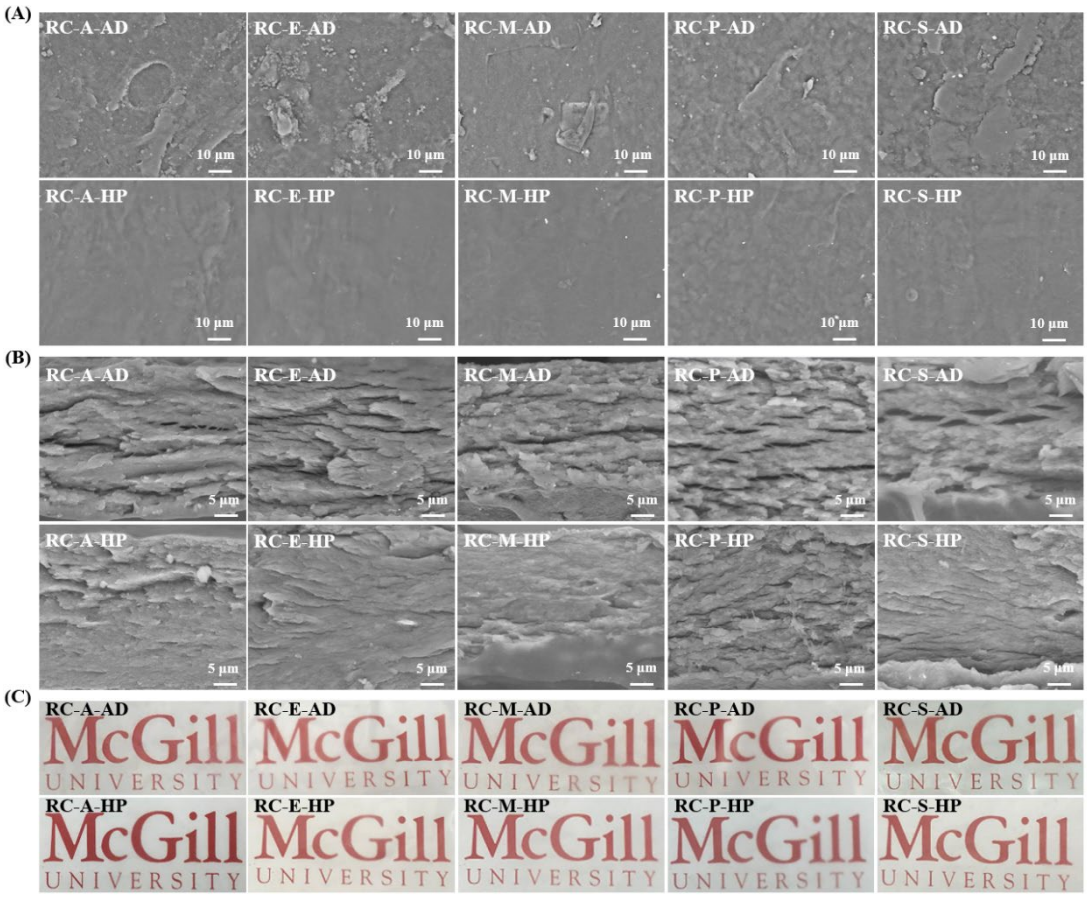

Fig. 4.3. SEM images of RC films: surface (A) and cross-section (B). Photos of RC films (C).

The mechanical properties of RC films are essential because food packaging materials need to maintain the integrity and preserve the quality of packaged food (Ai et al., 2021). As shown in Fig. 4.4 A and Fig. 4.4 C, the tensile strength and Young's modulus of RC films produced from pine were significantly higher than those of other RC films. It might be due to the variation of molecular weight and CI of cellulose from different sources (Aulin et al., 2010; De Silva & Byrne, 2017; Mokhena et al., 2021; Yousefi et al., 2013). For example, the higher M_v value of cellulose could enhance the intermolecular entanglement, leading to an improved tensile

strength of cellulose film (Jin et al., 2019); however, the aggregation and entanglement of cellulose chains also restricted the molecular orientation during dissolution and regeneration processes, and resulted in the decreased tensile strength (Xie et al. 2021). At the same time, the high content of the crystalline structure led to an enhanced tensile strength (Shi et al., 2021). As expected, the hot-pressed RC films possessed notable enhancement in tensile strength and modulus compared to the air-dried films. These different mechanical properties were attributed to the density and porosity (Cazón, Velazquez, & Vázquez, 2019). It has been demonstrated that pores and free volume affects the mechanical properties of the material, since the less solid material per unit volume, the weaker the resistance to deformation (Cao et al., 2020; Su, Rao, He, & Wei, 2020). The RC-P-HP sample exhibited the highest tensile strength of 85.00±3.26MPa and Young's modulus of 6.45±0.36GPa and was stronger than the RC films fabricated from bamboos in DMAc/LiCl solvent (81.09MPa) (Gao, Li, Zhang, Tang, & Chen, 2021), corncob residue in ionic liquid (70.63MPa) (Song, Chen, Chen, Xu, & Xu, 2021), bed sheets in NaOH/urea solution (76.21MPa) (Zhou & Wang, 2021), and cotton linter pulps in NaOH/urea solution (73.40MPa) (Reddy, Varada Rajulu, Rhim, & Seo, 2018).

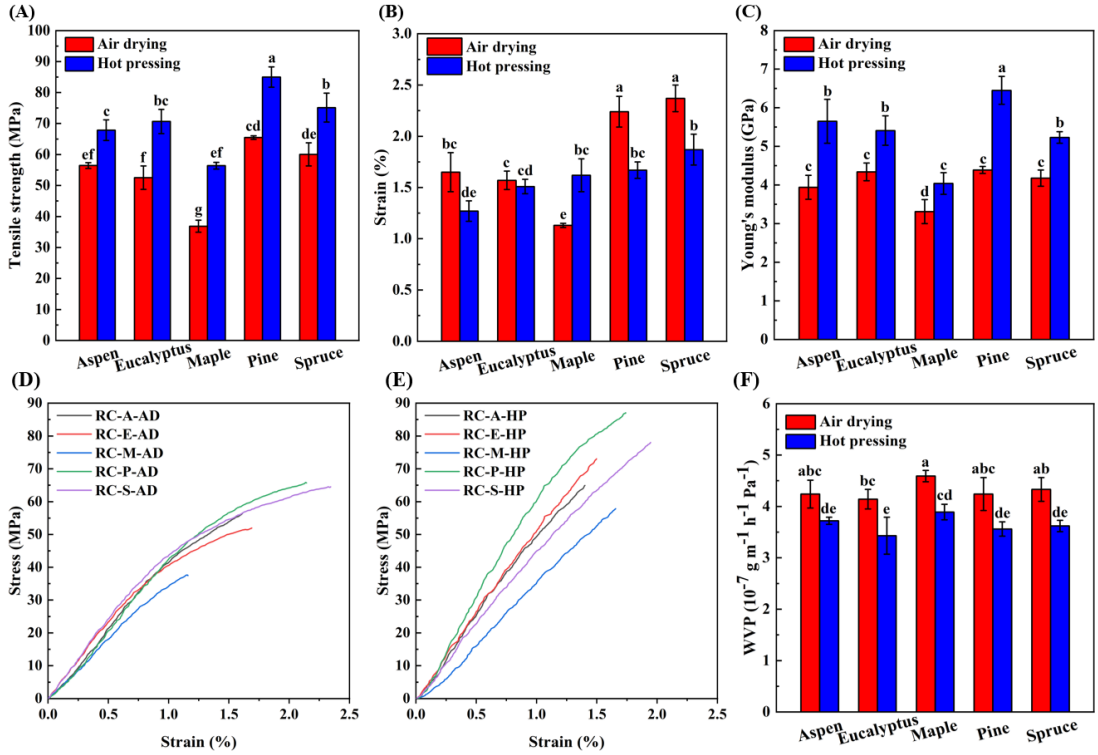

Fig. 4.4. Mechanical properties (A-E) and WVP (F) of RC films. Different letters on the tops of columns represented the significant difference ($p < 0.05$).

The WVP values of RC films dried by different methods are shown in Fig. 4.4 F. Despite the sources of wood pulps, the air-dried RC films displayed similar WVP values ranging from 4.14±0.19 to 4.59±0.11×10^{-7} g m^{-1} h^{-1} Pa^{-1}, while the hot pressing treatment significantly decreased the values to the range of 3.43±0.36 to 3.89±0.15×10^{-7} g m^{-1} h^{-1} Pa^{-1}. The hot-pressed films had reduced apparent porosity, which slowed down the diffusion of water vapor. It is well known that the water vapor barrier property of cellulose films is not ideal because of their hydrophilic nature, and chemical modifications are usually required (Li, Wang, Wang, Qin, & Wu, 2019). The improvement in barrier properties through hot pressing treatment could avoid using chemical reagents and eliminate possible contamination from chemical residues. It was worth noting that the WVP values of most RC films in this work were lower than those of RC films manufactured from oil palm biomass (4.68×10^{-7} g m^{-1} h^{-1} Pa^{-1}) (Amalini, Haida,

Imran, & Haafiz, 2019) and cotton linter pulp (8.21×10^{-6} g m^{-1} h^{-1} Pa^{-1}) (Reddy et al., 2018). Packaging materials with suitable mechanical and barrier properties can protect food products from physical damage, oxidation, loss of nutrients, and dehydration, and thereby extend the shelf life (Pandey, Sharma, & Gundabala, 2022; Yilmaz, Demirhan, & Ozbek, 2022). Based on the above-mentioned results, the RC-P-HP film with relatively good tensile strength and water vapor barrier property was selected for the shelf-life study and comparison with commercial plastic wrap. As shown in Fig. 4.5 A, the unpackaged cherry tomatoes became soft and exhibited obvious wrinkles on the surface on day 10, and completely deteriorated with a putrid odor on day 16. However, the tomatoes packaged with plastic wrap and RC-P-HP film well maintained their bright red color and hardness on day 10, and only showed minor shrinkages without putridity on day 16. The dehydration of fruits affects their shelf life and commercial value (Fich, Fisher, Zamir, & Rose, 2020). The weight loss of unwrapped and packaged cherry tomatoes over 16 days was monitored and displayed in Fig. 4.5 B. The unwrapped tomatoes lost about 21.72% of their original weight on day 16. This was lowered to 10.40% and 11.25% when commercial plastic wrap and RC-P-HP film were applied, respectively. The weight loss of cherry tomatoes was mainly due to water loss from transpiration and respiration processes. The WVP value of RC-P-HP ($3.56\pm0.14\times10^{-7}$g m^{-1} h^{-1} Pa^{-1}) was higher than the plastic wrap ($2.37\pm0.17\times10^{-8}$g m^{-1} h^{-1} Pa^{-1}). However, the OTR value of plastic wrap exceeded the detection limit (2000cc/m^2 day), and its OP value was higher than 0.02cc m^{-1} day^{-1} atm^{-1} compared to $3.01\pm0.49\times10^{-5}$cc m^{-1} day^{-1} atm^{-1} for RC-P-HP. It was reported that the composite film of gelatin and carboxymethyl cellulose with a WVP value of 5.47×10^{-7}g m^{-1} h^{-1} Pa^{-1} and OP of 1.32×10^{-4}cc m^{-1} day^{-1} atm^{-1} led to 23.22% weight loss of packed cherry tomatoes after 14 days' storage (Samsi, Kamari, Din, & Lazar, 2019). Thus, RC-P-HP effectively prevented the weight loss of cherry tomatoes due to the significantly reduced OP and relatively low WVP values.

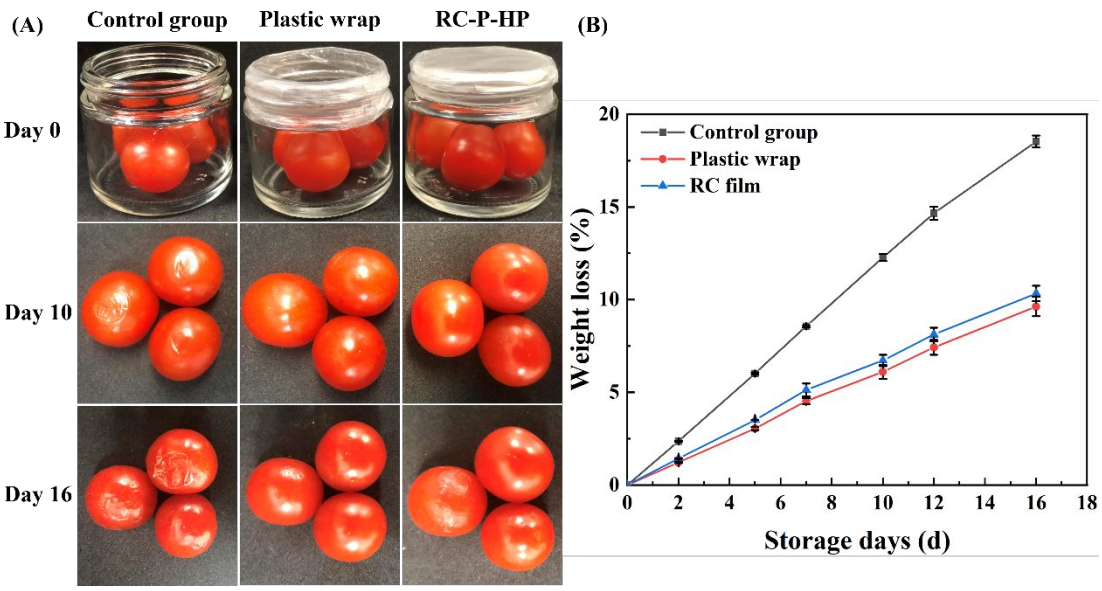

Fig. 4.5. Appearance (A) and weight loss (B) of cherry tomatoes under different packaging conditions.

4.5. Conclusion

After acid hydrolysis, five wood pulps were successfully dissolved in NaOH/urea aqueous solution. The type of wood pulps showed no remarkable impact on the structure of RC films, and all films were transparent for displaying the packaged products. Furthermore, the hot pressing process resulted in the RC films with smoother surfaces and fewer cavities compared to the air-dried films, which contributed to the dramatically improved mechanical strength and water vapor barrier property. Among all the samples, the RC-P-HP film made from pine showed the best properties and could effectively prevent the weight loss and deterioration of the wrapped cherry tomatoes for up to 16 days. This performance was comparable to the commercial plastic wrap, and thus the hot-pressed RC films had the potential applications in biodegradable food packaging.

4.6. References

Ai, B., Zheng, L., Li, W., Zheng, X., Yang, Y., Xiao, D., ..., Sheng, Z. (2021). Biodegradable

cellulose film prepared from banana pseudo-stem using an ionic liquid for mango preservation. *Frontiers in Plant Science, 12*, 234. DOI: 10.3389/fpls.2021.625878

Amalini, A. N., Haida, M. K. N., Imran, K., & Haafiz, M. K. M. (2019). Relationship between dissolution temperature and properties of oil palm biomass based-regenerated cellulose films prepared via ionic liquid. *Materials Chemistry and Physics, 221*, 382-389. DOI: 10.1016/j.matchemphys.2018.09.028

ASTM. (1995). Standard test methods for water vapor transmission of material, E96-95. *Annual book of ASTM standards, 4*, 697-704.

Aulin, C., Gällstedt, M., & Lindström, T. (2010). Oxygen and oil barrier properties of microfibrillated cellulose films and coatings. *Cellulose, 17*(3), 559-574. DOI: 10.1007/s10570-009-9393-y

Cai, J., & Zhang, L. (2005). Rapid dissolution of cellulose in LiOH/urea and NaOH/urea aqueous solutions. *Macromolecular Bioscience, 5*(6), 539-548. DOI: 10.1002/mabi.200400222

Cao, H., Luo, Z., Wang, C., Wang, J., Hu, T., Xiao, L., & Che, J. (2020). The stress concentration mechanism of pores affecting the tensile properties in vacuum die casting metals. *Materials, 13*(13), 3019. DOI: 10.3390/ma13133019

Cazón, P., Velazquez, G., & Vázquez, M. (2019). Novel composite films from regenerated cellulose-glycerol-polyvinyl alcohol: Mechanical and barrier properties. *Food Hydrocolloids, 89*, 481-491. DOI: 10.1016/j.foodhyd.2018.11.012

De Silva, R., & Byrne, N. (2017). Utilization of cotton waste for regenerated cellulose fibres: Influence of degree of polymerization on mechanical properties. *Carbohydrate Polymers, 174*, 89-94. DOI: 10.1016/j.carbpol.2017.06.042

Diggle, A., & Walker, T. R. (2020). Implementation of harmonized extended producer responsibility strategies to incentivize recovery of single-use plastic packaging waste in Canada. *Waste Management, 110*, 20-23. DOI: 10.1016/j.wasman.2020.05.013

Fich, E. A., Fisher, J., Zamir, D., & Rose, J. K. (2020). Transpiration from tomato fruit occurs primarily via trichome-associated transcuticular polar pores. *Plant Physiology, 184*(4), 1840-1852. DOI: 10.1104/pp.20.01105

Gao, X., Li, M., Zhang, H., Tang, X., & Chen, K. (2021). Fabrication of regenerated cellulose films by DMAc dissolution using parenchyma cells via low-temperature pulping from Yunnan-endemic bamboos. *Industrial Crops and Products, 160*, 113116. DOI: 10.1016/j.indcrop.2020.113116

Gong, X., Wang, Y., Tian, Z., Zheng, X., & Chen, L. (2014). Controlled production of spruce cellulose gels using an environmentally "green" system. *Cellulose, 21*(3), 1667-1678. DOI: 10.1007/s10570-014-0200-z

Guo, X., Chen, B., Wu, X., Li, J., & Sun, Q. (2020). Utilization of cinnamaldehyde and zinc oxide nanoparticles in a carboxymethylcellulose-based composite coating to improve the postharvest quality of cherry tomatoes. *International Journal of Biological Macromolecules, 160*, 175-182. DOI: 10.1016/j.ijbiomac.2020.05.201

Hasan, I., Wang, J., & Tajvidi, M. (2021). Tuning physical, mechanical and barrier properties of cellulose nanofibril films through film drying techniques coupled with thermal compression. *Cellulose, 28*(18), 11345-11366. DOI: 10.1007/s10570-021-04269-9

Huang, K., & Wang, Y. (2022). Recent applications of regenerated cellulose films and hydrogels in food packaging. *Current Opinion in Food Science, 43*, 7-17. DOI: 10.1016/j.cofs.2021.09.003

Huang, W., Wang, Y., Zhang, L., & Chen, L. (2016). Rapid dissolution of spruce cellulose in H_2SO_4 aqueous solution at low temperature. *Cellulose, 23*(6), 3463-3473. DOI: 10.1007/s10570-016-1047-2

Jia, C., Chen, C., Kuang, Y., Fu, K., Wang, Y., Yao, Y., ..., Xu, F. (2018). From wood to textiles: Top-down assembly of aligned cellulose nanofibers. *Advanced Materials, 30*(30), 1801347. DOI: 10.1002/adma.201801347

Jin, L., Gan, J., Hu, G., Cai, L., Li, Z., Zhang, L., ... & Xie, H. (2019). Preparation of cellulose films from sustainable CO_2/DBU/DMSO system. *Polymers*, *11*(6), 994. DOI: 10.3390/polym11060994

Ketola, A. E., Strand, A., Sundberg, A., Kouko, J., Oksanen, A., Salminen, K., ..., Retulainen, E. (2018). Effect of micro-and nanofibrillated cellulose on the drying shrinkage, extensibility, and strength of fibre networks. *BioResources, 13*(3), 5319-5342. DOI: 10.15376/biores.13.3.5319-5342

Lindman, B., Medronho, B., Alves, L., Costa, C., Edlund, H., & Norgren, M. (2017). The relevance of structural features of cellulose and its interactions to dissolution, regeneration, gelation and plasticization phenomena. *Physical Chemistry Chemical Physics, 19*(35), 23704-23718. DOI: 10.1039/C7CP02409F

Li, W., Wang, S., Wang, W., Qin, C., & Wu, M. (2019). Facile preparation of reactive hydrophobic cellulose nanofibril film for reducing water vapor permeability (WVP) in packaging applications. *Cellulose, 26*(5), 3271-3284. DOI: 10.1007/s10570-019-02270-x

Md Salim, R., Asik, J., & Sarjadi, M. S. (2021). Chemical functional groups of extractives, cellulose and lignin extracted from native *Leucaena leucocephala* bark. *Wood Science and Technology, 55*(2), 295-313. DOI: 10.1007/s00226-020-01258-2

Missio, A. L., Mattos, B. D., Otoni, C. G., Gentil, M., Coldebella, R., Khakalo, A., ..., Rojas, O. J. (2020). Cogrinding wood fibers and tannins: Surfactant effects on the interactions and properties of functional films for sustainable packaging materials. *Biomacromolecules, 21*(5), 1865-1874. DOI: 10.1021/acs.biomac.9b01733

Mokhena, T. C., Sadiku, E. R., Mochane, M. J., Ray, S. S., John, M. J., & Mtibe, A. (2021). Mechanical properties of cellulose nanofibril papers and their bionanocomposites: A review. *Carbohydrate Polymers, 273*, 118507. DOI: 10.1016/j.carbpol.2021.118507

Muthoka, R. M., Panicker, P. S., Agumba, D. O., Pham, H. D., & Kim, J. (2021). All-biobased transparent-wood: A new approach and its environmental-friendly packaging application. *Carbohydrate Polymers, 264*, 118012. DOI: 10.1016/j.carbpol.2021.118012

Pandey, S., Sharma, K., & Gundabala, V. (2022). Antimicrobial bio-inspired active packaging materials for shelf life and safety development: A review. *Food Bioscience*, *48*, 101730. DOI: 10.1016/j.fbio.2022.101730

Qing, Y., Sabo, R., Wu, Y., Zhu, J., & Cai, Z. (2015). Self-assembled optically transparent cellulose nanofibril films: Effect of nanofibril morphology and drying procedure. *Cellulose, 22*(2), 1091-1102. DOI: 10.1016/j.carbpol.2021.118012

Razali, N. A. M., Mohd Sohaimi, R., Othman, R. N. I. R., Abdullah, N., Demon, S. Z. N., Jasmani, L., ..., Norizan, M. N. (2022). Comparative study on extraction of cellulose fiber from rice straw waste from chemo-mechanical and pulping method. *Polymers, 14*(3), 387. DOI: 10.3390/polym14030387

Reddy, J. P., Varada Rajulu, A., Rhim, J.-W., & Seo, J. (2018). Mechanical, thermal, and water vapor barrier properties of regenerated cellulose/nano-SiO_2 composite films. *Cellulose, 25*(12), 7153-7165. DOI: 10.1007/s10570-018-2059-x

Rol, F., Billot, M., Bolloli, M., Beneventi, D., & Bras, J. (2020). Production of 100% cellulose nanofibril objects using the molded cellulose process: A feasibility study. *Industrial & Engineering Chemistry Research, 59*(16), 7670-7679. DOI: 10.1021/acs.iecr.9b06127

Samsi, M. S., Kamari, A., Din, S. M., & Lazar, G. (2019). Synthesis, characterization and application of gelatin–carboxymethyl cellulose blend films for preservation of cherry tomatoes and grapes. *Journal of food science and technology*, *56*(6), 3099-3108. DOI: 10.1007/s13197-019-03809-3

Shahi, N., Min, B., Sapkota, B., & Rangari, V. K. (2020). Eco-friendly cellulose nanofiber extraction from sugarcane bagasse and film fabrication. *Sustainability, 12*(15), 6015. DOI: 10.3390/su12156015

Shi, Z., Liu, Y., Xu, H., Yang, Q., Xiong, C., Kuga, S., & Matsumoto, Y. (2018). Facile dissolution of wood pulp in aqueous NaOH/urea solution by ball milling pretreatment. *Industrial Crops and Products, 118*, 48-52. DOI: 10.1016/j.indcrop.2018.03.035

Shi, S. C., Chen, C., Zhu, J. L., Li, Y., Meng, X., Huang, H. D., & Li, Z. M. (2021). Environmentally friendly regenerated cellulose films with improved dielectric properties via manipulating the hydrogen bonding network. *Applied Physics Letters*, *119*(2), 022903. DOI: 10.1063/5.0056164

Shi, H., Wu, L., Luo, Y., Yu, F., & Li, H. (2022). A facile method to prepare cellulose fiber-based food packaging papers with improved mechanical strength, enhanced barrier, and antibacterial properties. *Food Bioscience*, *48*, 101729. DOI: 10.1016/j.fbio.2022.101729

Song, Y., Chen, S., Chen, Y., Xu, Y., & Xu, F. (2021). Biodegradable and transparent films with tunable UV-blocking property from Lignocellulosic waste by a top-down approach. *Cellulose, 28*(13), 8629-8640. DOI: 10.1007/s10570-021-03994-5

Su, S.-l., Rao, Q.-h., He, Y.-H., & Wei, X. (2020). Effects of porosity on tensile mechanical properties of porous FeAl intermetallics. *Transactions of Nonferrous Metals Society of China, 30*(10), 2757-2763. DOI: 10.1016/S1003-6326(20)65418-8

Tang, X., Liu, G., Zhang, H., Gao, X., Li, M., & Zhang, S. (2021). Facile preparation of all-cellulose composites from softwood, hardwood, and agricultural straw cellulose by a simple route of partial dissolution. *Carbohydrate Polymers, 256*, 117591. DOI: 10.1016/j.carbpol.2020.117591

Tayeb, A. H., Tajvidi, M., & Bousfield, D. (2020). Paper-based oil barrier packaging using lignin-containing cellulose nanofibrils. *Molecules, 25*(6), 1344. DOI: 10.3390/molecules25061344

Wakabayashi, M., Fujisawa, S., Saito, T., & Isogai, A. (2020). Nanocellulose film properties tunable by controlling degree of fibrillation of TEMPO-oxidized cellulose. *Frontiers in Chemistry, 8*, 37. DOI: 10.3389/fchem.2020.00037

Wang, Q., Cai, J., Zhang, L., Xu, M., Cheng, H., Han, C. C., ..., Xiao, R. (2013). A bioplastic with high strength constructed from a cellulose hydrogel by changing the aggregated structure. *Journal of Materials Chemistry A, 1*(22), 6678-6686. DOI: 10.1039/C3TA11130J

Wang, Y., Zhao, Y., & Deng, Y. (2008). Effect of enzymatic treatment on cotton fiber dissolution in NaOH/urea solution at cold temperature. *Carbohydrate Polymers*, *72*(1), 178-184. DOI: 10.1016/j.carbpol.2007.08.003

Xie, K., Tu, H., Dou, Z., Liu, D., Wu, K., Liu, Y., ... & Fu, Q. (2021). The effect of cellulose molecular weight on internal structure and properties of regenerated cellulose fibers as spun from the alkali/urea aqueous system. *Polymer*, *215*, 123379. DOI:

10.1016/j.polymer.2021.123379

Yilmaz, P., Demirhan, E., & Ozbek, B. (2022). Development of *Ficus carica* Linn leaves extract incorporated chitosan films for active food packaging materials and investigation of their properties. *Food Bioscience*, *46*, 101542. DOI: 10.1016/j.fbio.2021.101542

Yousefi, H., Faezipour, M., Hedjazi, S., Mousavi, M. M., Azusa, Y., & Heidari, A. H. (2013). Comparative study of paper and nanopaper properties prepared from bacterial cellulose nanofibers and fibers/ground cellulose nanofibers of canola straw. *Industrial Crops and Products, 43*, 732-737. DOI: 10.1016/j.indcrop.2012.08.030

Zhou, C., & Wang, Y. (2021). Recycling of waste cotton fabrics into regenerated cellulose films through three solvent systems: A comparison study. *Journal of Applied Polymer Science, 138*(48), 51255. DOI: 10.1002/app.51255

Connecting Text

In Chapter 4, five wood pulps did not lead to significant structural difference in RC films, while the hot-pressing treatment resulted in a denser structured RC film with improved tensile strength and water vapor barrier property. However, the hygroscopic nature of cellulose diminished the superior mechanical properties of RC films and limited the application of RC films under high humidity and wet conditions. Chapter 5 aimed to enhance the water resistance of RC films under high humidity conditions without changing their disintegration rate. Firstly, CNC was isolated from wood pulp using concentrated H_2SO_4 solution. Secondly, RC films were dually modified by chemical vapor deposition of two organosilanes and incorporation of CNC. Thirdly, the effects of dual modifications on structure, mechanical, and barrier properties of RC films were investigated. Finally, the food packaging performance and disintegration ability of modified RC films were examined.

Chapter 5. Enhancing Water Resistance of Regenerated Cellulose films with Organosilanes and Cellulose Nanocrystals for Food Packaging

5.1. Abstract

Cellulose has been explored as potential alternative to traditional petroleum-based packaging materials, but its hygroscopic features lead to fast penetration of water and reduced mechanical properties of cellulose-based materials under humid and wet conditions. Chemical vapor deposition of organosilanes can incorporate hydrophobic moieties to overcome water sensitivity, but also decrease the strength of cellulose films. Herein, two commonly used organosilanes were selected to improve the water resistance of cellulose films, and cellulose nanocrystals were incorporated to compensate for the loss in mechanical strength. The results revealed that the films with dual modifications showed the unchanged tensile strength of around 57 MPa when the environmental relative humidity increased from 0 to 60% and the highest wet strength of about 12 MPa compared to the original and singly modified cellulose films. The water vapor permeability significantly decreased from 4.07×10^{-7} to about 3.3×10^{-7} $g \cdot m^{-1} \cdot h^{-1} \cdot Pa^{-1}$ after the modification, and all the films could completely disintegrate within 14 days. Moreover, the cookies preserved by the modified cellulose films for 100 days showed similar weight gain (~1.2%) and lower peroxide value (~5.6 meq/kg) than the ones covered by commercial plastic wrap. Therefore, this study presents a promising approach to develop cellulose films with enhanced water resistance for food packaging applications.

5.2. Introduction

Cellulose is an abundant and environmentally friendly natural polymer that has been developed as a potential alternative to replace traditional petroleum-based packaging materials (Zhao, Lyu, Lee, Cui, & Chen, 2019). Derived mainly from wood pulp, cellulose can be dissolved in aqueous NaOH/urea solution, overcoming dense hydrogen bonding and enabling its conversion into various forms of food packaging, including hydrogels (Zhao et al., 2022), films (Ramesh

& Radhakrishnan, 2019), coatings (Jin, Tang, Liu, Wang, & Ye, 2021), etc. Regenerated cellulose (RC) films are the primary form for developing biodegradable food packaging materials, owing to their rapid and efficient preparation process involving dissolution and regeneration. Furthermore, the films can be subjected to a hot-pressing treatment to significantly improve their tensile strength and gas barrier properties, while also achieving a dense structure and smooth surface (Huang, Maltais, Liu, & Wang, 2022).

Although the produced RC films have great potential in food packaging, the fast penetration of water molecules and swelling of RC films are commonly observed under wet or humid conditions, which are due to the natural hygroscopic features of cellulose. Besides, the absorbed water molecules weaken the intermolecular hydrogen bonding of cellulose, leading to the reduced mechanical strength and restricted barrier properties of RC films (Liao et al., 2012). Many efforts have been devoted to incorporating hydrophobic moieties onto hygroscopic surfaces, including impregnation of resins (Wu et al., 2018), incorporation of wax (Zhu, Ying, Zhang, Xu, & Chang, 2022), coating with surfactants (Wang, Liu, Chen, Zhang, & Lu, 2018), and chemical modifications such as acylation (Deng, Huang, Zhou, Chen, & Fu, 2016), esterification (LakshmiBalasubramaniam, Howell, Tajvidi, & Skonberg, 2022), silylation (Yu, Zhang, Tang, & Zhou, 2019), grafting (Yuan & Wen, 2018), etc. In recent years, researchers have focused on developing hydrophobic cellulose films to overcome the water sensitivity for packaging purpose. For instance, Li et al. (2019c) fabricated a hydrophobic cellulose film by attaching 10-undecylenoyl chloride onto cellulose nanofibril film (CNF) by vacuum filtration. Esterification with syringic acid and vanillic acid, using carbodiimide and tosyl chloride coupling agents, enhanced the hydrophobicity of CNF films (LakshmiBalasubramaniam et al., 2022), and another cellulose-based bioplastic was produced by esterifying cellulose with C6-fluorinated carboxylic acid (Guzman-Puyol et al., 2022).

A cost-effective method for imparting hydrophobicity to RC films is through the process of silylation, utilizing chemical vapor deposition (CVD) of organosilanes (Yu, Zhang, Tang, & Zhou, 2019). The CVD process is based on the chemical reaction between a heated substrate and gas-phase precursors. This convenient and scalable modification approach allows for uniform coverage of the surface of substrates, ensuring consistent hydrophobicity throughout the cellulose-based materials. For instance, Leal et al. (2020) reported the silanization of bacterial cellulose with trichloromethyl silane for a hydrophobic surface with a water contact angle of approximately 130º. Cheng and Gupta (2018) designed a roll-to-roll module to enable uniform coating of 1500 cm^2 of cellulose paper. Yu et al. (2019) fabricated a hydrophobic cellulose filter via CVD of reactive organosilane vapor for oil/water separation. CVD of organosilanes enables the transformation of cellulose-based materials into hydrophobic ones by coupling silane groups with the ─OH of cellulose through a condensation reaction. However, the reduced hydrogen bonding leads to a decreased tensile strength of modified films. Furthermore, Solala, Bordes, and Larsson (2018) reported that the water vapor barrier property of nanocellulose films was not enhanced after hydrophobic modification because of the unaltered porous structure. Therefore, the incorporation of nanofillers (clay, metallic nanoparticles, carbon nanotubes, nanocellulose, etc.) in the modified RC film is necessary to improve the mechanical and barrier properties. Among them, cellulose nanocrystals (CNC) have acquired increasing attention as nano-sized reinforcing agents of polymer matrices because of their abundance, renewability, biodegradability, high aspect ratio, high strength, and safety (Babaei-Ghazvini & Acharya, 2023).

We hypothesized that incorporating CNC can improve water resistance and tensile strength of organosilane-modified cellulose films, achieving better food preservation while maintaining their biodegradability. This is the first attempt to apply the dual modifications of CVD of

organosilanes and CNC to the hot-pressed RC films for potential food packaging applications. In this work, the effects of CVD of organosilanes and incorporation of CNC on the water resistance of RC films prepared from bleached pine pulp were investigated. Two commonly used organosilanes, methyltrimethoxysilane (MTMS) and 1H,1H,2H,2H-perfluorooctyltriethoxysilane (PFTS), were selected as examples, because MTMS is one of the most promising candidates for the fabrication of hydrophobic surfaces due to its low environmental impact, low overall cost, and low boiling point (102-104 °C) (Zheng & Fu, 2019; Yu, Zhang, Tang, & Zhou, 2019; Tang, Xie, Hess, & Breedveld, 2017), while PFTS is a common hydrophobization modifier and has been used to produce stable and durable superhydrophobic surfaces on cotton fabric (Li et al., 2020), metallic glass (Zhang et al., 2021b), wood (Pandit et al., 2020), paper (Teng et al., 2020), etc. The structure and properties including the disintegration rate of the modified RC films were characterized, and the capacity of cookie preservation for 100 days was compared to that of commercial plastic wrap.

5.3. Materials and methods

5.3.1 Materials

The bleached kraft pulps of pine were provided by FP Innovations (Pointe-Claire, QC, Canada). Sulfuric acid (95.0-98.0%) was purchased from Millipore-Sigma (Oakville, ON, Canada). Sodium hydroxide (>97.0%), urea (>99.6%), cellulose dialysis tubing (molecular weight cut-off 12-16 kDa), sodium bromide (99.0%), MTMS (97%), and PFTS (97%) were purchased from Fisher Scientific (Ottawa, ON, Canada).

5.3.2 Preparation of CNC

A grinding machine (KRUPS, ON, Canada) was applied as a mechanical pretreatment to reduce the size of pine pulps. The ground pine pulps (10 g) were hydrolyzed with 100 mL of H_2SO_4

solution (64 wt.%) at 800 rpm for 60 min at 45 °C. Acid hydrolysis was stopped by diluting the mixture with 10-fold ice water, and the excess H_2SO_4 solution was removed by centrifugation at 7500 rpm for 10 min at room temperature until a turbid suspension was obtained. The collected suspension was dialyzed against the DI water for 1 week in a dialysis membrane until the pH reached 7. The neutralized CNC was then freeze-dried and stored at room temperature. The morphology of CNC was observed by a Talos F200X G2 transmission electron microscope (TEM, Thermo Fisher Scientific, Waltham, MA, USA) at 200 kV.

5.3.3 Fabrication and modification of RC films

The ground pine pulps (2 g) were placed in 200 mL of H_2SO_4 aqueous solution (30 wt.%) for 48 h at 25 °C with continuous stirring at 200 rpm to reduce the molecular weight of cellulose from 5.26×10^5 g/mol to 1.90×10^5 g/mol, as demonstrated in our previous study (Huang et al., 2022). After acid hydrolysis, pine pulps were thoroughly washed with water and dried in an oven. An aqueous solution containing NaOH/urea/H_2O in a weight ratio of 7:12:81 pre-cooled to -12 °C was used to dissolve pine pulp cellulose at a concentration of 4 wt.% with continuous stirring at 2000 rpm for 10 min. When the solution temperature reached to 25 °C, CNC powder (5 wt.% based on the pine pulp content) was added to the solution and stirred for an additional 5 min at 2000 rpm, which was then cast on a glass plate with a thickness of about 0.8 mm and coagulated with 5 wt.% H_2SO_4 at room temperature for 5 min. The wet films were washed with water and then compressed by a hot press machine (3895, Carver Inc., USA) at 105 °C and 0.3 MPa for 10 min, followed by hot-pressing at 120 °C and 15 MPa for 10 min. The pristine RC films and CNC-reinforced RC films were coded as RC and RC-CNC, respectively. The CVD of organosilanes was performed according to the method of Yu et al. (2019). Specifically, RC or RC-CNC films (3 g) and a small glass vial containing the organosilane (MTMS or PFTS, 7 mL) were placed in a desiccator (diameter of 16.4 cm) under

heating conditions for three days. The heating temperatures for MTMS and PFTS were 120 °C and 150 °C, respectively. The MTMS and PFTS-modified films were coded as RC-M, RC-CNC-M, RC-P, and RC-CNC-P, respectively.

5.3.4 Characterization

5.3.4.1 Thickness and silane content of modified films

The thickness of the films was determined with a micrometer (resolution of 0.001 mm, Mitutoyo 547-400S, Japan) at 10 random points. The silane content of organosilane-modified films was measured by the gravimetric method (Yu et al., 2019):

$$Silane\ content\ (mg/g) = \frac{w_t - w_0}{w_0} \tag{1}$$

where w_t is the weight of modified film and w_0 is the initial weight of the film.

5.3.4.2 Fourier transform infrared spectroscopy (FT-IR)

The structures of RC and modified films were analyzed using a Cary 630 Fourier-transform infrared spectroscope with an attenuated total reflectance sampling module (FT-IR, Agilent Technologies, Santa Clara, CA, USA). The FT-IR spectra were recorded at a resolution of 2 cm^{-1} with 64 scans in the range of 4000-650 cm^{-1}, using the empty accessory as blank.

5.3.4.3 X-ray diffractometry (XRD)

The crystalline profile of RC and modified films was measured using a high-resolution X-ray diffractometer (Empyrean, Malvern Panalytical Ltd, Malvern, UK) in 2θ ranging from 5° to 40°. The crystallinity index (CI) was calculated as Eq. 2:

$$CI\ (\%) = \frac{A_c}{A_c + A_a} \times 100\% \tag{2}$$

where A_c denotes the crystalline area of the XRD pattern and A_a is the amorphous area of the

XRD pattern. The crystalline area is consequently obtained by subtracting the area of the amorphous regions of the sample from the area of the total XRD pattern.

5.3.4.4 Film morphology analysis

RC and modified films were stretched to break, and their surface and cross-sectional morphologies were observed by a Hitachi TM1000 SEM (Hitachi Co. Ltd., Tokyo, Japan) with an acceleration voltage of 4 kV after sputter-coating with a 4 nm layer of gold-palladium using a Leica EM ACE200 coater (Vaughan, ON, Canada).

5.3.4.5 Water contact angle (WCA)

The WCA of the films was measured by a contact angle apparatus (OCA 20, Dataphysics Instruments, Filderstadt, Germany) using the sessile drop method. A piece (1 cm × 1 cm) of sample was fixed on a microscope slide by double-faced adhesive tape to prevent the rolling of the flat surface during wetting. Water droplets (6 μL) were then placed on the sample surfaces. Images were captured and analyzed with the goniometer at 25 °C. The contact angle was measured and given by the goniometer based on the shape of the sessile drop, and the measurement was repeated for at least three samples of the same material with three tests for each sample.

5.3.4.6 Mechanical properties

To measure the mechanical properties of RC and modified films under different environments, the films were conditioned at 25 °C and i) 0% relative humidity (RH) with vacuum for three days (a condition that simulates a dry condition), ii) 60% RH with a saturated sodium bromide solution for three days (a condition that simulates an ambient environment), and iii) immersed in water for 12 h (a condition that simulates a wet environment), respectively. The dimension of film specimens was 50 mm × 20 mm × 0.03 mm (length × width × thickness). The tensile

strength, elongation at break, and Young's modulus of films were tested using an ADMET MTEST Quattro eXpert 7600 single-column testing system (MA, USA) with a load cell of 250 lb and a crosshead speed of 5 mm/min.

5.3.4.7 Water vapor permeability (WVP)

WVP of RC and modified films was determined based on the ASTM E96-92 standard. A dried film was taped on the top of a glass flask containing 3 g of anhydrous calcium chloride. The sealed glass flask was then located in a desiccator with water to reach 100% RH. The weight change of the flask was recorded periodically at 25 °C. The WVP (g m^{-1} h^{-1} Pa^{-1}) of films was calculated by Eq. 3:

$$WVP\ (g\ m^{-1}\ h^{-1}\ Pa^{-1}) = \frac{\Delta m \times k}{A \times \Delta T \times \Delta P} \tag{3}$$

where Δm is the weight change of the flask (g) during time ΔT (h), k is the thickness of each film (m), A is the exposed area of the film (7.85×10^{-5} m^2), and ΔP is the partial water vapor pressure difference between two sides of the film (Pa).

5.3.4.8 Oxygen permeability (OP)

The oxygen transmission rate of RC and modified films was determined at 23 °C and 0% RH using the Mocon Ox-Tran Model 2/22 (Mocon Co., Minneapolis, USA). The OP was calculated by Eq. 4:

$$OP\ (cm^3\ m^{-1}\ day^{-1}\ atm^{-1}) = \frac{OTR \times \ell}{\Delta P'} \tag{4}$$

where OTR is the oxygen transmission rate, ℓ is the thickness of the film, and $\Delta P'$ is the partial pressure of oxygen (kPa).

5.3.5 Preservation of cookies

Commercial white chocolate cranberry shortbread cookies were selected to evaluate the preservation effect of RC and modified films. About 16 g of cookies were placed in glass jars (diameter of 5.4 cm and height of 4.5 cm) and covered with plastic wrap (Kirkland Signature Stretch-Tite Plastic Wrap – 11 7/8 × 750 Feet), RC, RC-CNC, RC-CNC-M, and RC-CNC-P films, respectively. The cookies without any package were set as the control. All samples were stored in the desiccator at 25 °C and 60 % RH with a saturated sodium bromide solution for a maximum of 100 days to monitor the weight gain.

After 100 days of storage, the peroxide value (PV) of the fat fraction extracted from the milled cookies was determined based on the AOAC standard (AOAC, 2005). Specifically, 15 g of the crushed cookies were mixed with 30 mL petroleum ether and kept for 15 h. The filtrate was evaporated to remove petroleum ether and subsequently dissolved in 30 mL of chloroform-glacial acetic acid mixture (2/3, v/v). The sample was stirred after the addition of 1 mL of saturated KI aqueous solution, followed by the addition of 75 mL of water and 1 mL of 1% starch solution. The reaction solution was titrated with 0.01 N sodium thiosulfate. All samples were analyzed in duplicate. The PV was expressed as milli-equivalents of active oxygen per kilogram of fat (meq/kg) and calculated by Eq. 5:

$$PV\ (meq/kg) = \frac{(v_2 - v_1) \times 0.01 \times 1000}{w} \tag{5}$$

where v_2 and v_1 are the volumes (mL) of sodium thiosulfate solution consumed by the sample and the blank, respectively, and w is the sample weight (g).

5.3.6 Disintegration test

The disintegration test of RC and modified films was carried out based on the ISO-20200 standard (ISO, 2004). Briefly, a laboratory scale of a synthetic waste matrix consisting of 40 % sawdust, 30 % rabbit feed, 10 % ripe compost, 10 % corn starch, 5 % saccharose, 4 % corn oil,

and 1 % urea was prepared. After that, the dry waste was mixed with water in 45:55 ratio and heated to 58±2 °C to simulate the composting condition. The cellulose films were cut into 25 mm × 25 mm and buried at a depth of 6 cm in a composting reactor containing reconstituted wet waste, and water was added periodically to maintain the humidity in the compost. Before measuring the weight of the cellulose films, the synthetic waste matrix was carefully removed from the surface with tweezer. The degree of disintegration of the film was expressed by the mass reduction calculated from the initial weight (m_i) and the measured weight (m_d) by Eq. 6:

$$Mass\ reduction\ (\%) = \frac{m_i - m_d}{m_i} \times 100\% \tag{6}$$

5.3.7 Statistical analysis

The weight gain and PV of cookies during preservation were measured in duplicate. All other tests were done in triplicate. The experimental data were presented as the mean ± standard deviation. Analysis of variance (ANOVA) was applied for the statistical analysis, followed by multiple comparison tests via Duncan's multiple-range test. All the analyses were carried out through SPSS statistical software (version 26, IBM SPSS Inc., New York, NY) with significant differences within samples at $p < 0.05$.

5.4. Results and discussion

The thickness of hot-pressed RC films was 29±2 μm, which did not change after the incorporation of CNC and chemical modifications. The contents of MTMS and PFTS in RC-CNC-M and RC-CNC-P films were 39±8 mg/g and 43±5 mg/g, respectively. The TEM image of CNC is shown in Fig. 5.1A. The rod-shaped CNC had a length and diameter of 184.02±11.26 nm and 11.24±0.81 nm, respectively, and the aspect ratio was 13.04±0.14. FT-IR spectra and XRD diffraction patterns were collected to investigate the effects of CNC and organosilanes on the structure of RC films. As shown in Fig. 5.1B, RC-CNC film displayed a similar FT-IR

spectrum to the RC film, indicating no chemical reactions happened after incorporating CNC. The peaks at 3330 and 3269 cm^{-1} were ascribed to the O─H stretching of the hydrogen-bonded hydroxyl groups, which represented the intra- and intermolecular hydrogen bonds in cellulose, respectively (Li et al., 2019b). Besides, the asymmetric ─CH_2 bending vibration at 1427 cm^{-1} belonged to the cellulose I crystalline structure, while the ─C─O─C─ bridge stretching at 893 cm^{-1} represented the amorphous region and cellulose II crystalline structure (Huang, Tao, Ismail, & Wang, 2020). New peaks related to organosilanes were observed after chemical modification. For instance, two peaks were found in RC-CNC-M at 1260 and 780 cm^{-1}, which were attributed to the Si─C vibration (Yu et al., 2019). A slight increase in peak intensity near 1230 cm^{-1} was observed in RC-CNC-P due to the presence of C─F stretching in the pine pulps (Kowalczuk & Pitucha, 2019). Moreover, the modification of RC-CNC by the organosilanes led to a decrease in the intensities of the peaks at around 3360 and 3269 cm^{-1} owing to the formation of covalent bonds between ─OH of cellulose and organosilanes. As shown in Fig. 5.1C, the acid-hydrolyzed CNC exhibited the diffraction peaks at about 14.8° ($1\bar{1}0$), 16.3° (110), 22.5° (200), and 34° (040), for cellulose I structure with a CI of 75.24% (Beroual et al., 2021). The RC and RC-CNC films showed similar cellulose II structures with broad diffraction peaks at 20.2° and 22.6°, corresponding to (110) and (020) crystallographic planes, respectively (Huang et al., 2020). This result was in accordance with the regenerated cotton linter cellulose films reinforced by 5% cellulose nanowhiskers, in which the cellulose I structure was not obvious (Qi, Cai, Zhang, & Kuga, 2009). However, the incorporation of CNC resulted in an increase in CI values from 60.55% to 70.91%. The chemical modification of MTMS and PFTS did not affect the cellulose II structure of RC-CNC films, but slightly decreased the CI values to 68.46% and 64.21%, respectively. The morphology of RC films before and after modifications was observed by SEM. As shown in Fig. 5.1D and 5.1E, the RC and RC-CNC

films had smooth and uniform surfaces without any undissolved fibers. The incorporation of CNC did not lead to the obvious changes in the surface and cross-section of RC film. However, irregular aggregates of organosilanes were observed on the surfaces of RC-CNC films after chemical modification. The interactions between organosilanes and cellulose under heating condition have been proposed in three ways: organosilanes can (1) form monolayers on the surface of RC films via self-assembly, (2) react with surface ─OH groups to form covalently linked monolayers, and (3) condense with water and surface ─OH groups to form a highly cross-linked 3D network (Jin et al., 2011; Yu et al., 2019). The pristine RC films had a WCA value of 75.22°, which was not changed after the incorporation of CNC (77.49°). After the modification with MTMS and PFTS, more hydrophobic surfaces were observed with the increased WCA values of 109.71° and 102.53°, respectively.

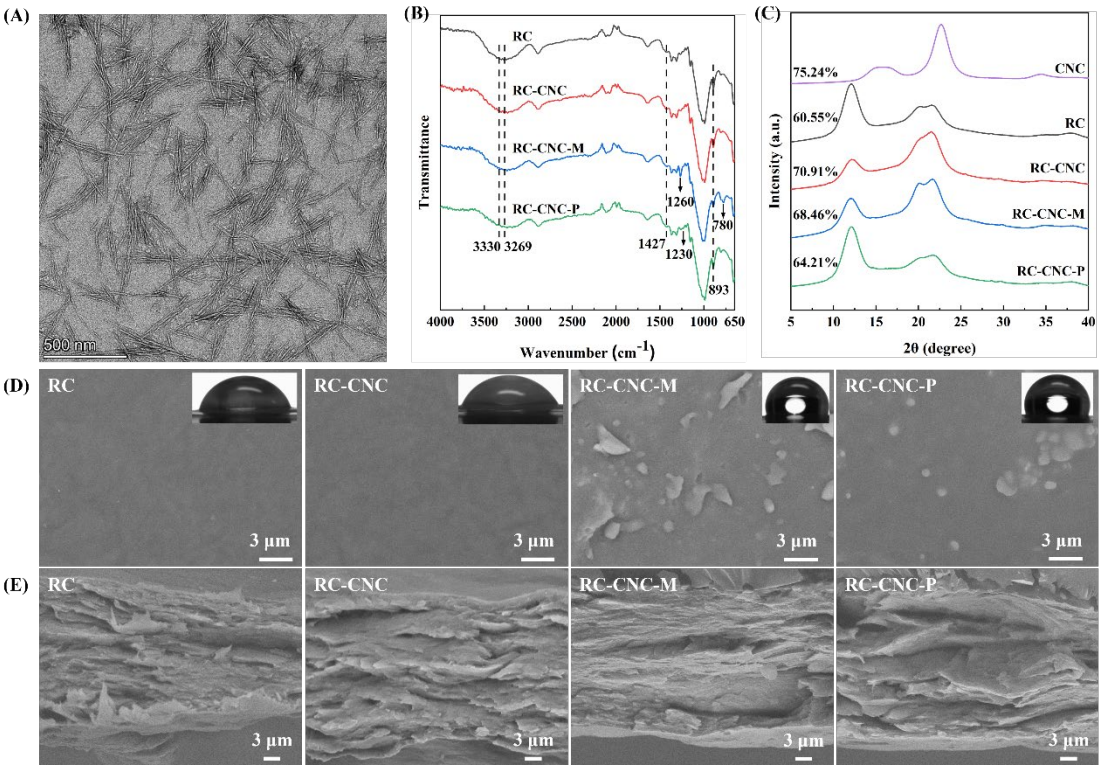

Fig. 5.1. (A) TEM image of CNC, (B) FT-IR spectra, (C) XRD patterns and crystallinity index, and (D) surface and (E) cross-sectional morphologies of RC and modified films. Inset: Water contact angle of RC and modified films.

As shown in Fig. 5.2, the tensile strength of RC films was 66.37±2.79 MPa under 0% RH. After chemical modification with MTMS and PFTS, this value decreased to 41.02±0.11 MPa (RC-M) and 42.92±1.58 MPa (RC-P), because the hydrogen bonding between cellulose chains was weakened. When exposed to 60% RH for 3 days, the tensile strength of RC films decreased significantly to 52.09±2.80 MPa, while those of RC-M and RC-P films had insignificant changes, which were 38.75±0.62 MPa and 39.57±1.4 MPa, respectively. It was worth noting that the incorporation of CNC compensated for the degradation of mechanical properties of the organosilane modified RC films, resulting in the tensile strengths of RC-CNC-M of 57.11±1.52 MPa (0% RH) and 56.79±3.67 MPa (60% RH) and RC-CNC-P of 59.67±1.09 MPa (0% RH) and 58.87±3.75 MPa (60% RH). Moreover, the hydrophobic modification limited the water

penetration and reduced the degradation of the mechanical properties under wet condition. The wet tensile strengths of RC-CNC-M and RC-CNC-P were 11.83±0.54 MPa and 12.95±0.11 MPa, respectively, which were comparable to the water-resistant cellulose nanopaper (11 MPa) (Zhang, Ismail, & Liimatainen, 2021a) and the refined and dip-coated cellulose paper (10.8 MPa) (Liu et al., 2022b), and stronger than the diisocyanate-modified hydrophobic filter paper (4.8 MPa) (Zhou et al., 2020) and the hydrophobic ethyl cellulose paper (7.8 MPa) (Liu et al., 2022a).

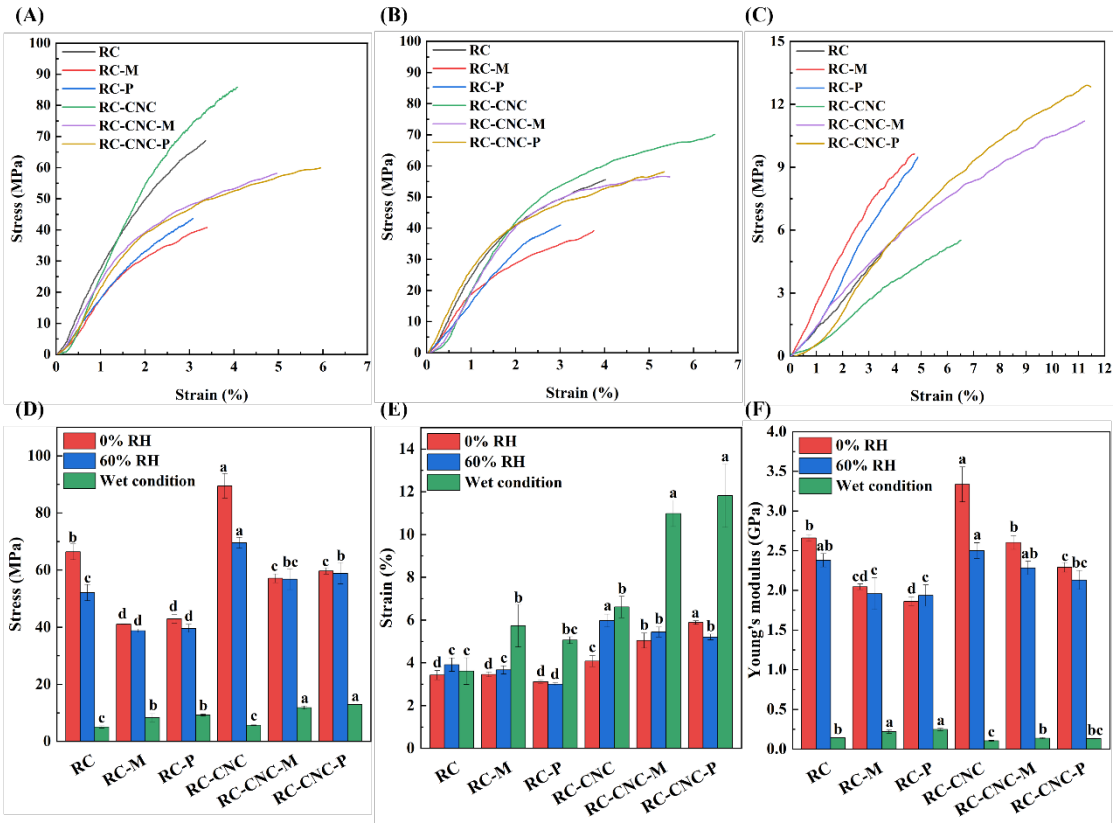

Fig. 5.2. Mechanical properties of RC and modified films under (A) 0% relative humidity, (B) 60% relative humidity, and (C) wet condition. (D) Stress, (E) strain, and (F) Young's modulus of RC and modified films under different conditions.

The WVP values of RC films before and after modifications are shown in Fig. 5.3A. The WVP of pristine RC film was 4.07±0.18×10^{-7} g m^{-1} h^{-1} Pa^{-1}. The addition of CNC led to the

increased crystalline structure and thus the longer water vapor diffusion pathway, so the WVP value of RC-CNC reduced to 3.74±0.18×10^{-7} g m^{-1} h^{-1} Pa^{-1}. The hydrophobic modification can decrease water vapor penetration by forming droplets on the surface and preventing the adsorption of water molecules (Li et al., 2019a), and the WVP values of RC-CNC-M and RC-CNC-P were 3.25±0.08×10^{-7} g m^{-1} h^{-1} Pa^{-1} and 3.35±0.19×10^{-7} g m^{-1} h^{-1} Pa^{-1}, respectively, which were lower than those of hydrophobic cellulose nanofibril films (1.22×10^{-5} g m^{-1} h^{-1} Pa^{-1}) (Li et al., 2019c), hydrophobic graphene oxide-incorporated RC films (4.86×10^{-7} g m^{-1} h^{-1} Pa^{-1}) (Xu et al., 2019), and hydrophobic acylated microfibrillated cellulose films (5.35 ×10^{-7} g m^{-1} h^{-1} Pa^{-1}) (Deng et al., 2016).

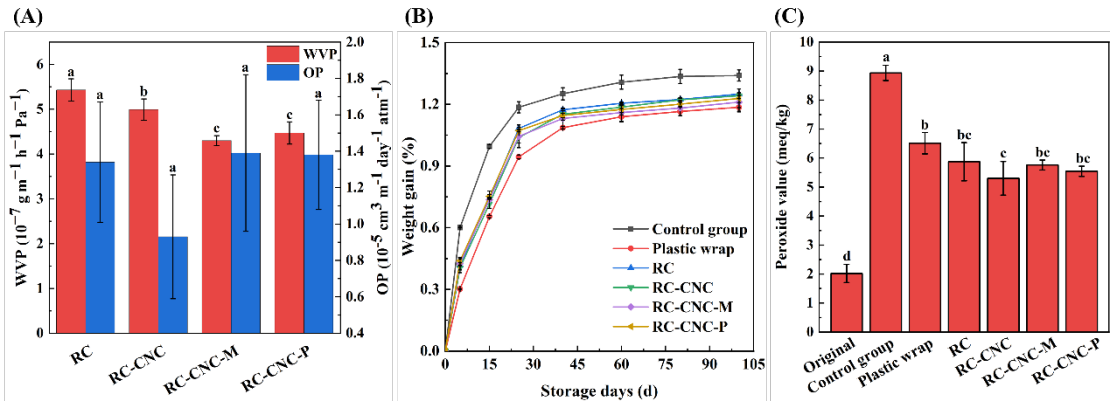

Fig. 5.3. (A) WVP and OP of RC and modified films. (B) Weight gain of cookies under different packaging conditions, and (C) peroxide values of cookies before (original) and after 100 days of storage.

The pristine RC film had an OP value of 1.34±0.33×10^{-5} cm^3 m^{-1} day^{-1} atm^{-1}. The addition of CNC to RC films increased the tortuosity, which hindered oxygen diffusion and led to a decrease in OP. However, the chemical modifications by two organosilanes interacted with the ─OH groups and decreased the polarity of RC films. This resulted in a slight increase in OP despite the incorporation of CNC. RC-CNC-M and RC-CNC-P had a similar OP of about

1.37×10^{-5} cm^3 m^{-1} day^{-1} atm^{-1} and an oxygen transmission rate of about 0.3 cm^3 m^{-2} day^{-1}, and thus could be considered as high oxygen barrier food packaging materials (<10 cm^3 m^{-2} day^{-1}) (Mirmehdi, Hein, de Luca Sarantópoulos, Dias, & Tonoli, 2018), which were better than the cellulose nanofibers and fluoropolymer coating packaging film (1.20×10^{-5} cm^3 m^{-1} day^{-1} atm^{-1}) (Kim, Choi, & Jin, 2020) and the composite packaging film consisting of RC, zinc oxide nanoparticles, and curcumin (2.93×10^{-3} cm^3 m^{-1} day^{-1} atm^{-1}) (Saedi, Kim, Shokri, Kim, & Shin, 2023).

The preservation effects of RC and modified films on cookies are shown in Fig. 5.3B, where all cookies had similar sigmoidal curves with rapid weight gains within the first 25 days followed by a gradual slowing down. The unpackaged cookies exhibited the highest increase in weight due to moisture absorption after 100 days (1.34±0.03%), while the use of plastic wrap and RC films (both unmodified and modified) obviously impeded the water vapor transmission. Although the plastic wrap had slightly better capacity of controlling weight gain (1.19±0.02%), the cookies wrapped by RC-CNC-M and RC-CNC-P showed the similar changes of 1.21±0.04% and 1.23±0.05%, respectively, and were relatively lower than those of RC and RC-CNC films. The PV value is an important indicator of the freshness and quality of fats and oils (Okparanta, Daminabo, & Solomon, 2018). The unpackaged cookies had the highest PV value of 8.94±0.26 meq/kg after 100 days. The plastic wrap significantly reduced the PV of cookies to 6.51±0.37 meq/kg, similar to the sample packaged with pristine RC film (5.88±0.66 meq/kg). The RC-CNC film showed the lowest PV value of 5.30±0.58 meq/kg, while RC-CNC-M and RC-CNC-P had a slight decrease in blocking oxygen due to the reduced polarity, resulting in the PV values of 5.76±0.17 and 5.55±0.18 meq/kg, respectively. The changes in the final PV values were due to the different OP and WVP of the packaging films. Specifically, oxygen can easily penetrate through high OP packaging films, resulting in higher rates of cookie oxidation during

the storage (Lu & Xu, 2010), while the reduction in WVP weakens the prooxidant feature of water and reduces the oxidation rate of lipids in the hydrolysis of triacylglycerols to diacylglycerols, monoacylglycerols, and free fatty acids (Mildner-Szkudlarz, Siger, Przygoński, Radziejewska-Kubzdela, & Zawirska-Wojtasiak, 2022).

Fig. 5.4A shows the effects of CNC and organosilane modifications on the disintegration process of RC films. Pristine RC film fully disintegrated in about 12 days, whereas RC-CNC film and chemically modified films needed about 14 days. The addition of CNC delayed the disintegration rate since it acted as a reinforcing agent and increased the crystallinity of RC films and prevented the penetration of water. The RC-CNC-MTMS and RC-CNC-PFTS films disintegrated slower in the first week due to the hydrophobic surface preventing water diffusion and penetration, but they also reached 100% disintegration on day 14.

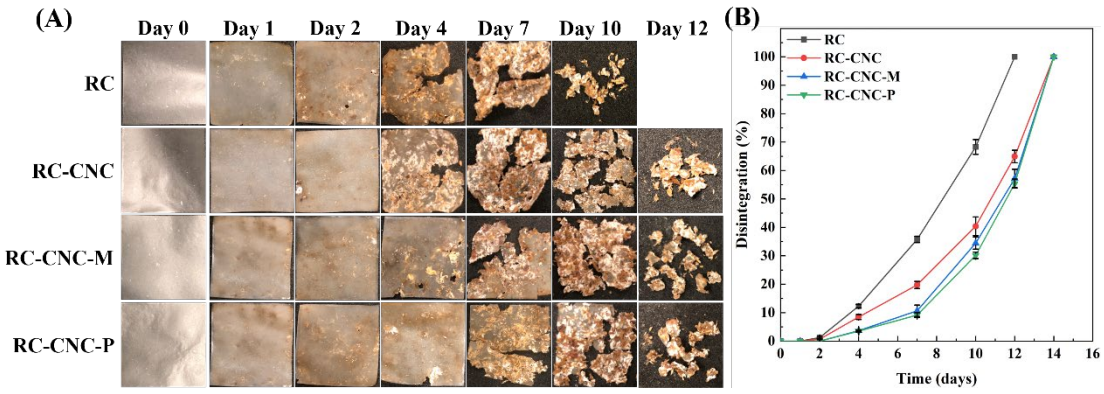

Fig. 5.4. (A) Visual appearance of RC and modified films at different composting times. (B) Degree of disintegration of RC and modified films under composting conditions.

5.5. Conclusion

The hypothesis has been confirmed that the dual modifications by incorporating CNC and coupling organosilanes successfully enhanced the water resistance and tensile strength of RC films. The selected two model organosilanes MTMS and PFTS showed similar effects on

modifying the hydrophobicity, where the water contact angles of RC-CNC-M and RC-CNC-P increased from 75.22° to 109.71° and 102.53°, respectively, compared to the unmodified RC film. The existence of CNC compensated for the deteriorated mechanical properties caused by the weakened intermolecular hydrogen bonding. The modified RC films exhibited the well-maintained tensile strength of around 57 MPa in the humid ambient environment (RH 60%), and the wet strength of about 12 MPa was much higher than those of the control samples and many other cellulose materials. Moreover, RC-CNC-M and RC-CNC-P possessed the significantly reduced WVP ($3.25\pm0.08\times10^{-7}$ g m^{-1} h^{-1} Pa^{-1} and $3.35\pm0.19\times10^{-7}$ g m^{-1} h^{-1} Pa^{-1}) and high oxygen barrier capacity (<1 cm^3 m^{-2} day^{-1}), leading to the comparable effect to the commercial plastic wrap in the cookie preservation test for 100 days. Importantly, the modified RC films maintained their ability to completely disintegrate within 14 days. Therefore, this work offers significant potential for developing sustainable packaging materials with good performance.

5.6. References

AOAC. (2005). Official Methods of Analysis 18th Edition. Pub AOAC International Maryland.

Babaei-Ghazvini, A., & Acharya, B. (2023). The effects of aspect ratio of cellulose nanocrystals on the properties of all CNC films: Tunicate and wood CNCs. *Carbohydrate Polymer Technologies and Applications,* 5, 100311.

Beroual, M., Trache, D., Mehelli, O., Boumaza, L., Tarchoun, A. F., Derradji, M., & Khimeche, K. (2021). Effect of the delignification process on the physicochemical properties and thermal stability of microcrystalline cellulose extracted from date palm fronds. *Waste and Biomass Valorization,* 12, 2779-2793.

Cheng, C., & Gupta, M. (2018). Roll-to-roll surface modification of cellulose paper via

initiated chemical vapor deposition. *Industrial & Engineering Chemistry Research,* 57(34), 11675-11680.

Deng, S., Huang, R., Zhou, M., Chen, F., & Fu, Q. (2016). Hydrophobic cellulose films with excellent strength and toughness via ball milling activated acylation of microfibrillated cellulose. *Carbohydrate Polymers,* 154, 129-138.

Guzman-Puyol, S., Tedeschi, G., Goldoni, L., Benítez, J. J., Ceseracciu, L., Koschella, A., . . . Heredia-Guerrero, J. A. (2022). Greaseproof, hydrophobic, and biodegradable food packaging bioplastics from C6-fluorinated cellulose esters. *Food Hydrocolloids,* 128, 107562.

Huang, K., Maltais, A., Liu, J., & Wang, Y. (2022). Wood cellulose films regenerated from NaOH/urea aqueous solution and treated by hot pressing for food packaging application. *Food Bioscience,* 50, 102177.

Huang, S., Tao, R., Ismail, A., & Wang, Y. (2020). Cellulose nanocrystals derived from textile waste through acid hydrolysis and oxidation as reinforcing agent of soy protein film. *Polymers,* 12(4), 958.

Huang, Z., Liu, C., Feng, X., Wu, M., Tang, Y., & Li, B. (2020). Effect of regeneration solvent on the characteristics of regenerated cellulose from lithium bromide trihydrate molten salt. *Cellulose,* 27, 9243-9256.

ISO. (2004). Plastics: determination of the degree of disintegration of plastic materials under simulated composting conditions in a laboratory-scale test.

Jin, K., Tang, Y., Liu, J., Wang, J., & Ye, C. (2021). Nanofibrillated cellulose as coating agent for food packaging paper. *International Journal of Biological Macromolecules,* 168, 331-338.

Jin, M., Wang, J., Yao, X., Liao, M., Zhao, Y., & Jiang, L. (2011). Underwater oil capture by a three-dimensional network architectured organosilane surface. *Advanced Materials,* 23(25), 2861-2864.

Kim, J.-K., Choi, B., & Jin, J. (2020). Transparent, water-stable, cellulose nanofiber-based packaging film with a low oxygen permeability. *Carbohydrate Polymers,* 249, 116823.

Kowalczuk, D., & Pitucha, M. (2019). Application of FTIR method for the assessment of immobilization of active substances in the matrix of biomedical materials. *Materials,* 12(18), 2972.

LakshmiBalasubramaniam, S., Howell, C., Tajvidi, M., & Skonberg, D. (2022). Characterization of novel cellulose nanofibril and phenolic acid-based active and hydrophobic packaging films. *Food Chemistry,* 374, 131773.

Leal, S., Cristelo, C., Silvestre, S., Fortunato, E., Sousa, A., Alves, A., . . . Gama, M. (2020). Hydrophobic modification of bacterial cellulose using oxygen plasma treatment and chemical vapor deposition. *Cellulose,* 27, 10733-10746.

Li, S., Liu, Y., Zheng, Z., Liu, X., Huang, H., Han, Z., & Ren, L. (2019a). Biomimetic robust superhydrophobic stainless-steel surfaces with antimicrobial activity and molecular dynamics simulation. *Chemical Engineering Journal,* 372, 852-861.

Li, W., Hu, J., Cheng, L., Chen, L., Zhou, L., Zhang, J., & Yuan, Y. (2019b). Study on thermal behavior of regenerated micro-crystalline cellulose containing slight amount of water induced by hydrogen-bonds transformation. *Polymer,* 185, 121989.

Li, W., Wang, S., Wang, W., Qin, C., & Wu, M. (2019c). Facile preparation of reactive hydrophobic cellulose nanofibril film for reducing water vapor permeability (WVP) in packaging applications. *Cellulose,* 26(5), 3271-3284.

Li, J., Wu, X., Jiang, P., Li, L., He, J., Xu, W., & Li, W. (2020). A facile method to fabricate durable super-hydrophobic cotton fabric. *Journal of Vinyl and Additive Technology*, *26*(1), 3-9.

Liao, R., Zhu, M., Zhou, X., Zhang, F., Yan, J., Zhu, W., & Gu, C. (2012). Molecular dynamics study of the disruption of H-bonds by water molecules and its diffusion behavior in amorphous cellulose. *Modern Physics Letters B,* 26(14), 1250088.

Liu, J., Wang, C., Ewulonu, C. M., Chen, X., Wu, M., & Huang, Y. (2022a). Fabrication of superhydrophobic and degradable cellulose paper materials for straw application. *Cellulose,* 29, 527-540.

Liu, S., Liu, X., Wang, Q., Wang, Y., Ji, X., Yang, G., . . . Ni, Y. (2022b). Superhydrophobic, strong and transparent paper made from cellulosic fibers. *Cellulose,* 29(3), 1993-2003.

Lu, L.-X., & Xu, F. (2010). Effects of initial oxygen concentration and oxygen-barrier property of film on fat oxidation rate of packed cookies. *European Food Research and Technology,* 231, 347-351.

Mildner-Szkudlarz, S., Siger, A., Przygoński, K., Radziejewska-Kubzdela, E., & Zawirska-Wojtasiak, R. (2022). Nε-(carboxymethyl) lysine, Available Lysine, and Volatile Compound Profile of Biscuits Enriched with Grape by-Product During Storage. *Plant Foods for Human Nutrition,* 77(2), 190-197.

Mirmehdi, S., Hein, P. R. G., de Luca Sarantópoulos, C. I. G., Dias, M. V., & Tonoli, G. H. D. (2018). Cellulose nanofibrils/nanoclay hybrid composite as a paper coating: Effects of spray time, nanoclay content and corona discharge on barrier and mechanical properties of the coated papers. *Food Packaging and Shelf Life,* 15, 87-94.

Okparanta, S., Daminabo, V., & Solomon, L. (2018). Assessment of rancidity and other

physicochemical properties of edible oils (mustard and corn oils) stored at room temperature. *Journal of Food and Nutrition Sciences,* 6(3), 70-75.

Pandit, S. K., Tudu, B. K., Mishra, I. M., & Kumar, A. (2020). Development of stain resistant, superhydrophobic and self-cleaning coating on wood surface. *Progress in Organic Coatings*, *139*, 105453.

Qi, H., Cai, J., Zhang, L., & Kuga, S. (2009). Properties of films composed of cellulose nanowhiskers and a cellulose matrix regenerated from alkali/urea solution. *Biomacromolecules,* 10(6), 1597-1602.

Ramesh, S., & Radhakrishnan, P. (2019). Cellulose nanoparticles from agro-industrial waste for the development of active packaging. *Applied Surface Science,* 484, 1274-1281.

Saedi, S., Kim, J. T., Shokri, M., Kim, J.-H., & Shin, G. H. (2023). Green seaweed (Ulva ohnoi) as a new eco-friendly source for preparing transparent and functional regenerated cellulose composite films. *Cellulose*, 1-19.

Shojaeiarani, J., Bajwa, D. S., & Chanda, S. (2021). Cellulose nanocrystal based composites: A review. *Composites Part C: Open Access,* 5, 100164.

Solala, I., Bordes, R., & Larsson, A. (2018). Water vapor mass transport across nanofibrillated cellulose films: effect of surface hydrophobization. *Cellulose,* 25(1), 347-356.

Tang, Z., Xie, L., Hess, D. W., & Breedveld, V. (2017). Fabrication of amphiphobic softwood and hardwood by treatment with non-fluorinated chemicals. *Wood Science and Technology*, *51*, 97-113.

Teng, Y., Wang, Y., Shi, B., Fan, W., Li, Z., & Chen, Y. (2020). Facile fabrication of superhydrophobic paper with durability, chemical stability and self-cleaning by roll coating with modified nano-TiO 2. *Applied Nanoscience*, *10*, 4063-4073.

Wang, Y., Liu, L., Chen, P., Zhang, L., & Lu, A. (2018). Cationic hydrophobicity promotes dissolution of cellulose in aqueous basic solution by freezing–thawing. *Physical Chemistry Chemical Physics,* 20(20), 14223-14233.

Wu, Y., Qian, Z., Lei, Y., Li, W., Wu, X., Luo, X., . . . Liu, S. (2018). Superhydrophobic modification of cellulose film through light curing polyfluoro resin in situ. *Cellulose,* 25(3), 1617-1623.

Xu, L., Teng, J., Li, L., Huang, H.-D., Xu, J.-Z., Li, Y., . . . Li, Z.-M. (2019). Hydrophobic graphene oxide as a promising barrier of water vapor for regenerated cellulose nanocomposite films. *ACS omega,* 4(1), 509-517.

Yu, L., Zhang, Z., Tang, H., & Zhou, J. (2019). Fabrication of hydrophobic cellulosic materials via gas–solid silylation reaction for oil/water separation. *Cellulose,* 26(6), 4021-4037.

Yuan, Z., & Wen, Y. (2018). Enhancement of hydrophobicity of nanofibrillated cellulose through grafting of alkyl ketene dimer. *Cellulose,* 25(12), 6863-6871.

Zhang, K., Ismail, M. Y., & Liimatainen, H. (2021). Water-resistant nanopaper with tunable water barrier and mechanical properties from assembled complexes of oppositely charged cellulosic nanomaterials. *Food Hydrocolloids,* 120, 106983.

Zhang, M., Sun, J., Wang, Y., Yu, M., Liu, F., Ding, G., ... & Liu, L. (2021). Preparation of stable and durable superhydrophobic surface on Zr-based bulk metallic glass. *Colloids and Surfaces A: Physicochemical and Engineering Aspects*, *631*, 127654.

Zhao, G., Lyu, X., Lee, J., Cui, X., & Chen, W.-N. (2019). Biodegradable and transparent cellulose film prepared eco-friendly from durian rind for packaging application. *Food Packaging and Shelf Life,* 21, 100345.

Zhao, Y., Zhou, S., Xia, X., Tan, M., Lv, Y., Cheng, Y., . . . Wang, H. (2022). High-performance

carboxymethyl cellulose-based hydrogel film for food packaging and preservation system. *International Journal of Biological Macromolecules,* 223, 1126-1137.

Zheng, X., & Fu, S. (2019). Reconstructing micro/nano hierarchical structures particle with nanocellulose for superhydrophobic coatings. *Colloids and Surfaces A: Physicochemical and Engineering Aspects*, *560*, 171-179.

Zhou, X., Fu, Y., Chen, L., Wang, R., Wang, X., Miao, Y., . . . Dai, H. (2020). Diisocyanate modifiable commercial filter paper with tunable hydrophobicity, enhanced wet tensile strength and antibacterial activity. *Carbohydrate Polymers,* 248, 116791.

Zhu, M., Ying, D., Zhang, H., Xu, X., & Chang, C. (2022). Self-healable hydrophobic films fabricated by incorporating natural wax into cellulose matrix. *Chemical Engineering Journal,* 446, 136791.

Connecting Text

In Chapter 5, the dual modifications by incorporating CNC and CVD of organosilanes enhanced the water resistance and tensile strength of RC films. In order to develop cellulose-based antibacterial food packaging, our previous studies have fabricated a chevaux-de-frise-like nanostructure through the coating of CNC onto RC films via vacuum filtration. Chapter 6 aimed to explore the effect of surface charge of CNC on the mechano-bactericidal activity and the performance of chevaux-de-frise-like nanostructure in meat preservation. Firstly, wood pulp was hydrolysed by hydrochloric acid to produce CNC (HCNC) with limited charges. Secondly, HCNC was modified by TEMPO oxidation or amination to produce CNC with highly negative (TCNC) or positive (ACNC) charges. Thirdly, the effects of chemical modifications on the charge and morphology of CNC were investigated. Finally, the topology, mechanical, barrier, and antimicrobial properties, and meat packaging performance of CNC-coated RC films were examined.

Chapter 6. Effect of Surface Charge on Mechano-Bactericidal Activity of Cellulose Nanocrystals Constructed Chevaux-de-Frise and Meat Preservation

6.1. Abstract

The nanostructured insect wings have inspired the development of antimicrobial surfaces with mechano-bactericidal activity. For the first time, a chevaux-de-frise-like nanostructure was fabricated through the coating of cellulose nanocrystals (CNC) onto regenerated cellulose (RC) films via vacuum filtration and the impact of contact time, temperature, and surface topography on eliminating foodborne bacteria was examined. Herein, our focus is to explore in more detail how the surface charge of CNC affects the mechano-bactericidal activity and the performance of chevaux-de-frise-like nanostructure in meat preservation. CNC with neutral (weak), negative, and positive charges were prepared by hydrochloric acid hydrolysis (HCNC), TEMPO oxidation (TCNC), and amination (ACNC), respectively, and showed similar reinforcing effects on the tensile strength (increased from 74.23 ± 1.20 to about 100 MPa) and water vapor barrier property (reduced from 1.83 ± 0.08 to about 1.20×10^{-7} g m^{-1} h^{-1} Pa^{-1}). Among them, RC-ACNC showed the highest log reduction against *Escherichia coli* (0.83 ± 0.06) and *Staphylococcus aureus* (0.69 ± 0.04) after 5 min contact, respectively, indicating the important role of attractive force in fast eliminating bacteria upon contact. It was worth noting that, during the meat preservation test, all three CNC-coated RC films exhibited a similar 0.4 log reduction of bacteria after day 4, likely due to the same physical attachment with an extended contact time. Therefore, the construction of chevaux-de-frise nanostructure from CNC on food packaging provides a sustainable strategy to contribute to preventing bacterial growth.

6.2. Introduction

Nanostructures such as nanopillars (Xie et al., 2022), nanospikes (Elbourne et al., 2019), and nanopins (Chu et al., 2016) that adorn the surfaces of insect wings (cicadas, dragonflies, and

damselflies) have the extraordinary ability to repel and inhibit bacteria through purely physical means (Ivanova et al., 2021; Mainwaring et al., 2016; Román-Kustas et al., 2020). Ivanova et al. (2012) reported that the shear stress induced by *Pseudomonas aeruginosa* (*P. aeruginosa*) adhering to the nanopillars of cicada wings led to cell membrane rupture within 3 min. A follow-up study performed by Dehghani et al. (2021) indicated that cicada wings inhibited 50% colony formation of *P. aeruginosa* through surface contact. Besides, Gram-positive bacteria, characterized by their robust and thick cell walls, exhibited greater resistance to mechano-bactericidal effects than Gram-negative bacteria (Zhao et al., 2023). Compared to chemical-based antimicrobial strategies, this inherent mechano-bactericidal surface has advantages in preventing the potential migration of harmful substances into food products. Moreover, the excessive usage of chemical antimicrobial agents can result in the development of antimicrobial resistance in pathogens, which can greatly reduce the effectiveness of antibiotics. Therefore, the construction of nanostructured surfaces with antimicrobial activities should be considered as a sustainable and efficient means to address bacterial threats.

In recent years, techniques like metal-assisted chemical etching (Luo et al., 2020), hydrothermal synthesis (Hayles et al., 2021), nanoimprint lithography (Lohmann et al., 2022), and electrochemical anodization (Maher et al., 2022) have been explored in the pursuit of synthetic nanostructured surfaces with antibacterial potential. Notably, most of these endeavors have employed metals and glass as substrates to engineer nanopillar-based antibacterial structures (Linklater et al., 2021), while the use of natural nanomaterials in constructing mechano-bactericidal surfaces remains an underexplored frontier. Cellulosic materials have garnered significant attention in recent years, and nanocellulose acts as a renewable high-performance building block and holds promise in various applications (Trache et al., 2020). Our previous research has demonstrated that cellulose nanocrystals (CNC) can be coated onto

the surface of regenerated cellulose (RC) films through vacuum filtration, resulting in the formation of chevaux-de-frise nanostructure with mechanical bactericidal activity that inhibited the bacterial growth of *Escherichia coli* and *Listeria monocytogenes* (Zhou et al., 2022). More efforts are required to understand this novel nanostructure, and one of the most important questions is how surface attachment affects antibacterial efficiency. Considering the negative charge on the majority of bacterial surfaces (Abbaszadegan et al., 2015), we hypothesized that the chevaux-de-frise constructed by positively charged CNC could facilitate the adhesion of bacteria in contrast to weak and strongly negatively charged CNC, resulting in a better mechano-bactericidal effect within a short contact time.

Therefore, in this study, three types of CNC with neutral (weak), negative, and positive charges were prepared by hydrochloric acid hydrolysis (HCNC), TEMPO oxidation (TCNC), and amination (ACNC), respectively. Their impact on the structure, surface topology, water vapor barrier property, mechanical properties, and mechano-bactericidal activity of RC films was evaluated. Subsequently, CNC-coated RC films were tested as active food packaging for meat preservation, and the growth of bacteria was monitored.

6.3. Materials and methods

6.3.1 Materials

Bleached spruce pulp was supplied by FP Innovations (Pointe-Claire, QC, Canada). Sodium bromide (99.0%), sodium hypochlorite (12% available chlorine), sodium borohydride (97%), sodium periodate (99%), sodium hydroxide (>97.0%), urea (>99.6%), ethylenediamine (>98%), and RC membrane dialysis tubes with a cut-off of 12-16 kDa were obtained from Fisher Scientific (Ottawa, ON, Canada). Sulfuric acid (95.0-98.0%), hydrochloric acid (37%), (2,2,6,6-Tetramethylpiperidin-1-yl)oxyl (TEMPO) (98%), and ethylene glycol (99%) were

purchased from Millipore-Sigma (Oakville, ON, Canada). Tryptic soy broth, Luria-Bertani broth, tryptic soy agar (TSA), and Luria-Bertani agar (LBA) were acquired from Becton, Dickinson and Company (Franklin Lakes, NJ, USA). Phosphate-buffered saline (10 × PBS) was supplied by VWR International (Mississauga, ON, Canada).

6.3.2 Preparation of CNC with different charges

Mechanical pretreatment involved grinding spruce pulp with a KRUPS grinder (Ontario, Canada) to reduce particle size. A quantity of 6 g of ground spruce pulp underwent hydrolysis with 180 mL of a 4 N HCl solution at 400 rpm and 80 °C for 6 h. The acid hydrolysis process was terminated by homogenizing the solution with ten-fold ice water. Subsequently, the excess HCl was eliminated through centrifugation at 7550 rpm for 10 minutes at 25 °C in 5 cycles. The HCl-hydrolyzed CNC was freeze-dried after dialysis and marked as HCNC. The yield of HCNC was 75.52 ± 1.32% (w/w).

The TEMPO-oxidized CNC (TCNC) was prepared using the TEMPO/NaBr/NaClO system as described by Zhang et al. (2020). The yield of TCNC was 86.81 ± 1.86% (w/w). The preparation of aminated cellulose nanocrystals (ACNC) followed the method described by Jin et al. (2015) with minor adjustments. $NaIO_4$ (4 g) was added to 200 mL HCNC suspension (0.5 wt.%) under dark conditions and stirred at 250 rpm and 45 °C for 5 h, which was stopped by introducing 10 mL of ethylene glycol. After dialysis, 11.12 mL of ethylenediamine was incorporated into 200 mL of dialdehyde CNC suspension (0.5 wt.%) to reach 30 equivalents/glucose unit. The mixture was stirred continuously at 200 rpm and 30 °C for 6 h, and then the resulting imine intermediate was reduced in situ with 0.58 g of $NaBH_4$ for 3 h at 25 °C. The product was then freeze-dried after dialysis. The yields of dialdehyde CNC and ACNC were 62.08 ± 2.64% and 87.14 ± 3.15%, respectively.

6.3.3 Preparation of chevaux-de-frise-like surfaces

The chevaux-de-frise-like surfaces were fabricated using all-cellulose materials based on our previous study (Zhou et al., 2022). Firstly, a quantity of 3 g of ground spruce pulp was continuously stirred in a 300 mL solution of 30 wt.% H_2SO_4 at 25 ℃ and 200 rpm for 48 h. This process reduced the molecular weight of spruce cellulose from 4.54×10^5 g/mol to 1.85×10^5 g/mol (Huang et al., 2022b). The hydrolyzed spruce pulp (0.75 g) was added into 25 mL of pre-cooled H_2SO_4 solution (64%, w/v) at -12 °C and stirred at 1700 rpm for 8 min. The mixture was centrifuged at 1000 rpm for 3 minutes to eliminate air bubbles, which were then cast onto a glass plate and regenerated in a NaOH solution (10%, w/v) at 25 ℃ for 7 min. The RC films underwent a 30 min washing process with running water. A 0.1 wt.% CNC suspension was then deposited dropwise on the RC film under vacuum filtration to yield a 3 wt.% dry weight of RC film, which was subsequently dried under ambient conditions. The original RC film was designated as RC, while the RC films coated with CNC were identified as RC-HCNC, RC-TCNC, and RC-ACNC, corresponding to the respective types of CNC employed.

6.3.4 Characterization

6.3.4.1 Zeta potential

The zeta potential measurements of HCNC, TCNC, and ACNC were carried out at room temperature by electrophoretic light scattering coupled with phase analysis light scattering (Zeta-PALS, Brookhaven Instruments Corporation, Holtsville, NY, USA).

6.3.4.2 Fourier transform infrared (FT-IR) spectroscopy

An Agilent Cary 630 FT-IR spectroscopy coupled with an ATR module (Agilent Technologies, Santa Clara, CA, USA) was used to examine the structures of RC film, HCNC, TCNC, and

ACNC, according to Huang et al. (2023a). The spectral range was 4000-500 cm^{-1} with 64 scans and the spectral resolution was 2 cm^{-1}.

6.3.4.3 X-ray diffractometry (XRD)

The crystalline characteristics of RC film, HCNC, TCNC, and ACNC were determined by a Panalytical Empyrean 3 X-ray diffractometer (Malvern Panalytical Ltd, Malvern, UK) with diffraction angle from 4° to 40°, according to Flores-Jerónimo et al. (2021). The crystallinity index (CI) was computed based on the crystalline area and total area.

6.3.4.4 Morphological analysis

The morphology of HCNC, TCNC, and ACNC was examined using a transmission electron microscope (Talos F200X G2, Thermo Fisher Scientific, Waltham, MA, USA). The morphology of RC and CNC-coated RC films were examined utilizing a field emission scanning electron microscope (FEI Quanta 450, Hillsboro, OR, USA) at 20 kV.

An atomic force microscope (MFP-3D, Asylum Research, Santa Barbara, CA, USA) was employed to investigate surface topographies of CNC-coated RC films. The surface roughness parameters of each sample were analyzed using Gwyddion software (version 2.6, Gwyddion Team).

6.3.4.5 Water contact angle (WCA)

A contact angle measurement system (OCA 20, Dataphysics Instruments, Filderstadt, Germany) was employed to determine the WCA of each film as described by Huang et al. (2023a).

6.3.4.6 Moisture uptake

A 2 cm × 2 cm square cut of the films was conditioned in a desiccator with a diameter of 17.2 cm at 25 °C using anhydrous calcium chloride to maintain 0% relative humidity (RH) until

constant weight (m_i) was achieved. Films were then conditioned in an environment simulating ambient conditions, set at 60% RH, using a saturated NaBr solution at 25 °C for 4 days to determine the weight (m_d). The moisture uptake of the films was computed using Equation 1:

$$Moisture\ uptake\ (\%) = \frac{m_d - m_i}{m_i} \times 100\% \quad (1)$$

6.3.4.7 Water vapor permeability (WVP)

ASTM E96-92 standard was employed to evaluate the WVP of RC and CNC-coated RC films as described by Huang et al. (2022b).

6.3.4.8 Mechanical properties

Films measuring 5 cm × 1 cm (length × width) were conditioned in a controlled environment (25 °C and 60% RH) for 4 days before determining mechanical properties. The stress-strain curve of each film was obtained using ADMET MTEST Quattro eXpert 7600 series (MA, USA) with a crosshead speed of 5 mm/min.

6.3.5 Bactericidal activity

Two bacteria strains were employed for the antibacterial assessment, encompassing *Staphylococcus aureus* (*S. aureus*) and *Escherichia coli* (*E. coli*). To reanimate strains, both bacteria were revived from -80 °C and streaked onto TSA and LBA plates, respectively, and then incubated at 37 °C for 24 hours. The isolated colonies were selected and inoculated into 4 mL of broth media, and the mixture was subjected to continuous shaking at 37 °C and 175 rpm for 16 h. Bacterial solutions were prepared at a concentration of approximately 10^8 CFU/mL and then diluted with PBS to the specified concentrations for subsequent experiments. The antimicrobial evaluations of RC and RC-CNC films were conducted following a previous study with minor adjustments (Zhou et al., 2022). Film samples were sliced into squares of 2 cm × 2

cm and deposited in a Petri dish to contact a 100 μL volume of bacterial suspension (at a concentration of approximately 10^5 CFU/mL) for 5 min.

6.3.6 Meat preservation

The pork tenderloin procured from a nearby grocery store was sliced into pieces of 1 cm × 1 cm × 0.3 cm (length × width × thickness). CNC-coated RC films were employed to wrap pork loin as an experimental group. The two control groups were kept unwrapped and covered with the original RC film, respectively. Each sample was positioned in a closed Petri dish and preserved at 4 °C. The total viable count (TVC) for each sample was assessed at 0, 2, 4, 6, and 8 days of storage, following the procedure outlined by Huang et al. (2023b).

6.3.7 Statistical analysis

One-way analysis of variance (ANOVA) and Duncan's test based on 95% confidence intervals were used to analyze significance by using SPSS 26.0 software (IBM SPSS Inc., New York, NY).

6.4. Results and discussion

The TEM images of different CNC samples are shown in Figure 6.1A. HCNC presented a rod-shaped structure with dimensions of 201.45 ± 36.22 nm and 10.53 ± 2.27 nm in length and diameter, respectively, contributing to an aspect ratio of 19.56 ± 3.43. After TEMPO oxidation, TCNC showed a similar average length of 194.34 ± 18.59 nm, diameter of 11.96 ± 2.25 nm, and aspect ratio of 19.17 ± 1.13. No significant difference was found for ACNC either (length of 182.64 ± 26.40 nm, diameter of 10.23 ± 3.91 nm, and aspect ratio of 18.37 ± 3.44). This result suggested that the chemical modifications did not impact the size and morphology of CNC. However, the chemical modifications successfully changed the surface charge of CNC. As shown in Figure 6.1B, HCNC displayed a weak zeta potential of -7.71 ± 1.01 mV. Carboxyl

groups were introduced on TCNC after TEMPO oxidation, leading to a highly negative zeta potential value of -69.89 ± 0.60 mV. The amino groups presented on ACNC resulted in a positive charge with a zeta potential of 38.16 ± 0.41 mV. In general, a CNC suspension is regarded as unstable when its absolute zeta potential value is less than 15 mV (Clogston & Patri, 2011). Thus, aggregated HCNC was observed by TEM, while TCNC and ACNC were well-dispersed.

The structures of pure RC film and three different types of CNC were studied by FT-IR and XRD. As shown in Figure 6.1C, typical cellulose bands were evident in all samples, including the O─H stretching at 3500-3200 cm^{-1}, C─H stretching vibration at 2885 cm^{-1}, asymmetric ─CH_2 bending vibration at 1427 cm^{-1}, O─H bending at 1315 cm^{-1}, and ─C─O─C─ bridge stretching at 893 cm^{-1} (Huang et al., 2022b). The presence of the N─H bending vibrational peak at 1650 cm^{-1} and the absence of the C═O stretching vibrational peak signified the conversion of dialdehyde CNC into ACNC (Jin et al., 2015). The peaks of ACNC at 3337 and 3279 cm^{-1} were due to the overlapped N─H and O─H stretching vibrations (Pokhrel et al., 2020), while the TCNC sample displayed a peak at 1598 cm^{-1} originating from C═O vibration introduced by TEMPO oxidation at the C6 position (Abou-Zeid et al., 2021). As shown in Figure 6.1D, RC film exhibited the diffraction peaks of cellulose II structure at 12.3° ($1\bar{1}0$) and 20.2° (110) with a crystallinity index of 30.78% (Huang et al., 2022a). All three CNC samples displayed similar diffraction peaks of crystalline cellulose polymorphism I_β at 14.8° ($1\bar{1}0$), 16.5° (110), 22.7° (200), and 34° (040) (Cao et al., 2021). Compared to HCNC, the crystallinity indexes of TCNC and ACNC decreased from 81.66% to 79.97% and 68.94%, respectively, which suggested that the crystalline structure of HCNC was slightly dismantled by oxidation and amination processes (Wu et al., 2020). Therefore, three CNC samples with similar

dimensions and crystalline structures but different surface charges were successfully obtained for the construction of a chevaux-de-frise-like nanostructure.

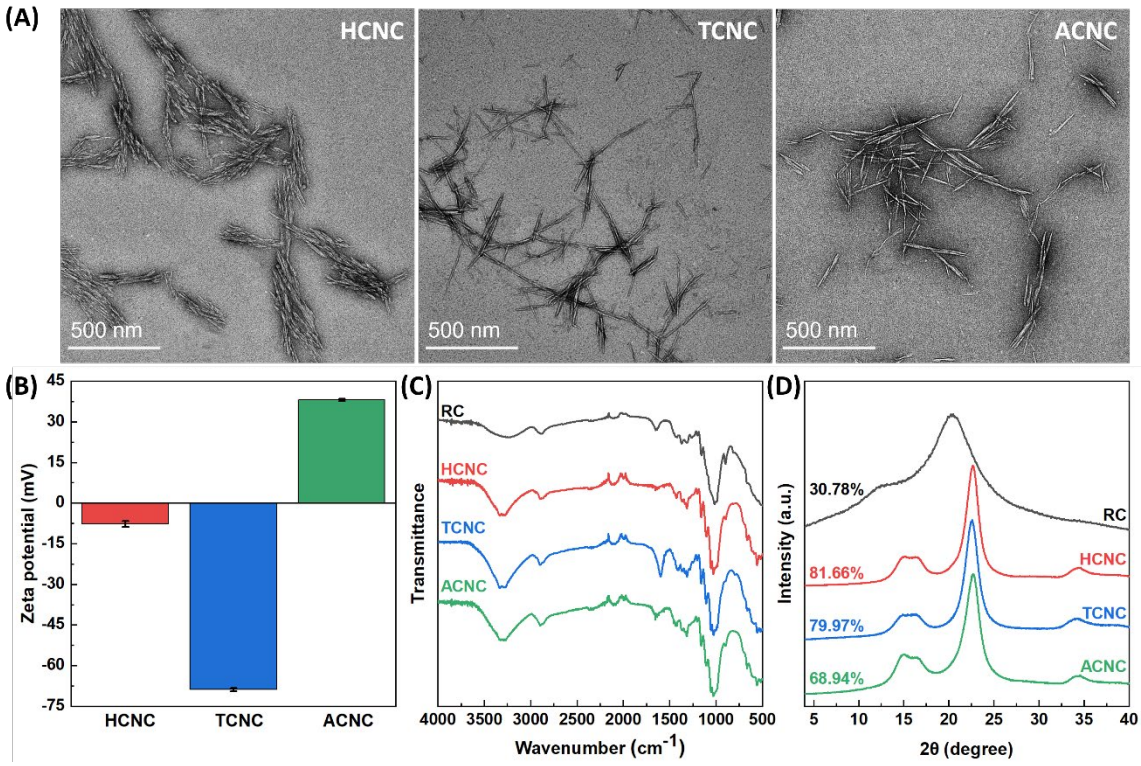

Figure 6.1. (A) TEM images and (B) zeta potential of different CNC samples. (C) FT-IR spectra and (D) XRD patterns and crystallinity index of RC film and CNC samples.

The morphology of RC and CNC-coated films was examined using FE-ESEM and AFM. As shown in Figure 6.2, pristine RC film did not have any undissolved fibers, and the thickness (~13 ± 1 μm) and cross-sectional morphology were not affected after depositing CNC. All three types of CNC were not vertically attached to the RC film like the nanopillars on insect wings. Instead, they formed an intricate and chevaux-de-frise-like nanostructure through interlacement. HCNC was partially clustered on the surface of the RC film due to its low charge, whereas TCNC and ACNC with higher absolute charges were randomly and uniformly distributed on the surface. The surface roughness parameters of CNC-coated films such as root-mean-square (RSM) roughness (R_q), average roughness (R_a), maximum height (R_{max}),

skewness (R_{sk}), and kurtosis (R_{ku}) were obtained through the analysis of AFM images and summarized in Table 1. All three modified films had similar values across these parameters, indicating that the charges of CNC did not have a significant effect on the formation of chevaux-de-frise. It has been reported that a positive correlation existed between bacterial adhesion and R_q within the range of 0.64 - 21 nm (Yang et al., 2022), and the graphite-like carbon wrinkled coating (R_q of 2.03 nm) resulted in a maximum absorption of up to 1.3×10^5 cells mm^{-2} for *P. aeruginosa* (Nguyen et al., 2019). Furthermore, the rough surfaces outperformed smooth surfaces in producing shear force for efficient mechano-bactericidal action due to R_{sk} and R_{ku} (Dehghani et al., 2021; Luan et al., 2018), where R_{sk} quantifies the asymmetry of the height probability distribution and R_{ku} signifies the sharpness of the roughness profile. Dehghani et al. have compared two nanopillars-decorated cicada wings with different roughness parameters and found that the higher R_{sk} and R_{ku} values of cicada wings led to better bactericidal efficiency against *P. aeruginosa* (Dehghani et al., 2021). The nanostructured Ti surface had the R_{sk} of 0.1 and R_{ku} of 2.5, and exhibited inhibition rates of 80.7 ± 12.0% and 86.8 ± 11.6% towards susceptible and resistant *Staphylococcus aureus*, respectively (Wandiyanto et al., 2019), while in this study, the CNC-coated RC films had the similar R_{sk} (0.15 - 0.33) and R_{ku} (2.48 - 2.64) values.

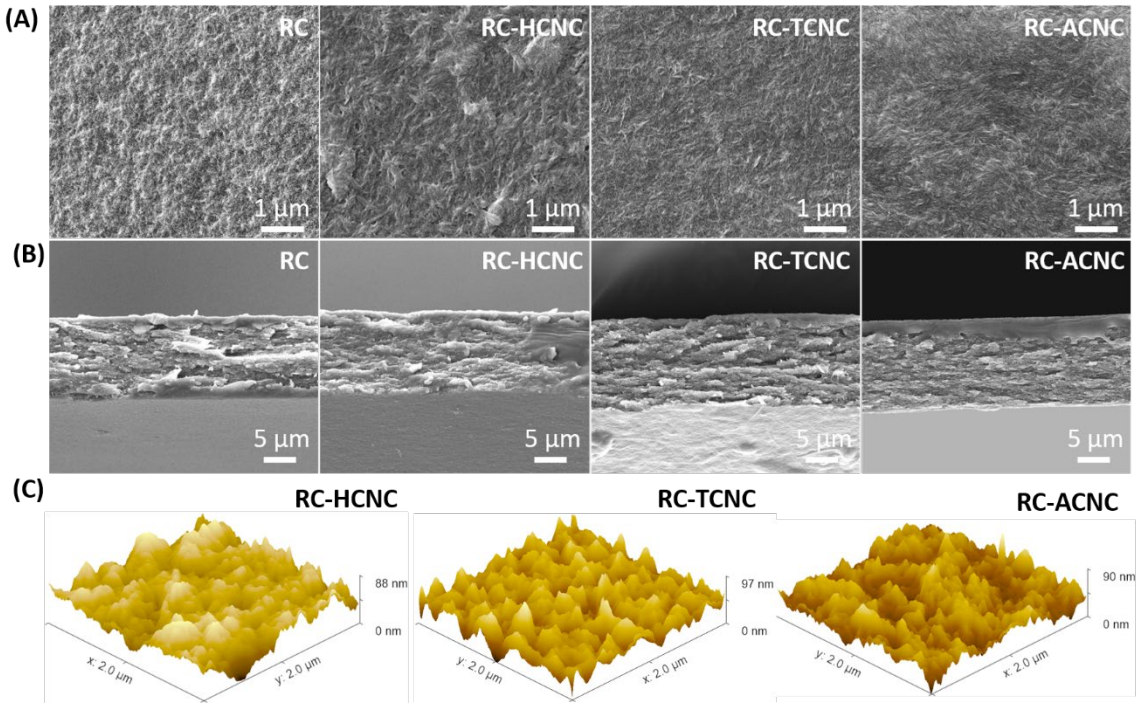

Figure 6.2. (A) Surface and (B) cross-sectional morphologies of RC and CNC-coated RC films. (C) Surface topology of CNC-coated RC films.

Table 6.1. Surface roughness parameters of CNC-coated RC films.

Samples	RMS roughness (nm)	Roughness average (nm)	Maximum height (nm)	Surface skewness	Surface kurtosis
RC-HCNC	10.99	8.68	96.86	0.15	2.61
RC-TCNC	11.18	8.68	88.47	0.15	2.64
RC-ACNC	10.63	8.58	90.01	0.33	2.48
Graphite-like carbon coating (Nguyen et al., 2019)	2.03	/	/	0.59	2.32
Nanostructured Ti surfaces (Wandiyanto et al., 2019)	8.8	6.2	/	0.1	2.5

As depicted in Figure 6.3A, an increase in the WCA from 41.85 ± 2.57° to 64.90 ± 2.84°, 59.68 ± 3.91°, and 64.66 ± 1.74° was observed for RC films after HCNC, TCNC, and ACNC

coatings, respectively. It was because of that the dispersed CNC trapped surrounding air pockets to form a network of air cushions (Figure 6.3B), leading to the decreased contact area and penetration rate of water droplets (Hu et al., 2016). This further resulted in the reduced moisture uptake of RC film from 14.49 ± 1.73% to 9.54 ± 0.40%, 8.51 ± 1.33%, and 10.93 ± 0.66% for RC-HCNC, RC-TCNC, and RC-ACNC, respectively. Figure 6.3D shows the WVP of RC and CNC-coated RC films. The original RC film displayed a WVP value of 1.83 ± 0.08 $\times 10^{-7}$ g m^{-1} h^{-1} Pa^{-1}. The deposition of CNC and the formation of air cushions constructed a tortuous path for water vapor diffusion and decreased WVP values of RC-HCNC, RC-TCNC, and RC-ACNC to 1.11 ± 0.01, 1.20 ± 0.04, and 1.20 ± 0.09 $\times 10^{-7}$ g m^{-1} h^{-1} Pa^{-1}, respectively, which were lower than those of other antimicrobial films such as ZnO nanopillars-incorporated cellulose film (8.46 $\times 10^{-7}$ g m^{-1} h^{-1} Pa^{-1}) (Xie et al., 2022) and ZnO reinforced cellulose-based film (7.88 $\times 10^{-7}$ g m^{-1} h^{-1} Pa^{-1}) (Pan et al., 2022), and similar to xanthan/hydroxypropyl methylcellulose/tea polyphenols composite film (1.20 $\times 10^{-7}$ g m^{-1} h^{-1} Pa^{-1}) (Chen et al., 2022). As shown in Figure 6.3F, the original RC film had a tensile strength of 74.23 ± 1.20 MPa, which was improved to 95.03 ± 5.73 MPa, 105.06 ± 4.24 MPa, and 104.83 ± 8.86 MPa with HCNC, TCNC, and ACNC coatings, respectively. The tensile strength of CNC-coated RC films was higher than those of other reported nanostructured antimicrobial packaging materials, including chitosan/nano-ZnO/organoclay composite film (38.86 ± 1.49 MPa) (Rodrigues et al., 2020), ZnO nanopillars-incorporated cellulose film (55.0 MPa) (Xie et al., 2022), and bionic polystyrene film with nanopillar structure (40.0 MPa) (Du et al., 2023). Similar to our previous observation (Huang et al., 2023a), RC-HCNC, RC-TCNC, and RC-ACNC exhibited higher Young's modulus but decreased tensile strain values compared to RC film, because the rigid CNC surface coating well bonded to the RC matrix and formed a scaffolding effect to improve the resistance to loading, and at the same time, restrict the extension of RC films.

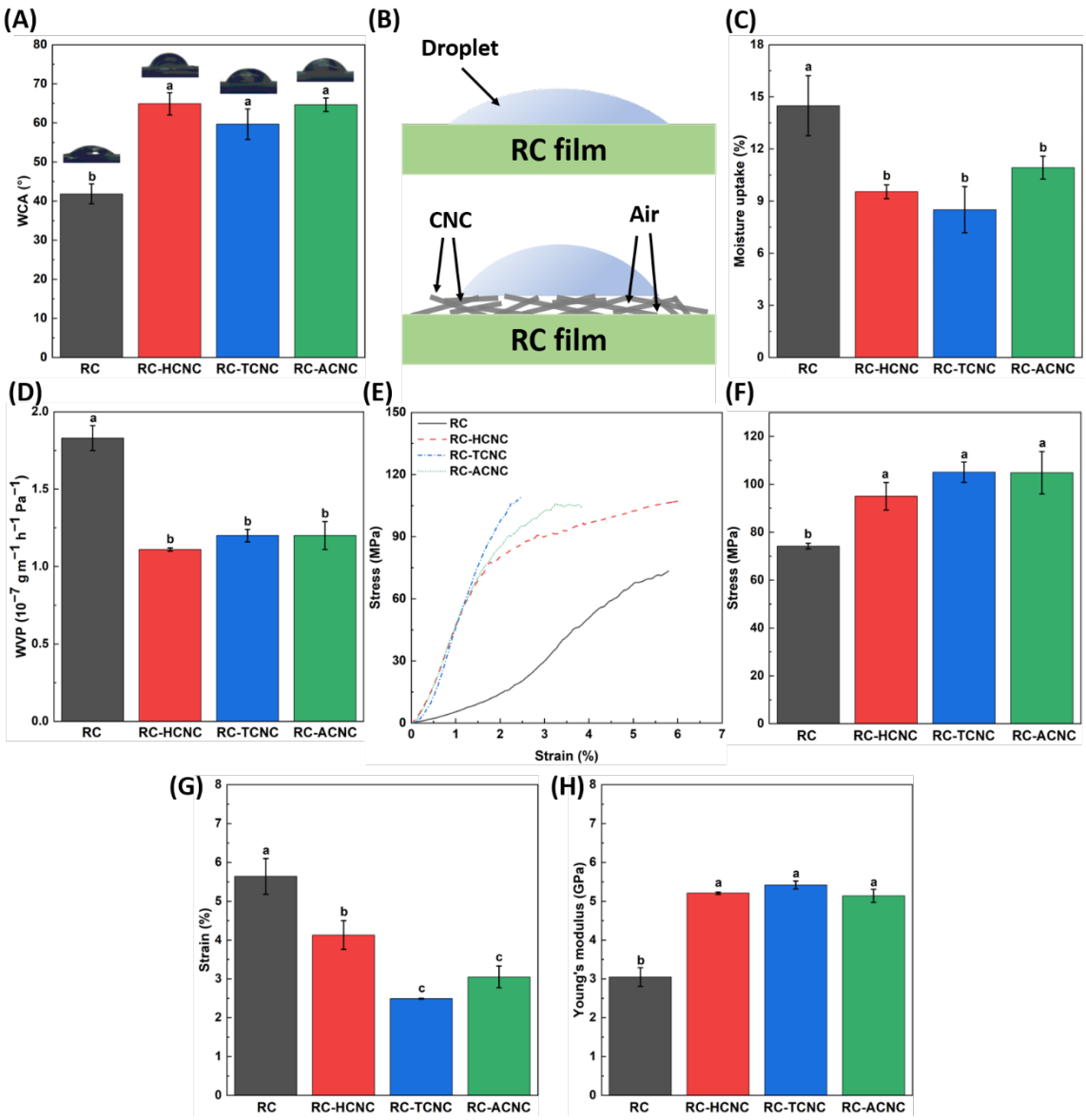

Figure 6.3. (A) WCA of RC and CNC-coated RC films. (B) Schematic illustration of water droplets on RC and CNC-coated RC films. (C) Moisture uptake, (D) WVP, and (E-H) mechanical properties of RC and CNC-coated RC films.

As shown in Figure 6.4A, after 5 min of contact, pristine RC film did not show any antibacterial effect. RC-ACNC exhibited significant bactericidal activity against *E. coli* and *S. aureus* with 0.83 ± 0.06 and 0.69 ± 0.04 log reductions, respectively. However, RC-HCNC and RC-TCNC had similar roughness parameters to RC-ACNC but did not have obvious antibacterial

properties. It might be ascribed to the fact that the positively charged RC-ACNC was effective in quickly attracting bacteria to achieve an antimicrobial effect, while the strong negative charges of RC-TCNC affected the contact between bacteria and chevaux-de-frise-like nanostructure. The weakly charged RC-HCNC formed bundles with a smaller surface area, leading to a decrease in bactericidal activity (Ivanova et al., 2020). The cellulose films decorated with ZnO nanopillars showed about 0.27 and 0.24 log reductions for *E. coli* and *S. aureus*, respectively, ascribing to the mechanical rupture of cell walls (Xie et al., 2022). Nevertheless, our previous studies have elucidated that the production of reactive oxygen species was not the main driving force for CNC-coated RC films to inhibit bacteria and the structure of bacteria did not change after contact (Zhou et al., 2022), so the mechano-bactericidal properties of RC-ACNC might be based on sub-lethal mechanical damage that did not immediately kill the bacteria but resulted in apoptosis-like cell death (Zhao et al., 2022). Besides, RC-ACNC was more effective in inhibiting the growth of *E. coli* than *S. aureus*. A comparable outcome was noted on a silicon nanopillar surface, where a greater efficacy against gram-negative bacteria of *P. aeruginosa* was observed compared to gram-positive bacteria of *S. aureus*. This heightened effectiveness was associated with more evident deformation, which was attributed to the variations in the rigidity of the cell's outer walls (Ivanova et al., 2020).

The RC and CNC-coated RC films were applied as antimicrobial packaging for meat preservation. As shown in Figure 6.4B, the initial TVC value of raw pork loins was 4.95 ± 0.12 log CFU/g, which was slightly higher than the reported values of 4.7 and 4.41 log CFU/g (Leelaphiwat et al., 2022; Vargas Romero et al., 2021). The bacteria in pork packaged by RC film and unwrapped pork grew very rapidly during the storage period, whereas all three CNC-coated films had significant inhibitory effects on bacterial growth, although the bactericidal activity was only presented on the contact interface between the pork and films. RC-ACNC

had about 0.3 log reduction on day 2, and this value slightly increased to 0.4 log reduction on day 4. Surprisingly, RC-HCNC and RC-TCNC did not show obvious antimicrobial properties in the 5-minute contact experiment but could inhibit the growth of bacteria during pork preservation, and the TVC values gradually increased to a similar 0.4 log reduction as RC-ACNC. It indicated that the physical attachment of the chevaux-de-frise-like nanostructures on pork surfaces could gradually compensate for the antimicrobial effect caused by the lack of attractive force. Therefore, the deposition of CNC on the surface of packaging films can be considered as a preliminary antimicrobial measure and be used synergistically in combination with other antimicrobial approaches to extend the shelf life of packaged foods.

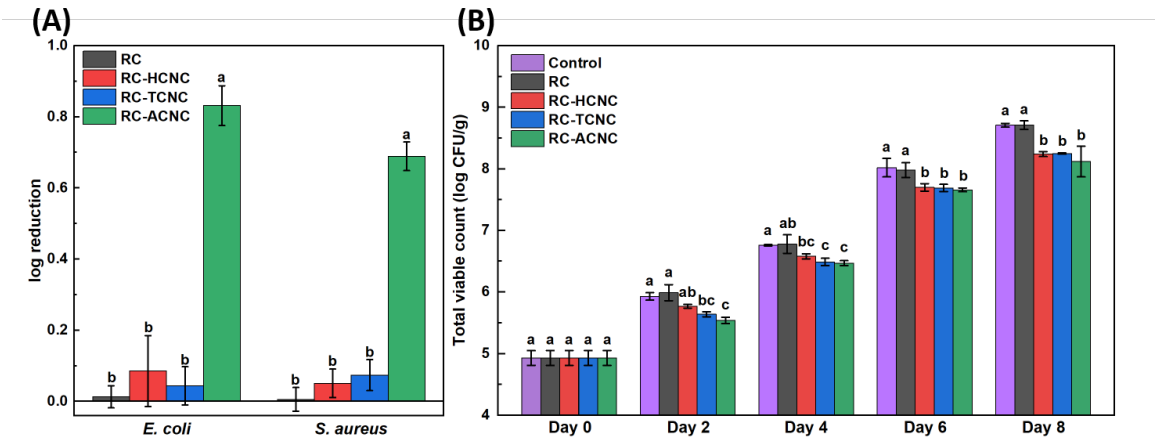

Figure 6.4. (A) Antimicrobial activities of RC and modified films. (B) TVC of pork loins during storage at 4 °C.

6.5. Conclusion

Three CNC samples were obtained by acid hydrolysis, TEMPO oxidation, and amination, and exhibited similar morphology and crystalline structure but different surface charges. The chevaux-de-frise-like nanostructures were formed by coating three CNC samples on the surface of RC films via vacuum filtration, which enhanced the tensile strength (to about 100 MPa) and water vapor barrier property (to about 1.20×10^{-7} g m^{-1} h^{-1} Pa^{-1}). The hypothesis has been

confirmed that RC-ACNC with a positively charged surface was more effective in attracting negatively charged foodborne bacteria, leading to higher antibacterial activities against *E. coli* and *S. aureus* after 5 min contact. The RC-ACNC coated RC film also showed a stronger bacterial inhibition capacity in the first 2 days of meat storage, but the difference among the three CNC coatings was not significant after day 4. It was probably attributed to the tight contact between packaging films and meat that physically forced bacteria to adhere to the chevaux-de-frise-like surfaces. Therefore, this work demonstrates the importance of attractive force and tight contact between CNC-constructed chevaux-de-frise and bacteria for inhibiting bacterial growth and the potential to build sustainable nanostructures for active food packaging.

6.6. References

Abbaszadegan, A., Ghahramani, Y., Gholami, A., Hemmateenejad, B., Dorostkar, S., Nabavizadeh, M., & Sharghi, H. (2015). The effect of charge at the surface of silver nanoparticles on antimicrobial activity against gram-positive and gram-negative bacteria: a preliminary study. *Journal of Nanomaterials*, *16*(1), 53-53.

Abou-Zeid, R. E., Kamal, K. H., Abd El-Aziz, M., Morsi, S., & Kamel, S. (2021). Grafted TEMPO-oxidized cellulose nanofiber embedded with modified magnetite for effective adsorption of lead ions. *International Journal of Biological Macromolecules*, *167*, 1091-1101.

Cao, X., Wang, Y., Chen, H., Hu, J., & Cui, L. (2021). Preparation of different morphologies cellulose nanocrystals from waste cotton fibers and its effect on PLLA/PDLA composites films. *Composites Part B: Engineering*, *217*, 108934.

Chen, J., Zheng, M., Tan, K. B., Lin, J., Chen, M., & Zhu, Y. (2022). Development of xanthan gum/hydroxypropyl methyl cellulose composite films incorporating tea polyphenol and

its application on fresh-cut green bell peppers preservation. *International Journal of Biological Macromolecules*, *211*, 198-206.

Chu, X., Aydin, F., & Dutt, M. (2016). Modeling interactions between multicomponent vesicles and antimicrobial peptide-inspired nanoparticles. *Acs Nano*, *10*(8), 7351-7361.

Clogston, J. D., & Patri, A. K. (2011). Zeta potential measurement. *Characterization of nanoparticles intended for drug delivery*, 63-70.

Dehghani, S., Mashreghi, M., Nezhad, A. H. N., Karimi, J., Hosseinpour, S., & Davoodi, A. (2021). Exploring mechano-bactericidal nature of *Psalmocharias* cicadas wings: an analytical nanotopology investigation based on atomic force microscopy characterization. *Surfaces and Interfaces*, *26*, 101407.

Du, Y., Wu, T., Zhou, W., Li, C., Ding, C., Chen, P., Xie, H., & Qu, J. (2023). Cicada wing-inspired transparent polystyrene film integrating self-cleaning, antifogging, and antibacterial properties. *ACS Applied Materials & Interfaces*, *15*(39), 46538-46549.

Elbourne, A., Coyle, V. E., Truong, V. K., Sabri, Y. M., Kandjani, A. E., Bhargava, S. K., Ivanova, E. P., & Crawford, R. J. (2019). Multi-directional electrodeposited gold nanospikes for antibacterial surface applications. *Nanoscale Advances*, *1*(1), 203-212.

Flores-Jerónimo, G., Silva-Mendoza, J., Morales-San Claudio, P. C., Toxqui-Terán, A., Aguilar-Martínez, J. A., & Chávez-Guerrero, L. (2021). Chemical and mechanical properties of films made of cellulose nanoplatelets and cellulose fibers obtained from banana pseudostem. *Waste and Biomass Valorization*, 1-9.

Hayles, A., Hasan, J., Bright, R., Palms, D., Brown, T., Barker, D., & Vasilev, K. (2021). Hydrothermally etched titanium: A review on a promising mechano-bactericidal surface for implant applications. *Materials Today Chemistry*, *22*, 100622.

Hu, Z., Sun, M., Lv, M., Wang, L., Shi, J., Xiao, T., Cao, Y., Wang, J., & Fan, C. (2016). Deciphering buried air phases on natural and bioinspired superhydrophobic surfaces using synchrotron radiation-based X-ray phase-contrast imaging. *NPG Asia Materials*, *8*(9), e306-e306.

Huang, C., Yu, H., Abdalkarim, S. Y. H., Li, Y., Chen, X., Yang, X., Zhou, Y., & Zhang, L. (2022a). A comprehensive investigation on cellulose nanocrystals with different crystal structures from cotton via an efficient route. *Carbohydrate Polymers*, *276*, 118766.

Huang, K., Maltais, A., Liu, J., & Wang, Y. (2022b). Wood cellulose films regenerated from NaOH/urea aqueous solution and treated by hot pressing for food packaging application. *Food Bioscience*, *50*, 102177.

Huang, K., Maltais, A., & Wang, Y. (2023a). Enhancing water resistance of regenerated cellulose films with organosilanes and cellulose nanocrystals for food packaging. *Carbohydrate Polymer Technologies and Applications*, *6*, 100391.

Huang, S., Zou, S., & Wang, Y. (2023b). Construction of compostable packaging with antibacterial property and improved performance using sprayed coatings of modified cellulose nanocrystals. *Carbohydrate Polymers*, *305*, 120539.

Ivanova, E. P., Hasan, J., Webb, H. K., Truong, V. K., Watson, G. S., Watson, J. A., Baulin, V. A., Pogodin, S., Wang, J. Y., & Tobin, M. J. (2012). Natural bactericidal surfaces: Mechanical rupture of *Pseudomonas aeruginosa* cells by cicada wings. *Small*, *8*(16), 2489.

Ivanova, E. P., Linklater, D. P., Aburto-Medina, A., Le, P., Baulin, V. A., Nguyen, H. K. D., Curtain, R., Hanssen, E., Gervinskas, G., & Ng, S. H. (2021). Antifungal versus antibacterial defence of insect wings. *Journal of Colloid and Interface Science*, *603*,

886-897.

Ivanova, E. P., Linklater, D. P., Werner, M., Baulin, V. A., Xu, X., Vrancken, N., Rubanov, S., Hanssen, E., Wandiyanto, J., & Truong, V. K. (2020). The multi-faceted mechano-bactericidal mechanism of nanostructured surfaces. *Proceedings of the National Academy of Sciences*, *117*(23), 12598-12605.

Jin, L., Li, W., Xu, Q., & Sun, Q. (2015). Amino-functionalized nanocrystalline cellulose as an adsorbent for anionic dyes. *Cellulose*, *22*, 2443-2456.

Leelaphiwat, P., Pechprankan, C., Siripho, P., Bumbudsanpharoke, N., & Harnkarnsujarit, N. (2022). Effects of nisin and EDTA on morphology and properties of thermoplastic starch and PBAT biodegradable films for meat packaging. *Food Chemistry*, *369*, 130956.

Linklater, D. P., Baulin, V. A., Juodkazis, S., Crawford, R. J., Stoodley, P., & Ivanova, E. P. (2021). Mechano-bactericidal actions of nanostructured surfaces. *Nature Reviews Microbiology*, *19*(1), 8-22.

Lohmann, S. C., Tripathy, A., Milionis, A., Keller, A., & Poulikakos, D. (2022). Effect of flexibility and size of nanofabricated topographies on the mechanobactericidal efficacy of polymeric surfaces. *ACS Applied Bio Materials*, *5*(4), 1564-1575.

Luan, Y., Liu, S., Pihl, M., van der Mei, H. C., Liu, J., Hizal, F., Choi, C.-H., Chen, H., Ren, Y., & Busscher, H. J. (2018). Bacterial interactions with nanostructured surfaces. *Current Opinion in Colloid & Interface Science*, *38*, 170-189.

Luo, L., Zhou, Y., Xu, X., Shi, W., Hu, J., Li, G., Qu, X., Guo, Y., Tian, X., & Zaman, A. (2020). Progress in construction of bio-inspired physico-antimicrobial surfaces. *Nanotechnology Reviews*, *9*(1), 1562-1575.

Maher, S., Linklater, D., Rastin, H., Le Yap, P., Ivanova, E. P., & Losic, D. (2022). Tailoring additively manufactured titanium implants for short-time pediatric implantations with enhanced bactericidal activity. *ChemMedChem*, *17*(2), e202100580.

Mainwaring, D. E., Nguyen, S. H., Webb, H., Jakubov, T., Tobin, M., Lamb, R. N., Wu, A. H.-F., Marchant, R., Crawford, R. J., & Ivanova, E. P. (2016). The nature of inherent bactericidal activity: insights from the nanotopology of three species of dragonfly. *Nanoscale*, *8*(12), 6527-6534.

Nguyen, D. H., Wang, J., Sbarski, I., Juodkazis, S., Crawford, R. J., & Ivanova, E. P. (2019). Influence of amorphous, carbon-derived wrinkled surface topologies on the colonization of *Pseudomonas aeruginosa* bacteria. *Advanced Materials Interfaces*, *6*(7), 1801890.

Pan, Y., Xie, Y., & Cai, P. (2022). Cellulose-based films reinforced by in-situ generated ZnO for antimicrobial packaging. *Cellulose*, *29*(17), 9375-9391.

Pokhrel, S., Shrestha, M., Slouf, M., Sirc, J., & Adhikari, R. (2020). Eco-friendly urea-formaldehyde composites based on corn husk cellulose fiber. *International Journal of Composite Materials*, *10*(2), 29-36.

Rodrigues, C., de Mello, J. M. M., Dalcanton, F., Macuvele, D. L. P., Padoin, N., Fiori, M. A., Soares, C., & Riella, H. G. (2020). Mechanical, thermal and antimicrobial properties of chitosan-based-nanocomposite with potential applications for food packaging. *Journal of Polymers and the Environment*, *28*, 1216-1236.

Román-Kustas, J., Hoffman, J. B., Reed, J. H., Gonsalves, A. E., Oh, J., Li, L., Hong, S., Jo, K. D., Dana, C. E., & Miljkovic, N. (2020). Molecular and topographical organization: Influence on cicada wing wettability and bactericidal properties. *Advanced Materials*

Interfaces, *7*(10), 2000112.

Trache, D., Tarchoun, A. F., Derradji, M., Hamidon, T. S., Masruchin, N., Brosse, N., & Hussin, M. H. (2020). Nanocellulose: from fundamentals to advanced applications. *Frontiers in Chemistry*, *8*, 392.

Vargas Romero, E., Lim, L.-T., Suarez Mahecha, H., & Bohrer, B. M. (2021). The effect of electrospun polycaprolactone nonwovens containing chitosan and propolis extracts on fresh pork packaged in linear low-density polyethylene films. *Foods*, *10*(5), 1110.

Wandiyanto, J. V., Cheeseman, S., Truong, V. K., Al Kobaisi, M., Bizet, C., Juodkazis, S., Thissen, H., Crawford, R. J., & Ivanova, E. P. (2019). Outsmarting superbugs: bactericidal activity of nanostructured titanium surfaces against methicillin-and gentamicin-resistant *Staphylococcus aureus* ATCC 33592. *Journal of Materials Chemistry B*, *7*(28), 4424-4431.

Wu, Q., Xu, J., Wu, Z., Zhu, S., Gao, Y., & Shi, C. (2020). The effect of surface modification on chemical and crystalline structure of the cellulose III nanocrystals. *Carbohydrate Polymers*, *235*, 115962.

Xie, Y., Pan, Y., & Cai, P. (2022). Cellulose-based antimicrobial films incroporated with ZnO nanopillars on surface as biodegradable and antimicrobial packaging. *Food Chemistry*, *368*, 130784.

Yang, K., Shi, J., Wang, L., Chen, Y., Liang, C., Yang, L., & Wang, L.-N. (2022). Bacterial anti-adhesion surface design: Surface patterning, roughness and wettability: A review. *Journal of Materials Science & Technology*, *99*, 82-100.

Zhao, S., Li, Z., Linklater, D. P., Han, L., Jin, P., Wen, L., Chen, C., Xing, D., Ren, N., & Sun, K. (2022). Programmed death of injured *Pseudomonas aeruginosa* on mechano-

bactericidal surfaces. *Nano Letters*, *22*(3), 1129-1137.

Zhao, X., Xu, Z., Wei, Z., Sun, Y., & Zhou, Q. (2023). Nature-inspired mechano-bactericidal nanostructured surfaces with photothermally enhanced antibacterial performances. *Progress in Organic Coatings*, *182*, 107599.

Zhang, H., Chen, Y., Wang, S., Ma, L., Yu, Y., Dai, H., & Zhang, Y. (2020). Extraction and comparison of cellulose nanocrystals from lemon (*Citrus limon*) seeds using sulfuric acid hydrolysis and oxidation methods. *Carbohydrate Polymers*, *238*, 116180.

Zhou, C., Girouard, F., O'Brien, B., Ronholm, J., & Wang, Y. (2022). Construction of chevaux-de-frise from cellulose nanocrystals to enable mechano-bactericidal activity on recycled waste cotton films. *Green Chemistry*, *24*(3), 1109-1113.

Zhou, C., & Wang, Y. (2021). Recycling of waste cotton fabrics into regenerated cellulose films through three solvent systems: A comparison study. *Journal of Applied Polymer Science*, *138*(48), 51255.

Chapter 7. General Discussion

Cellulose presents a promising alternative for mitigating the environmental impact caused by the accumulation of non-degradable petroleum-based packaging materials (Su et al., 2023). Its advantages include inexpensiveness, low density, non-toxicity, versatility, and excellent mechanical properties (Joo et al., 2023). However, cellulose's complex molecular structure and the strong hydrogen bonding between its molecules make it difficult to dissolve in common solvents such as water and ethanol. The development of various solvents, such as NMMO, LiCl/DMAc, ionic liquids, and alkaline aqueous solutions, has enabled the production of RC films with diverse structures and properties (Baghaei & Skrifvars, 2020). Cellulose-based food-packaging materials, such as cellophane, have been widely utilized. Nonetheless, with the growing demand for improved food protection, there is an urgent need to explore novel food packaging materials with multiple functional properties. This can be achieved by constructing cellulose-based composites with the incorporation of functional polymers and/or additives to enhance mechanical properties, optical properties, barrier properties, thermal stability, and antimicrobial properties (Baghaei & Skrifvars, 2020). This study investigates strategies to produce sustainable food packaging from wood cellulose.

In Chapter 3, the structures and properties of wood cellulose films obtained from concentrated H_2SO_4 and NaOH/urea aqueous solutions were compared. Mechanical and barrier properties are crucial for evaluating the packaging performance of films. Tensile strength is defined as the maximum stress a material can withstand while being stretched or pulled before breaking. Results showed that RC films obtained from H_2SO_4 solution (RC-H4) exhibited higher tensile strength (109.78±2.14 MPa), folding endurance (20-28 times), and torsion angle (42°) compared to those from NaOH/urea solution (62.90±2.27 MPa, un-foldable, and 12°). The cellulose content from 3 to 5 wt.% in H_2SO_4 solution positively correlated with tensile strength without affecting foldability. Additionally, RC-H4 demonstrated better water vapor barrier

property and transparency but lower thermal stability compared to RC-N4. Further analyses revealed differences in film morphology, molecular weight, crystallinity, and other properties between the two solvent systems. Notably, RC films from the H_2SO_4 solution exhibited more amorphous structure, attributed to sulfate ions disrupting hydrogen bonding during regeneration (Sadeghalvad et al., 2021). This amorphous structure contributed to improved foldability of RC films. In contrast, RC-N4 films showed higher porosity and crystallinity, affecting moisture uptake and light transmittance. The findings suggest potential applications for RC films regenerated from both solvents, each with unique properties. RC films from H_2SO_4 solution could be suitable for applications requiring higher mechanical strength and foldability, while those from NaOH/urea solution could be beneficial for applications requiring higher porosity for reagent accessibility and subsequent modifications. Overall, this study provides valuable insights into the sustainable processing of wood cellulose through different aqueous solvents, offering a promising alternative to non-degradable plastics. The comparison of RC films obtained from different solutions highlights the effect of solvent systems on the structure of RC films, facilitating the development of high-performance RC films from abundant forestry resources.

In Chapter 4, wood cellulose films obtained from NaOH/urea solution were used to investigate the effect of different wood species and drying methods on the structure and properties of RC films. Three hardwood (aspen, eucalyptus, and maple) and two softwood (pine and spruce) pulps were firstly acid hydrolyzed and then dissolved in NaOH/urea aqueous solution, followed by air-drying or hot-pressing treatment to obtain RC films. Different wood species did not lead to the variation in the thickness of RC films while hot-pressing treatment decreased the average thickness of RC films from 33 ± 3 μm to 27 ± 1 μm. Hot-pressing produced denser RC films, as evidenced by increased density (from 0.95 to 1.15 g/cm^3), decreased porosity (from 35% to

22.5%), and reduced free space and cavities in the cross-sectional area of the films. FT-IR and XRD analyses indicated that the wood species and treatment methods resulted in similar chemical structure and cellulose II crystalline structures in the RC films, without any chemical modifications. However, hot-pressing produced smoother, more uniform film surfaces with denser internal structures, enhancing film transparency. Tensile strength was influenced by the molecular weight, CI value, and density of the films. Hot-pressed pine films, with a high viscosity-average molecular weight of 1.46×10^5 g/mol, CI value of 55.65%, and density of about 1.15 g/cm^3, exhibited the highest tensile strength of 85.00 ± 3.26 MPa, outperforming commercial cellophane (18 MPa) (Zhao et al., 2019).

Besides, the denser hot-pressed RC films reduced the water vapor diffusion pathway, leading to lowered WVP values from 4.14 ± 0.19 to $4.59 \pm 0.11 \times 10^{-7}$ g m^{-1} h^{-1} Pa^{-1} to 3.43 ± 0.36 to $3.89 \pm 0.15 \times 10^{-7}$ g m^{-1} h^{-1} Pa^{-1}. The hot-pressed pine films were compared with commercial plastic wrap for packaging cherry tomatoes, showing similar weight loss percentages and shrinkage after 16 days of storage without putridity. Considering the higher WVP ($3.56 \pm 0.14 \times 10^{-7}$ g m^{-1} h^{-1} Pa^{-1}) but lower OP ($3.01 \pm 0.49 \times 10^{-5}$ cc m^{-1} day^{-1} atm^{-1}) values of hot-pressed pine films than those of plastic wraps ($2.37 \pm 0.17 \times 10^{-8}$g m^{-1} h^{-1} Pa^{-1} and more than 0.02 cc m^{-1} day^{-1} atm^{-1}), the weight loss of packaged cherry tomatoes was primarily due to the water loss from transpiration and respiration processes (Jalali et al., 2020). Overall, RC films obtained from different wood species exhibited similar dissolution and regeneration processes, leading to no significant structural differences and morphology. Hot-pressing treatment provided a sustainable option to enhance the mechanical and barrier properties of RC films without adding any chemical additives, extending the shelf life of packaged cherry tomatoes similar to commercial plastic wraps.

However, the hygroscopic nature of cellulose facilitated the absorption of moisture from the

environment, which posed a threat to the tensile strength and integrity of films during transportation and storage processes (Cheng et al., 2022). Therefore, in Chapter 5, we aimed to enhance the water resistance of RC films under high humidity or even wet conditions without compromising their degradability. CNC was isolated from wood pulp through an acid hydrolysis process and added to cellulose solution to produce CNC-reinforced RC films, followed by the CVD of two organosilane examples (MTMS and PFTS) for dual modification. The presence of peaks at 1260 and 780 cm^{-1} due to the Si─C vibration and peaks at 1230 cm^{-1} due to the C─F stretching confirmed the modification of RC films by MTMS and PFTS, respectively (Yu et al., 2019; Kowalczuk & Pitucha, 2019), but they did not change the thickness of RC films (29 ± 2 μm). The addition of CNC increased the CI value of RC films from 60.55% to 70.91% without changing their cellulose II structure, which was then decreased to 68.46% and 64.21% after modification of MTMS and PFTS, respectively. The chemical modification increased water contact angle (higher than 100°) while detrimentally affected the tensile strength of RC films. For instance, the RC films modified with MTMS and PFTS showed the reduced tensile strength from 66.37 ± 2.79 MPa to 41.02 ± 0.11 MPa and 42.92 ± 1.58 MPa under 0% RH, respectively, due to decreased hydrogen bonding between cellulose chains. Therefore, the addition of CNC, which acted as nanofillers, was necessary for RC films to compensate for the degraded mechanical strength to 57.11 ± 1.52 MPa and 59.67 ± 1.09 MPa, respectively. The dual-modified films with increased hydrophobicity maintained the tensile strength of MTMS (56.79 ± 3.67 MPa) and PFTS (58.87 ± 3.75 MPa) modified RC films with the addition of CNC at 60% RH. In comparison, the pristine RC films showed a decreased tensile strength of 52.09 ± 2.80 MPa at 60% RH. Immersing the modified films into water for 12 h as an extreme condition yielded a tensile strength of about 12 MPa, better than the 4.5 MPa of pristine RC films. Moreover, the dual modification decreased the water vapor

penetration and adsorption, resulting in the reduced WVP values of RC films from 4.07 ± 0.18 × 10^{-7} g m^{-1} h^{-1} Pa^{-1} to about 3.3 × 10^{-7} g m^{-1} h^{-1} Pa^{-1}. It should be noted that the addition of CNC and dual modification did not change the OP value of modified RC films (about 1.37 ×10^{-5} cm^3 m^{-1} day^{-1} atm^{-1}), which could be explained by the fact that CNC decreased the oxygen diffusion pathway and organosilanes interacted with hydroxyl groups and decreased the polarity of RC films. The modified films were used to preserve chocolate cookies at 25 °C and 60% RH for 100 days and compared with commercial plastic wrap. The weight gain of preserved cookies packaged with modified films was comparable to that of plastic wraps. PV values were determined to evaluate the freshness of oils inside of cookies, and lower values indicated a fresher food (Srivastava & Mishra, 2021). Surprisingly, the dual-modified RC films led to similar PV values of cookies to those packaged in plastic wraps, because both oxygen and moisture caused the degradation of lipids. The disintegration test indicated that dual modification only delayed the full disintegration process by 2 days (from 12 days to 14 days), which was due to the decreased water penetration into RC films. Overall, this study presented a simple and feasible method to improve the water-resistance of RC films without changing their disintegration capacity, providing a significant potential for developing sustainable packaging materials with good performance.

Another promising application of cellulose-based films is antimicrobial packaging, which uses cellulose as a matrix to incorporate various antimicrobial ingredients such as metallic nanoparticles and chemical preservatives (Zhang et al., 2021). However, excessive usage of chemical antimicrobial agents can result in the development of antimicrobial resistance in pathogens and may migrate into food products, posing harmful effects. One of the novel and promising strategies was to fabricate nanostructured cellulose film with mechano-bactericidal ability, mimicking the nanopillars and nanospikes on the surface of the insect wings (Linklater

et al., 2021). Our previous study successfully fabricated a chevaux-de-frise-like nanostructure by depositing acid-hydrolyzed CNC on the surface of RC films using vacuum filtration and investigated the effects of cellulose concentrations, contact time, and temperature on the mechano-bactericidal activity. Therefore, Chapter 6 aimed to investigate the effect of the surface charge of CNC on the mechanical and barrier properties, mechano-bactericidal activity, and meat preservation performance of nanostructured RC films. The hydrochloric acid hydrolyzed CNC (HCNC) with limited charges was modified by TEMPO oxidation or amination to produce CNC with highly negative (TCNC) or positive (ACNC) charges. The TEM observation proved that chemical modification did not change the rod shape of three different CNC, which showed similar lengths in the range of 180 to 200 nm and diameters in the range of 10 to 12 nm. The surface charge of HCNC was -7.71 ± 1.01 mV, which changed to -69.89 ± 0.60 mV and 38.16 ± 0.41 mV after incorporating carboxyl groups and amino groups, respectively. FT-IR analysis showed a peak at 1598 cm^{-1} from C═O vibration introduced by TEMPO oxidation (Fan et al., 2022). Besides, the presence of the N─H bending vibrational peak at 1650 cm^{-1} and the increased peak intensities at 3337 and 3279 cm^{-1} were due to the overlapped N─H and O─H stretching vibrations, indicating the anchoring of amino groups on CNC (Koshani et al., 2022). The morphology of pristine and CNC-coated RC films was observed by FE-SEM. It should be noted that all CNC were not vertically attached to the surface of RC films like nanostructured insect wings, but rather formed an interlaced chevaux-de-frise-like nanostructure. The aggregation of HCNC was found during TEM and FE-SEM observations, which was due to the low surface charge to dispense homogeneously. The topology and roughness parameters of three differently charged RC films were determined by AFM. An uneven surface with a maximum height of about 90 nm was found for three CNC-coated RC films and the root-mean-square roughness was about 11 nm. The rougher surface of

CNC-coated RC films compared to graphite-like carbon coating and nanostructured Ti surface provided more opportunities for bacterial adhesion (Nguyen et al., 2019; Wandiyanto et al., 2019). Besides, the similar improvement of barrier properties of RC films after CNC-coating was indicated by WCA, moisture uptake, and WVP, which was due to the formation of air cushions that prevented the penetration of water droplets. A similar tensile strength of about 100 MPa was found for three CNC-coated RC films, which was due to the scaffolding effect of CNC to improve the resistance to loading. For mechano-bactericidal activities of CNC-coated RC films, RC-ACNC films with positive surface charges inhibited the growth of *E. coli* and *S. aureus* with 0.83 ± 0.06 and 0.69 ± 0.04 log reductions after 5 min of contact, respectively. Notably, RC-HCNC and RC-TCNC had similar roughness parameters to those of RC-ACNC but did not exhibit any antibacterial properties within 5 min of contact. In comparison, the cellulose film decorated with ZnO nanopillars showed about 0.27 and 0.24 log reduction for *E. coli* and *S. aureus*, respectively, which was mainly due to the mechanical rupture of cell walls (Xie, Pan & Cai, 2022). Our previous study elucidated that the production of reactive oxygen species was not the main driving force for CNC-coated RC films to inhibit bacteria and their nanostructured surfaces were not sufficient to cause significant deformation of the attached cells (Zhou et al., 2022). Several studies have demonstrated that the elongation and deformation of the cells were affected by the height and aspect ratio of nanopillars. For instance, the distortion and rupture of *S. aureus* were more evident when the height of the anodic aluminium oxide nanopillar increased from 200 nm to 400 nm (Wu et al., 2018). However, a decreased antimicrobial effect caused by cell deformation was observed when the height of the silica nanopillars increased from 360 nm to 400 nm, which was attributed to the fact that the nanopillars with high aspect ratios were more flexible and more easily clustered together to form bundles with a larger surface area, thus altering the surface nanostructures and

leading to a decrease in the bactericidal activity (Ivanova et al., 2020). In this study, the mechano-bactericidal properties of RC-ACNC might be based on sub-lethal mechanical damage to adherent bacteria that did not immediately kill the bacteria but resulted in apoptosis-like cell death. Besides, RC-ACNC was more effective against Gram-negative bacteria (*E. coli*) than Gram-positive bacteria (*S. aureus*). A comparable outcome was noted on a silicon nanopillar surface, where it exhibited greater efficacy against *P. aeruginosa* compared to *S. aureus*. This heightened effectiveness was associated with more evident deformation, which was attributed to variations in the rigidity of the cell outer walls (Ivanova et al., 2020). Wu et al. (2018) reported that the antimicrobial behavior of nanostructured surfaces was also affected by surface roughness, nanopillar height, distribution distance, and nanopillar density. Films with lower R_q (4.4 nm) and higher nanopillar density (~70 pillars μm^{-2}) only showed 0.11 log reduction against *S. aureus*, which was improved to 1.70 log reduction by increasing R_q (39.1 nm) and optimizing nanopillar density (~40 pillars μm^{-2}). The RC and CNC-coated RC films were applied as antimicrobial packaging for meat preservation. The initial TVC value of raw pork loins was 4.95 ± 0.12 log CFU/g and grew very rapidly during the storage period, whereas all three CNC-coated films had significant inhibitory effects on bacterial growth, although the bactericidal activity was only presented on the contact interface between the pork and films. RC-ACNC had about 0.3 log reduction on day 2, and this value slightly increased to 0.4 log reduction on day 4. Although RC-HCNC and RC-TCNC did not show any significant antimicrobial effects in a short 5-minute contact experiment, they demonstrated the ability to inhibit bacterial growth during meat preservation. Despite the lack of immediate effectiveness, their gradual impact resulted in a reduction of TVC comparable to that observed with RC-ACNC. This highlights the importance of the physical attachment of chevaux-de-frise-like nanostructures to pork surfaces, compensating for the initial absence of attractive force.

Therefore, the deposition of CNC onto packaging film surfaces can serve as an essential preliminary antimicrobial measure to extend the shelf life of packaged foods. This study underscored the significance of attractive forces and close contact between CNC-constructed nanostructures and bacteria in inhibiting bacterial growth. It not only provided insights into the development of sustainable nanostructures for active food packaging but also emphasized the potential of such strategies in addressing food safety and preservation challenges.

Chapter 8. Contribution to Knowledge and Recommendations for Future Research

8.1. Conclusion

The primary objective of this thesis was to develop wood cellulose-based sustainable food packaging as the alternatives to traditional petroleum-based plastics. The literature review showed that cellulose can be dissolved into different solvents to fabricate RC films and the applications of RC films in food packaging can be mainly classified into three aspects: biodegradable packaging, active packaging, and intelligent packaging (Chapter 2). Therefore, we compared different methods to produce RC films and investigate their potential as biodegradable food packaging materials with improved functions (Chapter 3-6).

Chapter 3 compared RC films regenerated from concentrated H_2SO_4 and NaOH/urea aqueous solutions. It was found that the choice of solvent significantly influenced the structure and properties of the resulting films. RC films from NaOH/urea solution exhibited a loose layered structure with high crystallinity index values but were relatively brittle, whereas those from H_2SO_4 solution displayed higher density with more amorphous regions and good foldability. Moisture uptake of RC films was determined by both the crystalline structure and porosity. Water vapor barrier property was affected by the density of RC films and thermal stability was influenced by the crystallinity of RC films.

In Chapter 4, five different wood pulp species were dissolved in NaOH/urea solutions and dried at ambient and hot-pressing conditions to prepare RC films. It was observed that different wood pulps did not significantly impact the structure of RC films. However, hot-pressing treatment markedly improved the density of RC films, leading to enhanced tensile strength and water vapor barrier property. The hot-pressed RC films obtained from pine had highest tensile

strength of 85.00 ± 3.26 MPa and lowest water vapor permeability of 3.59 ± 0.14 × 10^{-7} g m^{-1} h^{-1} Pa^{-1}, and exhibited the similar capacity as the commercial plastic wrap during the preservation of cherry tomatoes for up to 16 days.

Chapter 5 reported the modification of RC films by incorporating CNC and coupling organosilanes to improve their water resistance and mechanical properties while maintaining biodegradability. The dual modifications successfully increased water contact angles of RC films and maintained tensile strength of around 57 MPa in RH 60% environment. Moreover, modified films had WVP of about 3.3 × 10^{-7} g m^{-1} h^{-1} Pa^{-1} and high oxygen barrier capacity of less than 1 cm^3 m^{-2} day^{-1}, and were comparable to the commercial plastic wrap in the cookie preservation test for 100 days. Importantly, the modified RC films maintained their ability to completely disintegrate within 14 days.

In Chapter 6, three different CNC samples with neutral, negative, and positive charges were coated on the surface of RC films to obtain chevaux-de-frise-like nanostructure. Three different CNC led to similar reinforcing effects on the tensile strength (increased from 74.23 ± 1.20 to about 100 MPa) and water vapor barrier property (reduced from 1.83 ± 0.08 to about 1.20 × 10^{-7} g m^{-1} h^{-1} Pa^{-1}) of RC films. RC films coated with positively charged CNC had the highest log reduction against *Escherichia coli* (0.83 ± 0.06) and *Staphylococcus aureus* (0.69 ± 0.04) after 5 min contact, respectively. Besides, all three CNC-coated RC films exhibited a similar 0.4 log reduction of bacteria in packaged pork loins after day 4, likely due to the same physical attachment with an extended contact time.

Overall, wood pulps were proved to be a potential source for the fabrication of cellulose-based sustainable food packaging with multifunction to replace conventional non-degradable plastics. Enhanced water resistance through dual modifications and mechano-bactericidal property by deposition of CNC provide a foundation for further advancements in the field of advanced packaging materials, addressing environmental concerns associated with plastic pollution and promoting a more sustainable future.

8.2. Contribution to original knowledge

The important contributions of this research to knowledge are as follows:

1. This study systematically revealed the effects of two different aqueous solutions (concentrated H_2SO_4 and NaOH/urea aqueous solutions) on the structure and properties of RC films.

2. This study demonstrated the structure and properties of RC films obtained from different wood species and drying methods and evaluated the performance of hot-pressed RC film for preserving cherry tomatoes.

3. This work provided a dual modification strategy through the incorporation of CNC and chemical vapor deposition of organosilanes to improve water resistance of RC films without changing their disintegration rate.

4. This work revealed the effect of surface charge of CNC on the mechano-bactericidal property and meat preservation performance of nanostructured RC films, contributing to creating antimicrobial food packaging without any chemical preservatives.

8.3. Recommendations for future research

Building upon the current study, future research directions may include:

1. Optimization of solvent systems: Further exploration of alternative solvent systems to optimize the regeneration process and enhance the properties of RC films.

2. Scale-up and commercialization: Investigating the scalability of the developed RC films and modifications for commercial production, including cost analysis and environmental impact assessment.

3. Long-term stability studies: Conducting long-term stability studies on RC films with various modifications to assess their durability and performance over extended periods under different storage conditions.

4. Exploration of additional functional additives: Exploring the incorporation of other functional additives, such as antioxidants or UV-blocking agents, to further enhance the protective properties of RC films for specific food packaging applications.

5. RC films with self-healing ability: Developing RC films with self-healing properties to improve their longevity and robustness. This can involve incorporating microcapsules and constructing dynamic bonds to repair damaged films spontaneously. By maintaining the integrity and effectiveness of the packaging over time, such self-healing films can significantly extend the shelf life and usability of biodegradable food packaging materials.

General References List

Baghaei, B., & Skrifvars, M. (2020). All-cellulose composites: a review of recent studies on structure, properties and applications. *Molecules*, *25*(12), 2836.

Cheng, Y., Zhang, X., Zhang, J., He, Z., Wang, Y., Wang, J., & Zhang, J. (2022). Hygroscopic hydrophobic coatings from cellulose: Manipulation of the aggregation morphology of water. *Chemical Engineering Journal*, *441*, 136016.

Dhar, P., Tarafder, D., Kumar, A., & Katiyar, V. (2015). Effect of cellulose nanocrystal polymorphs on mechanical, barrier and thermal properties of poly (lactic acid) based bionanocomposites. *RSC Advances*, *5*(74), 60426-60440.

El Seoud, O. A., Kostag, M., Jedvert, K., & Malek, N. I. (2019). Cellulose in ionic liquids and alkaline solutions: Advances in the mechanisms of biopolymer dissolution and regeneration. *Polymers*, *11*(12), 1917.

Fan, F., Zhu, M., Fang, K., Cao, E., Yang, Y., Xie, J., ... & Cao, X. (2022). Extraction and characterization of cellulose nanowhiskers from TEMPO oxidized sisal fibers. *Cellulose*, *29*(1), 213-222.

Gardner, K. H., & Blackwell, J. (1974). The structure of native cellulose. *Biopolymers: Original Research on Biomolecules*, *13*(10), 1975-2001.

Han, J. H. (Ed.). (2005). *Innovations in food packaging*. Academic Press. Elsevier.

Ivanova, E. P., Linklater, D. P., Werner, M., Baulin, V. A., Xu, X., Vrancken, N., ... & Crawford, R. J. (2020). The multi-faceted mechano-bactericidal mechanism of nanostructured surfaces. *Proceedings of the National Academy of Sciences*, *117*(23),

12598-12605.

Jalali, A., Linke, M., Geyer, M., & Mahajan, P. V. (2020). Shelf life prediction model for strawberry based on respiration and transpiration processes. *Food Packaging and Shelf Life*, *25*, 100525.

Joo, S. W., Berkani, M., Mashifana, T., Kamyab, H., Wang, C., & Vasseghian, Y. (2023). Sustainable cellulose-based hydrogels for water treatment and purification. *Industrial Crops and Products*, *205*, 117525.

Koshani, R., Eiyegbenin, J. E., Wang, Y., & van de Ven, T. G. (2022). Synthesis and characterization of hairy aminated nanocrystalline cellulose. *Journal of Colloid and Interface Science*, *607*, 134-144.

Kowalczuk, D., & Pitucha, M. (2019). Application of FTIR method for the assessment of immobilization of active substances in the matrix of biomedical materials. *Materials*, *12*(18), 2972.

Li, R., Zhang, L., & Xu, M. (2012). Novel regenerated cellulose films prepared by coagulating with water: Structure and properties. *Carbohydrate Polymers*, *87*(1), 95-100.

Li, X., Li, H. C., You, T. T., Wu, Y. Y., Ramaswamy, S., & Xu, F. (2019). Fabrication of regenerated cellulose membranes with high tensile strength and antibacterial property via surface amination. *Industrial Crops and Products*, *140*, 111603.

Linklater, D. P., Baulin, V. A., Juodkazis, S., Crawford, R. J., Stoodley, P., & Ivanova, E. P. (2021). Mechano-bactericidal actions of nanostructured surfaces. *Nature Reviews Microbiology*, *19*(1), 8-22.

Nguyen, D. H., Wang, J., Sbarski, I., Juodkazis, S., Crawford, R. J., & Ivanova, E. P. (2019). Influence of amorphous, carbon-derived wrinkled surface topologies on the colonization of *Pseudomonas aeruginosa* bacteria. *Advanced Materials Interfaces*, *6*(7), 1801890.

Pirich, C. L., Picheth, G. F., Fontes, A. M., Delgado-Aguilar, M., & Ramos, L. P. (2020). Disruptive enzyme-based strategies to isolate nanocelluloses: A review. *Cellulose*, *27*, 5457-5475.

Robertson, G. L. (2013). *Food packaging: Principles and practice* (3rd ed.). CRC Press.

Roy, P., Mohanty, A. K., & Misra, M. (2022). Microplastics in ecosystems: Their implications and mitigation pathways. *Environmental Science: Advances*, *1*(1), 9-29.

Sadeghalvad, B., Khorshidi, N., Azadmehr, A., & Sillanpää, M. (2021). Sorption, mechanism, and behavior of sulfate on various adsorbents: A critical review. *Chemosphere*, *263*, 128064.

Shaghaleh, H., Xu, X., & Wang, S. (2018). Current progress in production of biopolymeric materials based on cellulose, cellulose nanofibers, and cellulose derivatives. *RSC Advances*, *8*(2), 825-842.

Srivastava, S., & Mishra, H. N. (2021). Development of microencapsulated vegetable oil powder based cookies and study of its physicochemical properties and storage stability. *LWT*, *152*, 112364.

Su, Z., Cui, L., Zhang, H., Xiao, L., Chi, B., Xu, H., ... & Wang, X. (2023). Robust, waterproof, and degradable cellulose-based polyimine vitrimer for plastic replacement. *Chemical*

Engineering Journal, *471*, 144501.

Tu, H., Zhu, M., Duan, B., & Zhang, L. (2021). Recent progress in high-strength and robust regenerated cellulose materials. *Advanced Materials*, *33*(28), 2000682.

Véronique, C. O. M. A. (2008). Bioactive packaging technologies for extended shelf life of meat-based products. *Meat Science*, *78*(1-2), 90-103.

Wandiyanto, J. V., Cheeseman, S., Truong, V. K., Al Kobaisi, M., Bizet, C., Juodkazis, S., ... & Ivanova, E. P. (2019). Outsmarting superbugs: Bactericidal activity of nanostructured titanium surfaces against methicillin-and gentamicin-resistant *Staphylococcus aureus* ATCC 33592. *Journal of Materials Chemistry B*, *7*(28), 4424-4431.

Wu, S., Zuber, F., Maniura-Weber, K., Brugger, J., & Ren, Q. (2018). Nanostructured surface topographies have an effect on bactericidal activity. *Journal of Nanobiotechnology*, *16*, 1-9.

Xie, Y., Pan, Y., & Cai, P. (2022). Cellulose-based antimicrobial films incroporated with ZnO nanopillars on surface as biodegradable and antimicrobial packaging. *Food Chemistry*, *368*, 130784.

Yu, L., Zhang, Z., Tang, H., & Zhou, J. (2019). Fabrication of hydrophobic cellulosic materials via gas–solid silylation reaction for oil/water separation. *Cellulose*, *26*, 4021-4037.

Zhang, S., Luo, L., Sun, X., & Ma, A. (2021). Bioactive peptides: A promising alternative to chemical preservatives for food preservation. *Journal of Agricultural and Food Chemistry*, *69*(42), 12369-12384.

Zhao, G., Lyu, X., Lee, J., Cui, X., & Chen, W. N. (2019). Biodegradable and transparent cellulose film prepared eco-friendly from durian rind for packaging application. *Food Packaging and Shelf Life*, *21*, 100345.

Zhao, H., Li, C. F., Yu, X., Zhong, N., Hu, Z. Y., Li, Y., ... & Hu, J. (2022). Mechanistic understanding of cellulose β-1,4-glycosidic cleavage via photocatalysis. *Applied Catalysis B: Environmental*, *302*, 120872.

Zhou, C., Girouard, F., O'Brien, B., Ronholm, J., & Wang, Y. (2022). Construction of chevaux-de-frise from cellulose nanocrystals to enable mechano-bactericidal activity on recycled waste cotton films. *Green Chemistry*, *24*(3), 1109-1113.